NOTICE

The quality of this microform is heavily dependent upon the quality of the original thesis submitted for microfilming. Every effort has been made to ensure the highest quality of reproduction possible.

If pages are missing, contact the university which granted the degree.

Some pages may have indistinct print especially if the original pages were typed with a poor typewriter ribbon or if the university sent us an inferior photocopy.

Previously copyrighted materials (journal articles, published tests, etc.) are not filmed.

Reproduction in full or in part of this microform is governed by the Canadian Copyright Act, R.S.C. 1970, c. C-30.

AVIS

La qualité de cette microforme dépend grandement de la qualité de la thèse soumise au microfilmage. Nous avons tout fait pour assurer une qualité supérieure de reproduction.

S'il manque des pages, veuillez communiquer avec l'université qui a conféré le grade

La qualité d'impression de certaines pages peut laisser à désirer, surtout si les pages originales ont été dactylographiées à l'aide d'un ruban usé ou si l'université nous a fait parvenir une photocopie de qualité inférieure.

Les documents qui font déjà l'objet d'un droit d'auteur (articles de revue, tests publiés, etc.) ne sont pas microfilmés.

La reproduction, même partielle, de cette microforme est soumise à la Loi canadienne sur le droit d'auteur, SRC 1970, c. C-30.

Two-Dimensional Modelling of Local River Ice Cover Melting due to a Side Thermal Effluent

Philip R. Plouffe

A Thesis

in

The Department

of

Civil Engineering

Presented in Partial Fulfillment of the Requirements
for the Degree of Master of Engineering at
Concordia University
Montréal, Québec, Canada

August 1987

ISBN 0-315-41600-9

ABSTRACT

Two-Dimensional Modelling of Local River Ice Cover Melting due to a Side Thermal Effluent

Philip R. Plouffe

Thermal effluent is discharged from municipalities, industries and thermal power plants. In northern regions, where rivers are ice covered for a considerable period of the year, these thermal effluents have the effect of lessening ice cover thickness or completely melting the ice cover over long reaches, predominately downstream of the effluent discharge. Ice free reaches may be employed for beneficial purposes such as allowing year round navigation and flood prevention, by elimination of ice jamming.

The extent of ice melting is dependant on the river hydrodynamic characteristics, the effluent source characteristics and the prevailing meteorological conditions.

This thesis deals with the development and testing of a two-dimensional numerical model, for the local melting of a river ice cover due to a side thermal effluent. The river hydrodynamics are modelled using the depth integrated St. Venant equations for shallow water, incorporating the effect of the ice cover on the flow. Temperature distribution is determined from the two-dimensional unsteady depth averaged energy equation. These equations are solved by employing a modified McCormack and upwinding, finite difference schemes. Heat exchange between the river and atmosphere is evaluated from the meteorological variables, for ice covered and open river conditions. Ice thickness is simulated by use of the atmospheric heat exchange processes and heat transfer from the river flow to the ice cover.

A comparison is carried out with field data to determine the validity of the model results.

ACKNOWLEDGEMENT

I would like to express special thanks to my thesis advisor, Dr. Semaan Sarraf, for his encouragement and guidance during the completion of this thesis.

I also wish to thank Dr. George Ashton of CRREL for the provision of the field data used in this work.

Finally, I want to express sincere appreciation for the support of my parents, Roland and Shirley Plouffe, during my studies.

TABLE OF CONTENTS

LIST OF FIGURES

LIST OF TABLES

LIST OF SYMBOLS

A	=	energy equation discritization coefficient, in m s^{-1}
a	=	annual variation in solar radiation constant, in cal $cm^{-2}day^{-1}$
b	=	annual variation in solar radiation constant
C	=	cloud cover, in tenths
C_c	=	coefficient for ice cover reduction in conductive heat transfer
C_e	=	coefficient for ice cover reduction in evapo-condensation heat flux
C_{el}	=	celerity, in m s^{-1}
C_p	=	specific heat of water, in cal kg^{-1} °C^{-1}
C_{wi}	=	heat transfer constant water to ice, in cal $s^{-0.2}$ $m^{-2.6}$ °C^{-1}
c	=	empirical constant for atmospheric radiation
DD	=	diffusion conductance, in m s^{-1}
D_x	=	longitudinal dispersion coefficient x direction, in m^2 s^{-1}
D_y	=	longitudinal dispersion coefficient y direction, in m^2 s^{-1}
d	=	empirical constant for atmospheric radiation
e_a	=	air vapour pressure, in mb
e_s	=	saturation vapour pressure, in mb
F	=	conservative variable, in m^3 s^{-2}
FF	=	convective strength, in m s^{-1}
f	=	Coriolis parameter, in s^{-1}
G	=	conservative variable, in m^3 s^{-2}
g	=	gravitational acceleration, in m s^{-2}

h	=	water depth, in m
h_{wi}	=	heat transfer coefficient from water to ice cover, in cal m^{-2} s^{-1} $°C^{-1}$
K_i	=	ice thermal conductivity, in cal $m^{-1}s^{-1}$ $°C^{-1}$
k_c	=	empirical constant for atmospheric radiation
k_n	=	coefficient for free convection
k_x	=	longitudinal dispersion constant x direction
k_y	=	longitudinal dispersion constant y direction
L_i	=	ice heat of fusion, in cal kg^{-1}
L_x	=	McCormack operator x-direction backward predictor, forward corrector
L_y	=	McCormack operator y-direction backward predictor, forward corrector
L'_x	=	McCormack operator x-direction forward predictor, backward corrector
L'_y	=	McCormack operator y-direction forward predictor, backward corrector
n	=	Manning's coefficient
n_b	=	Manning's coefficient of river bed
n_i	=	Manning's coefficient of underside of ice cover
P	=	Peclet number
q_{wi}	=	heat transfer water to ice cover, in cal $m^{-2}s^{-1}$
R	=	hydraulic radius, in m
S	=	conservative variable, in m^3 s^{-2}

S_{fx} = friction slope longitudinal direction

S_{fy} = friction slope transverse direction

S_{ox} = bed slope longitudinal direction

S_{oy} = bed slope transverse direction

T = water temperature, in °C

T_a = air temperature, in °C

T_{ak} = air temperature, in °K

T_f = freezing point temperature, in °C

T_i = ice cover internal temperature, in °C

T_s = top surface temperature, in °C

T_{sk} = ice top surface temperature, in °K

t = time, in s

Δt = time step, in s

Δt_2 = one half the time step, in s

U = unit discharge longitudinal direction, in $m^2 s^{-1}$

U^* = shear velocity longitudinal direction, in $m s^{-1}$

u = flow velocity longitudinal direction, in $m s^{-1}$

V = unit discharge transverse direction, in $m^2 s^{-1}$

V^* = shear velocity transverse direction, in $m s^{-1}$

VV = resultant water velocity, in $m s^{-1}$

V_a = wind velocity at 2 m above surface, in $m s^{-1}$

v = flow velocity transverse direction, in $m s^{-1}$

x = space coordinate longitudinal direction, in m

Δx = grid spacing x direction, in m

y = space coordinate transverse direction, in m

Δy = grid spacing y direction, in m

Z_f = bed elevation, in m

z = space coordinate vertical direction, in m

α = surface albedo

α_s = empirical constant for ice surface albedo

α_i = empirical constant for ice surface albedo

β_i = fraction of solar radiation which penetrates ice-water interface

$\Delta\theta_s$ = ice thickness change at top surface, in m

$\Delta\theta_w$ = ice thickness change at bottom surface, in m

ε = turbulant viscosity coefficient, in $m^2 s^{-1}$

ε_s = emissivity of water or ice surface

θ = ice thickness, in m

ρ = water density, in kg m^{-3}

ρ_i = ice density, in kg m^{-3}

σ = Stefan-Boltzman constant, in cal cm^{-2} day^{-1}

τ_i = bulk extinction coefficient, in cm^{-1}

τ_{sx} = wind induced surface stress longitudinal direction, in kg s^{-2} m^{-1}

τ_{sy} = wind induced surface stress transverse direction, in kg s^{-2} m^{-1}

Φ = source term, in °C s^{-1}

ϕ = heat transfer to water, in cal cm^{-2} day^{-1}

ϕ_b = effective back radiation, in cal cm^{-2} day^{-1}

ϕ_{ba} = atmospheric radiation, in cal cm^{-2} day^{-1}

ϕ_{bn} = net atmospheric radiation, in cal cm^{-2} day^{-1}

ϕ_{bs} = longwave radiation emitted by the river surface, in cal cm^{-2} day^{-1}

ϕ_c = conductive heat transfer, in cal cm^{-2} day^{-1}

ϕ_e = evapo-condensation flux, in cal cm^{-2} day^{-1}

ϕ_{lat} = latitude on earth's surface, in degrees

ϕ_{ri} = incoming shortwave radiation, in cal cm^{-2} day^{-1}

ϕ_s = net shortwave radiation, in cal cm^{-2} day^{-1}

ϕ_{sp} = shortwave penetration into the waterbody, in cal cm^{-2} day^{-1}

ψ = empirical constant for ice surface albedo

CHAPTER 1
INTRODUCTION

Throughout the world large amounts of waste heat are being rejected to the environment and in particular to watercourses. Thermal power plants, industries and municipalities discharge thermal effluent to nearby streams. In cold regions where rivers are ice covered for part of the year, these effluents have the effect of reducing ice cover thickness, or completely suppressing its formation over long reaches. In the case of power plant discharges, these ice free reaches often extend several kilometers downstream of the effluent source.

A model which would predict the melting of river ice cover due to a thermal effluent is of considerable interest to people dealing with hydraulics and navigation in cold regions as the discharge of thermal effluents increase. This model would evaluate the outcome of a new effluent source, before construction, as is often required by environmental studies. A possible beneficial use of this model would be the design of effluent sourses to keep navigation channels and harbours ice free. Closure of shipping routes cause economic loss, as is the case in Canada where the St. Lawrence Seaway must close for the winter period. These effluents would allow an extension of the navigation season or year round navigation. Electricity can be easily transmitted over long distances allowing beneficial placement of generation facilities. Steam generation of electricity typically rejects 58 to 67% [Paily 1974] of the energy used to the environment, predominately in the form of cooling water from the station condensors. The ice free reaches also eliminate flood damage caused by ice jamming during river ice breakup. This is another possible benefit from use of the model to design effluent discharges to prevent ice formation at critical river sections. Thermal effluent can create dangerous

conditions in recreational and urban areas by weakening the ice cover in some regions. The model would also be of use to calculate the effects of the thermal effluent for this purpose.

River ice cover melting is dependent on a large number of parameters. The region of ice cover melting is determined by the magnitude of the effluent discharge, the river flow pattern and the meteorological conditions.

A number of researchers have previously studied this subject. Dingman et al [Dingman, Weeks & Yeh 1967] performed a one-dimensional solution of the energy equation neglecting the diffusion term. A steady state solution was calculated using an uniform, assumed velocity field. Paily et al [Paily 1974; Paily, Macagno & Kennedy 1974; Paily & Macagno 1974] solved the one-dimensional energy equation including the effect of longitudinal dispersion. The solution used an uniform, assumed velocity field. The unsteady case was included in the model. In addition, linearized heat loss relations were developed. Ashton [Ashton 1979] solved the one-dimensional quasi-steady energy equation. Heat transfer processes at the ice cover interfaces were considered as well as varying meteorological conditions, using a linear heat transfer relation. An assumed velocity field was uniform and steady. Shen and Chiang [Shen & Chiang 1984] developed a one-dimensional model of the ice cover growth and decay on the St. Lawrence River. The model used an uniform velocity field and included a complete ice cover and open water heat transfer formulation. Al-Salah et al [Al-Salah, Sarraf & Kahawita 1987] performed an analytical solution of the one-dimensional energy equation, including coverging or diverging river flow. A linear heat transfer relation was used in the solution.

Field studies have been conducted to evaluate the process of river ice cover melting by a thermal effluent. Dingman et al [Dingman & Weeks 1970] carried out a study on

the North Saskatchewan River at Edmonton, Alberta. Despite operational difficulties useful information was obtianed. Ashton [Ashton 1981] conducted an extensive study on the Mississippi River at Bettendorf, Iowa. Field data on many aspects of ice melting was collected during the study period. Hayes and Ashton [Hayes & Ashton 1985] collected data from power plants in the Pittsburgh, Pennsylvania area to further test their model. The field studies allow verification of model results and assumptions.

In the present work, river ice cover melting by a thermal effluent is modelled by a two-dimensional numerical model. The river flow is determined from the solution of the St. Venant shallow water equations. The unsteady two-dimensional energy equation is the basis of the water temperature calculation. Heat transfer processes between the river and the atmosphere is incorporated both for the open water and ice covered cases. Melting of the ice surface on the top and underside is considered. The heat transfer between ice cover and water is also evaluated. This model accounts for variability in the river geometry and changes in the flow pattern caused by the ice conditions, by calculation of the velocity field. A two-dimensional solution of the flow pattern and temperature distribution allows modelling of the ice cover melting in the longitudinal as well as the transverse direction. The heat transfer processes and ice cover thickness change is addressed by considering the dominant heat transfer terms in river ice cover melting by a thermal effluent and the ice thickness equations.

CHAPTER 2

MATHEMATICAL FORMULATION

2.1 Hydrodynamic Equations

The river flow field is calculated by use of the shallow water or depth averaged hydrodynamic equations, to model the flow of the thermal effluent, which causes melting of the ice cover. These equations express the principles of conservation of mass and momentum stated by the three-dimensional Navier-Stokes equations. In the case of free surface flow, these equations are integrated over the depth using the hydrostatic pressure approximation. The result is the St. Venant shallow water equations for free surface flows. The St. Venant shallow water equations are expressed here in conservative form [Garcia 1983]:

Continuity equation:

$$\frac{\partial h}{\partial t} + \frac{\partial U}{\partial x} + \frac{\partial V}{\partial y} = 0 \qquad (2.1)$$

Conservation of momentum equation in x direction:

$$\frac{\partial U}{\partial t} + \frac{\partial F}{\partial x} + \frac{\partial G}{\partial y} = gh(S_{ox} - S_{fx}) + fV - \frac{1}{\rho}\tau_{sx} + \frac{\partial}{\partial x}(\varepsilon\frac{\partial U}{\partial x}) + \frac{\partial}{\partial y}(\varepsilon\frac{\partial U}{\partial y}) \qquad (2.2)$$

Conservation of momentum equation in y direction:

$$\frac{\partial V}{\partial t} + \frac{\partial G}{\partial x} + \frac{\partial S}{\partial y} = gh(S_{oy} - S_{fy}) - fU - \frac{1}{\rho}\tau_{sy} + \frac{\partial}{\partial x}(\varepsilon\frac{\partial V}{\partial x}) + \frac{\partial}{\partial y}(\varepsilon\frac{\partial V}{\partial y}) \qquad (2.3)$$

where the conservative variables F, G and S are defined as:

$$F = F(x,y,t) = u^2h + 1/2\ gh^2 \qquad (2.4)$$

$$G = G(x,y,t) = uvh \tag{2.5}$$

$$S = S(x,y,t) = v^2h + 1/2\ gh^2 \tag{2.6}$$

x and y are the horizontal coordinates in the longitudinal and transverse directions respectively; t is the time; $h = h(x,y,t)$ is the water depth; $U = u(x,y,t) = uh$ and $V = v(x,y,t) = vh$ which are the unit width discharges in the longitudinal and transverse directions respectively; S_{ox} and S_{oy} are the river bed slopes given by equations (2.7) and (2.8) respectively;

$$S_{ox} = \frac{\partial Z_f}{\partial x} \tag{2.7}$$

$$S_{oy} = \frac{\partial Z_f}{\partial y} \tag{2.8}$$

Z_f is the bed elevation; S_{fx} and S_{fy} are the friction slopes approximated by Manning's formula expressed in equations (2.9) and (2.10) respectively;

$$S_{fx} = \frac{n^2 u\sqrt{(u^2+v^2)}}{h^{4/3}} \tag{2.9}$$

$$S_{fy} = \frac{n^2 v\sqrt{(u^2+v^2)}}{h^{4/3}} \tag{2.10}$$

n is the Manning's surface roughness coefficient; g is the gravitational acceleration value; f is the Coriolis parameter; τ_{sx} and τ_{sy} are the surface stresses developed from wind currents; ε is the turbulent viscosity coefficient and ρ is the water density which is assumed constant.

The diffusion of momentum due to the turbulence terms are not normally significant for large scale problems unless near field mixing is considered. The modelling of the near field mixing would require a complete turbulence model. In this present work a constant coefficient of turbulent viscosity is satisfactory.

2.1.1 Ice Cover Effects on Hydrodynamics

To account for the effect of a floating ice cover in the hydrodynamic equations, modification of the hydrostatic pressure terms is necessary. The additional pressure due to the weight of the ice cover is accounted for by adding 90% of the ice thickness to the water depth in hydrostatic pressure terms. The value of 90% is employed due to a nine tenths density ratio between ice and water. The conservative variables F and S are redefined as:

$$F = F(x,y,t) = uh + 1/2\, g(h + 0.9\theta)^2 \qquad (2.11)$$

$$S = S(x,y,t) = vh + 1/2\, g(h + 0.9\theta)^2 \qquad (2.12)$$

where θ is the thickness of the ice cover. The friction slope term in the x and y conservation of momentum equations, $gh(S_{ox} - S_{fx})$ and $gh(S_{oy} - S_{fy})$ respectively, also is modified by the addition of 90% of the ice thickness to the water depth.

The friction slopes S_{fx} and S_{fy}, formula is modified due to the presence of the ice cover. The formulas are redefined as:

$$S_{fx} = \frac{n^2 u\sqrt{(u^2 + v^2)}}{R^{4/3}} \qquad (2.13)$$

$$S_{fy} = \frac{n^2 v\sqrt{(u^2 + v^2)}}{R^{4/3}} \qquad (2.14)$$

where R is the hydraulic radius. In the case of open water the hydraulic radius is set equal to the water depth, by use of the wide river assumption [Chow 1957]. For the case of ice covered flow in a wide river, the hydraulic radius is one half the river depth. This accounts for the increased friction caused by a two fold increase in the wetted perimeter of the river [Burrel & Davar 1982].

The Manning coefficient used in the friction slope calculation for an open river is determined by the bed friction. For ice covered flow a combined Manning coefficient taking into account the roughness of the river bed and ice cover underside is required. The combined Manning coefficient is obtained form the Nezhikhovskiy formula [Wankiewicz 1984]:

$$n = \left(\frac{n_b^{3/2} + n_i^{3/2}}{2} \right)^{2/3} \qquad (2.15)$$

where n_b is the bed roughness coefficient and n_i is the ice underside roughness coefficient.

2.2 Energy Equation

The temperature distribution in the river flow field is calculated by use of the energy equation. The energy equation is based on the principal of conservation of heat transported and dispersed by the flow. The space-time temperature distribution of the river is expressed as a function of the flow properties. An increase in the river water temperature caused by the thermal effluent, which leads to melting of the ice cover is simulated by this equation.

The two-dimensional unsteady heat energy conservation equation governing the temperature distribution in a vertically homogeneous stream is given as [Wake & Rumer 1979]:

$$\frac{\partial TH}{\partial t} + \frac{\partial TU}{\partial x} + \frac{\partial TV}{\partial y} = \frac{\partial}{\partial x}\left(hD_x \frac{\partial T}{\partial x}\right) + \frac{\partial}{\partial y}\left(hD_y \frac{\partial T}{\partial y}\right) + h\,\Phi \qquad (2.16)$$

where T is the water temperature; D_x is the longitudinal dispersion coefficient in the x direction; D_y is the longitudinal dispersion coefficient in the y direction and Φ is the source term which represents the heat flux at the water-air or water-ice interface.

2.2.1 Dispersion Coefficients

The solution of the energy equation requires the evaluation of the dispersion coefficient terms. These terms are determined from the following equations [Ashton 1979]:

$$D_x = k_x U^* R \qquad (2.17)$$

$$D_y = k_y V^* R \qquad (2.18)$$

where k_x is the longitudinal dispersion constant in the x direction; k_y is the longitudinal dispersion constant in the y direction; U* is the shear velocity in the longitudinal direction and V* is the shear velocity in the transverse direction. The shear velocities are defined as:

$$U^* = \sqrt{S_{fx}\, g\, R} \qquad (2.19)$$

$$V^* = \sqrt{S_{fy}\, g\, R} \qquad (2.20)$$

Engman [Engman 1977] found that the presence of an ice cover reduces the dispersion constants by 50%. However by the use of the hydraulic radius, which is reduced by one half in the case of an ice covered river, one value may be used for the dispersion constant.

The longitudinal dispersion constant is influenced by the processes of mixing over the flow cross section and variation of the longitudinal velocity. In field situations the value is determined by channel irregularities in the horizontal and vertical directions, wind and waves. Elder [Elder 1959] found the value of the dispersion constant in laboratory channels to be 5.9. In rivers a large variation in the dispersion constant is measured, with much larger values being found. The dispersion constant values are summarized in Table 2.1.

2.3 Atmospheric Heat Transfer Equations

Heat exchange occurs between the atmosphere and river. When the river is not ice covered heat exchange occurs at the air-water interface and for an ice covered river at the air-ice interface. This surface condition influences the individual heat transfer processes.

The components of the heat exchange include shortwave (solar) radiation, longwave radiation, evapo-condensation flux and conductive heat transfer. The meteorological factors determining these components are cloud cover, air temperature, wind velocity and air vapour pressure. Heat transfer from precipitation and geothermal heat transfer through the river bed is not significant in modelling the melting of river ice by thermal effluent. The effect of snow cover is not included but the ice edge is normally washed free of snow by wave action. During winter periods when the air temperature is considerably lower than the temperature of the river and solar radiation is

Table 2.1 Longitudinal Dispersion Measurements [after Paily 1974]

Reference	Channel	Depth h (cm)	Width b (m)	Shear Velocity u* (cm/sec)	Observed Dispersion Coefficient E (m^2/sec)	C = E/hu*	E Predicted (m^2/sec)
Thomas (1958)	Chicago Ship Canal	807	48.8	1.91	3.0	20	
State of Calif. (1962)	Sacramento River	400		5.1	15	74	
Owens et al. (1964)	River Derwent	26		14	4.6	131	
Glover (1964)	South Platte River	46		6.9	16.2	510	
Schuster (1965)	Yuma Mesa A Canal	345		3.45	0.75	8.6	
Fischer (1967a)	Trapezoidal Laboratory Channel with roughened sides	3.5	.40	2.02	.123	174	.131
		4.7	.43	3.59	.253	150	.251
		3.5	.40	3.51	.415	338	.371
		3.5	.34	3.48	.250	205	.250
		2.1	.33	3.28	.400	392	.450
		2.1	.19	3.88	.220	270	.166
Fischer (1968b)	Green-Duwamish River, Washington	110	20	4.9	6.5 to 8.5	120 to 160	7.8
Yotsukura et al. (1970)	Missouri River	270	200	7.4	1500	7500	

Table 2.1 (Continued)

Reference	Channel	Depth h (cm)	Width b (m)	Shear Velocity u* (cm/sec)	Observed Dispersion Coefficient E (m^2/sec)	C = E/hu*	E Predicted (m^2/sec)
Godfrey and Frederick (1970) (Predicted Values of E from Fischer, 1968b)	Copper Creek, Va. (below gage)	49	16	8.0	20	500	6.0
		85	18	10.0	21	250	28
		49	16	8.0	9.5	245	11.4
	Clinch River, Tenn.	85	47	6.7	14	235	15
		210	60	10.4	54	245	86
		210	53	10.7	47	210	55
	Copper Creek, Va. (above gage)	40	19	11.6	9.9	220	2.8
	Powell River, Tenn.	85	34	5.5	9.5	200	9.1
	Clinch River, Va.	58	36	4.9	8.1	280	30
	Coachella Canal, Calif.	156	24	4.3	9.6	140	3.9
Fukuoka (1971)	Sinuous rectangular Laboratory Channel, smooth sides, smooth and rough bottoms - 25 experiments	2.3 to 7.0	.13 to .25	1.1 to 2.7		5.8 to 35	

at a minimum, considerable heat loss from the river to the atmosphere occurs. This results in the cooling of the river, formation and thickening of ice cover and cooling of the effluent flow, reducing ice melting.

The heat exchange processes are summarized in Fig. 2.1.

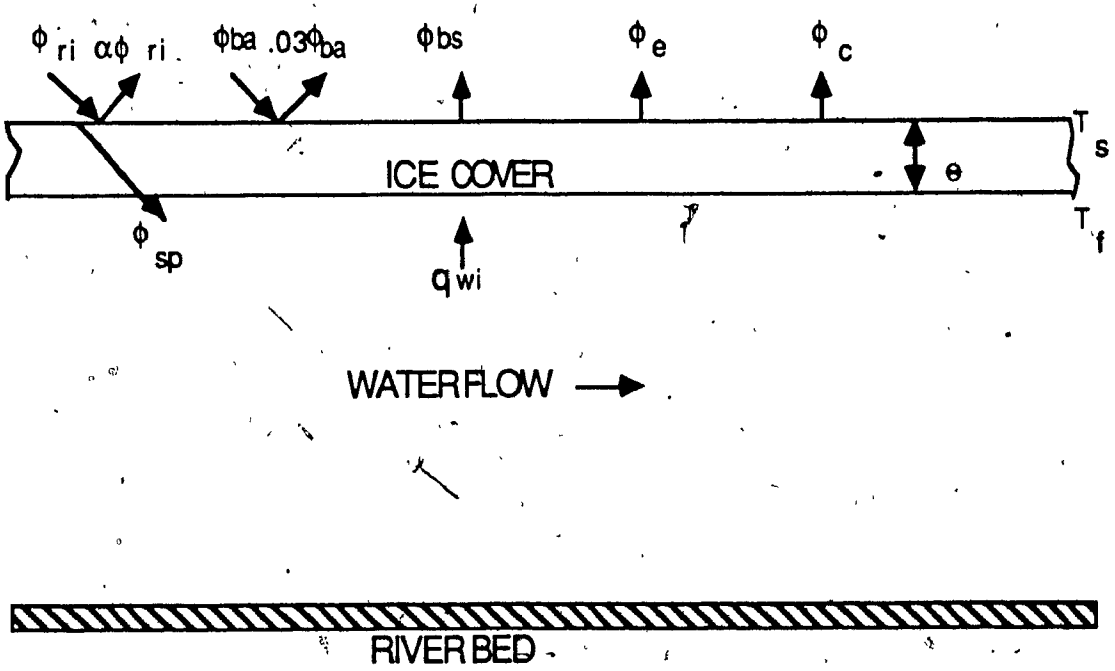

Fig. 2.1 Heat Transfer Processes on the Ice Cover

Heat transfer values from the equations used are converted to units of cal m^{-2} s^{-1} for use in subsequent calculations.

2.3.1 Shortwave (Solar) Radiation

The incoming solar radiation for an area may be determined from weather records,

if such data has been recorded. Often the only available data is on cloud cover conditions. The incoming solar radiation may be calculated using the cloud cover data from [Shen & Chiang 1984]:

$$\phi_{ri} = [a - b\,(\phi_{lat} - 50)]\,(1 - 0.0065C^2) \qquad (2.21)$$

where ϕ_{ri} is the incoming shortwave radiation in cal cm^{-2} day^{-1}; ϕ_{lat} is the latitude on the earth's surface in degrees; C is the cloud coyer in tenths (ranging from 0 for a clear sky to 10 for a completely overcast sky) and a and b which are constants that reflect the annual variation in solar radiation intensity. The values of the constants a and b are given in Table 2.2 for the winter period.

Table 2.2 Annual Variation of Solar Radiation Constants [after Shen & Chiang 1984]

Month	a, in calorie-centimeters^{-2} -day^{-1}	b
Dec.	100	8.2
Jan.	142	11.0
Feb.	228	11.2
March	394	12.7
April	554	8.4

A portion of this solar radiation reaching a surface is reflected back and not absorbed.

For the water surface the net solar radiation is given by [Shen & Chiang,1984]:

$$\phi_s = (1 - \alpha)\, \phi_{ri} \qquad (2.22)$$

where ϕ_s is the net shortwave radiation in cal cm^{-2} day^{-1} and α is the surface albedo. The value of this albedo is equal to 0.1 [Shen & Chiang 1984].

For the ice cover surface the albedo value depends on the material behaviour of the ice cover. The albedo is calculated using [Shen & Chiang 1984]:

$$\alpha = \alpha_i \qquad T_a \le 0^\circ C \qquad (2.23)$$

$$\alpha = \alpha_a + (\alpha_i - \alpha_a) e^{-\psi T_a} \qquad T_a \ge 0^\circ C \qquad (2.24)$$

where α_i, α_a and ψ are empirical constants and T_a is the air temperature in °C. The values of the constants are $\alpha_i = 0.41$, $\alpha_a = 0.25$ and $\psi = 0.7$ [Shen & Chiang1984].

A portion of this solar radiation penetrates the ice cover and acts as an internal heat source in the waterbody. This shortwave radiation penetration is calculated from the Bouguer-Lambert exponential law [Shen & Chiang 1984]:

$$\phi_{sp} = \beta_i\, \phi_s\, e^{-\tau_i \theta} \qquad (2.25)$$

where ϕ_{sp} is the penetration of shortwave radiation into the waterbody in cal cm^{-2} day^{-1}

β_i is the fraction of absorbed solar radiation which penetrates the ice-water interface and

τ_i is the bulk extinction coefficient. The value of β_i is set equal to 1.0 due to the small difference in the refractive indices of ice and water. The bulk extinction coefficient is 0.07 cm^{-1} [Shen & Chiang 1984].

2.3.2 Longwave Radiation

The longwave radiation heat transfer is made up of two components. These components are the longwave radiation emitted from the river surface and the net absorbed atmospheric radiation.

Radiation emission from the river surface is evaluated from the Stefan-Boltzman law of radiation including the emissivity of the river's surface [Shen &Chiang 1984]:

$$\phi_{bs} = \varepsilon_s \sigma T_{sk}^4 \qquad (2.26)$$

where ϕ_{bs} is the longwave radiation emitted by the river surface in cal cm^{-2} day^{-1}; ε_s is the emissivity of the water or ice surface; σ is the Stefan-Boltzman constant and T_{sk} is the water or ice surface temperature in °K. The Stefan-Boltzman constant is 1.171 x 10^{-7} cal cm^{-2} day^{-1} and the emissivity of both the water and ice surface is 0.97 [Shen & Chiang 1984].

The atmospheric radiation for an area may be determined from weather records, if such data has been recorded. Atmospheric radiation may also be calculated from cloud cover data using Bolz's formula [Shen & Chiang 1984]:

$$\phi_{ba} = \sigma T_{ak}^4 (c + d\sqrt{e_a})(1 + k_c C^2) \qquad (2.27)$$

where ϕ_{ba} is the atmospheric radiation in cal cm^{-2} day^{-1}; T_{ak} is the air temperature in °K; c, d and k_c are empirical constants and e_a is the air vapour pressure in mb. Empirical constant values for c, d and k_C are 0.55, 0.052 and 0.0017 respectively [Shen & Chiang 1984].

The reflectivity of the ice or water surface may be taken as 0.03. Net atmospheric radiation is therefore [Shen & Chiang 1984]:

$$\phi_{bn} = 0.97\ \phi_{ba} \qquad (2.28)$$

where ϕ_{bn} is the net atmospheric radiation in cal cm^{-2} day^{-1}.

Considering the two components of the longwave radiation, the effective back radiation is given by [Shen & Chiang 1984]:

$$\phi_b = \phi_{bs} - \phi_{bn} \qquad (2.29)$$

where ϕ_b is the effective back radiation in cal cm^{-2} day^{-1}.

2.3.3 Evapo-Condensation Flux

Evapo-condensation heat flux which occurs at the water surface is determined by the Rimsha-Dochenko formula [Shen & Chiang 1984]:

$$\phi_e = (1.56\ k_n + 6.08\ V_a)\ (e_s - e_a) \qquad (2.30)$$

where ϕ_e is the evapo-condensation heat flux in cal cm^{-2} day^{-1}; V_a is the wind velocity at 2 m above the water surface in m s^{-1} and e_s is the saturation vapour pressure at the

surface temperature in mb.

To account for the effect of free convection the coefficient k_n is calculated [Shen & Chiang 1984]:

$$k_n = 8.0 + 0.35 (T_s - T_a) \qquad (2.31)$$

where k_n is a coefficient that accounts for free convection and T_s is the surface temperature in °C.

Presence of an ice cover will reduce the evaporation process. A coefficient of estimated value 0.5 is added to the Rimsha-Dochenko formula [Shen & Chiang 1984]:

$$\phi_e = C_e (1.56 k_n + 6.08 V_a) (e_s - e_a) \qquad (2.32)$$

where C_e is a coefficient which accounts for the reduction in surface evaporation due to the presence of an ice cover.

Saturation vapour pressure may be calculated using the Goff-Gatch formula [Paily, Macagno & Kennedy 1974]:

$$\log e_s = -7.90298 \left(\frac{373.16}{T_{sk}} - 1 \right) + 5.02808 \log \left(\frac{373.16}{T_{sk}} \right)$$

$$- 1.3816 \times 10^{-3} \left(10^{11.344 \left(1 - \frac{T}{373.16} \right)} - 1 \right)$$

$$+ 8.1328 \times 10^{-3} \left(10^{-3.39149 \left(\frac{373.16}{T_{sk}} - 1 \right)} - 1 \right) + \log (1013.246) \qquad (2.33)$$

2.3.4 Conductive Heat Transfer

Heat exchange occurring from conduction at the water surface is determined by use of the Rimsha-Dochenko formula [Shen & Chaing 1984]:

$$\phi_c = (k_n + 3.9\ V_a)\ (T_s - T_a) \tag{2.34}$$

where ϕ_c is the conductive heat exchange in cal cm^{-2} day^{-1}.

Ice cover presence reduces conductive heat transfer, necessitating the introduction of a coefficient of estimated value 0.5 [Shen & Chiang 1984]:

$$\phi_c = C_c\ (k_n + 3.9\ V_a)\ (T_s - T_a) \tag{2.35}$$

where C_c is a coefficient which accounts for the reduction in conductive heat transfer due to the presence of an ice cover.

2.4 Ice Equations

River ice cover consists of a floating slab with heat transfer and thickness changes occurring at both the top and bottom surfaces. The top surface exchanges heat with the atmosphere and at the bottom surface heat exchange occurs with the river flow.

The top surface of the floating ice cover is assumed to be well drained, with no surface water present during thawing periods. Water is only present at the bottom surface, to cause ice cover thickening.

Within the ice cover heat transfer is governed by one-dimensional heat conduction. Top surface temperature is determined from meteorological conditions. Bottom surface temperature at the water-ice interface is set to the freezing point temperature. These surface temperatures are shown in Fig. 2.1.

Across the ice cover thickness the asumption of a linear temperature profile is adopted. The temperature profile in the ice cover is given by [Shen & Chiang 1984]:

$$\frac{\partial T_i}{\partial z} = \frac{T_f - T_s}{\theta} \tag{2.36}$$

where T_i is the ice cover internal temperature in °C; z is the distance from the top surface in m and T_f is the freezing point temperature. The freezing point temperature for fresh water is 0°C.

To model the ice cover behaviour the heat exchange processes at both surfaces must be studied. These processes are the heat transfer at the top surface which provides the top surface temperature and top surface melting and the bottom surface heat transfer and bottom surface ice thickness growth or reduction. These heat transfer processes are shown on Fig. 2.1.

Ice cover melting due to a thermal effluent is most influenced by the heat transfer and melting at the bottom surface caused by the increased water temperature.

2.4.1 Top Surface Temperature

Top surface temperature of the ice cover is determined by the heat exchanges occurring at the air-ice interface. A number of these heat exchange processes are dependant on the surface temperature namely, longwave radiation, evapo-condensation flux and conductive heat exchange. The procedure to solve for the surface temperature consists of evaluating each top surface heat exchange process, using the surface temperature of the previous time step for processes which include the surface temperature, and then solving for the new surface temperature. Top surface temperature

is calculated from [Shen & Chiang 1984]:

$$\phi_s (1 - \beta_i e^{-\tau_i \theta}) - \phi_b - \phi_e - \phi_c + K_i \frac{T_f - T_s}{\theta} = 0 \qquad (2.37)$$

where K_i is the thermal conductivity of ice. The thermal conductivity of ice is 0.53 cal m^{-1} s^{-1} $°C^{-1}$ [Shen & Chiang 1984].

2.4.2 Top Surface Ice Melting

When the top surface temperature calculation is performed the surface temperature may exceed 0°C, the melting pont of ice. For this situation the top surface temperature is set to 0°C and the top surface melting is calculated from [Shen & Chiang 1984]:

$$\phi_s (1 - \beta_i e^{-\tau_i \theta}) - \phi_b - \phi_e - \phi_c + K_i \frac{T_f - T_s}{\theta} = - \rho_i L_i \frac{\Delta \theta_s}{\Delta t} \qquad (2.38)$$

where ρ_i is the density of ice; L_i is the latent heat of fusion of ice and $\Delta\theta_s$ is the change in the ice thickness at the upper surface during the time step Δt. The density of ice is 920 kg m^{-3} and the heat of fusion of ice is 8.0×10^4 cal kg^{-1} [Shen & Chiang 1984].

2.4.3 Bottom Surface Heat Transfer

Heat transfer from the water to the underside of the ice cover has a significant effect on ice melting caused by a thermal effluent. The turbulent heat transfer from the water to the ice cover is given by [Shen & Chiang 1984]:

$$q_{wi} = h_{wi} (T - T_f) \qquad (2.39)$$

where q_{wi} is the heat transfer from the water to the ice cover in cal m^{-2} s^{-1}. The heat transfer coefficient is determined from considering the ice covered river flow as a closed conduit flow where h_{wi} is found from [Shen & Chiang 1984; Hayes & Ashton 1979]:

$$h_{wi} = C_{wi} \frac{VV^{0.8}}{h^{0.2}} \tag{2.40}$$

where h_{wi} is the heat transfer coefficient water to ice in cal m^{-2} s^{-1} $^{\circ}C^{-1}$ and C_{wi} is the heat transfer constant. The value of C_{wi} is 387.4 cal $s^{-0.2}$ $m^{-2.6}$ $^{\circ}C^{-1}$ [Shen & Chiang 1984]. The resultant velocity is found from:

$$VV = \sqrt{(u^2 + v^2)} \tag{2.41}$$

where VV is the resultant velocity in m s^{-1}.

2.4.4 Bottom Surface Ice Melting

At the bottom surface of the ice cover water is present allowing melting or growth of the ice cover, depending on the ice cover heat exchanges. The ice cover thickness change is determined from [Shen & Chiang 1984]:

$$K_i \frac{T_f - T_s}{\theta} - q_{wi} = \rho_i L_i \frac{\Delta\theta_w}{\Delta t} \tag{2.42}$$

where $\Delta\theta_w$ is the change in the ice thickness at the water interface during the time step

Δt. This equation utilizes the assumption of the linear temperature profile through the ice cover.

2.5 Source Term Calculation

The energy equation contains a source term which represents the heat flux between the water and the surroundings. This source term contains different components depending on whether the river is ice covered or not. Heat exchange components with the water are illustrated in Fig. 2.1. For the case with an ice cover [Shen & Chiang 1984]:

$$\phi = \phi_{sp} - q_{wi} \tag{2.43}$$

and for the case without an ice cover:

$$\phi = \phi_s - \phi_b - \phi_e - \phi_c \tag{2.44}$$

The source term in the energy equation is calculated from:

$$\Phi = \frac{\phi}{C_p h \rho} \tag{2.45}$$

where C_p is the specific heat of water. The specific heat of water is 1000 cal kg^{-1} $°C^{-1}$ [Paily 1974].

CHAPTER 3

NUMERICAL FORMULATION

3.1 Hydrodynamic Equations

Solution of the hydrodynamic equations utilize a modified McCormack finite difference scheme.

3.1.1 Modified McCormack Scheme

The modified McCormack scheme is an explicit, forward time central space scheme. The scheme is a fractional step method involving the division of a finite difference operator into a sequence of simpler steps. The two-dimensional operation is split into a sequence of one-dimensional operations. Each operator is further split into a predictor-corrector sequence. The use of a symmetric sequence allows for second order accuracy in space and time.

A finite difference grid is overlain on the river to discritize the hydrodynamic equations. In this work a fully dense grid is used, with all values defined at each grid point. Fig. 3.1 shows the fully dense grid. Subscripts of i indicate points in the x direction and j subscripts indicate points in the y direction.

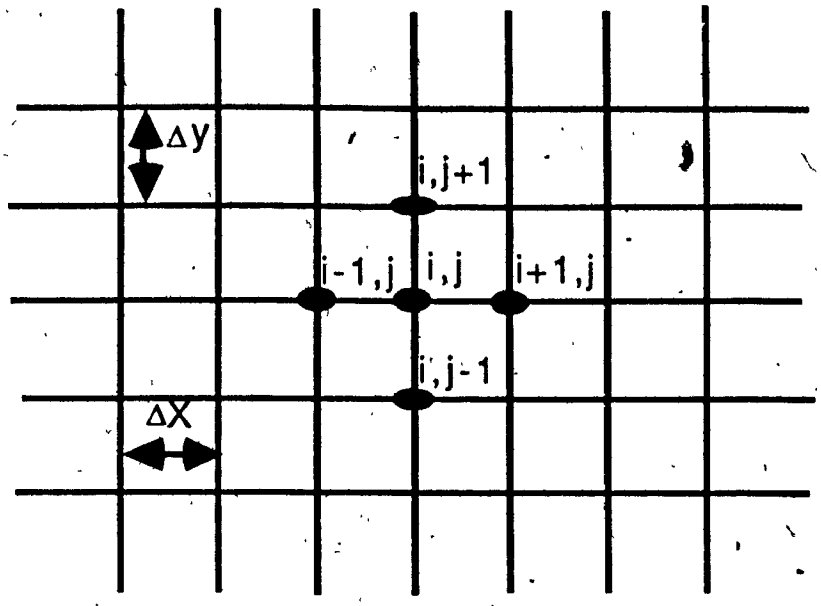

Fig. 3.1 Fully Dense Finite Difference Grid

The usual finite difference notation of a superscript to denote time step is employed. A superscript of n denotes the present time step and n + 1 denotes the next time step [Anderson, Tannehill & Pletcher 1984].

In the McCormack scheme the differentiation is carried out by a series of one dimensional operators. The L_x operator calculates x derivatives and the L_y operator calculates y derivatives. The modified McCormack scheme splits both the x and y derivatives into two time steps, each one half of the original time step. By splitting both x and y derivatives, as opposed to the original scheme where only one direction was split, no preferred alignment in the flow direction of the scheme is necessary. The modified McCormaek scheme uses the series of operators:

$$[Lx \quad Ly \quad L'y \quad L'x] \tag{3.1}$$

where in the operators Lx and Ly, backward differences are used in the predictor step and forward differences are used in the corrector step. In the L'x and L'y operators, forward differences are used in the predictor step and backward differences are used in the corrector step.

3.1.2 Discritization of the Hydrodynamic Equations

In the Lx operator only x derivatives are considered. Backward differences are used for the predictor step. The discritization of the hydrodynamic equations are [Garcia 1983]:

$$h_{i,j}^{n+1/2} = h_{i,j}^{n} - \frac{\Delta t_2}{\Delta x}(U_{i,j}^{n} - U_{i-1,j}^{n}) \tag{3.2}$$

$$U_{i,j}^{n+1/2} = U_{i,j}^{n} - \frac{\Delta t_2}{\Delta x}(F_{i,j}^{n} - F_{i-1,j}^{n}) + g\,\Delta t_2 \left(\frac{h_{i,j}^{n} + h_{i-1,j}^{n}}{2}\right)\left(-\left(\frac{Z_{fi,j} - Z_{fi-1,j}}{\Delta x}\right) - S_{fxi,j}^{n}\right)$$

$$+ \Delta t_2 \left(f V_{i,j}^{n} - \frac{\tau_{sxi,j}^{n}}{\rho}\right) + \varepsilon \frac{\Delta t_2}{\Delta x^2}(U_{i-1,j}^{n} - 2U_{i,j}^{n} + U_{i+1,j}^{n}) \tag{3.3}$$

$$V_{i,j}^{n+1/2} = V_{i,j}^{n} - \frac{\Delta t_2}{\Delta x}(G_{i,j}^{n} - G_{i-1,j}^{n}) + \varepsilon \frac{\Delta t_2}{\Delta x^2}(V_{i-1,j}^{n} - 2V_{i,j}^{n} + V_{i+1,j}^{n}) \tag{3.4}$$

where Δt_2 is one half the time step Δt and Δx is the grid spacing in the x direction.

The Lx corrector step is discritized using forward differences:

$$h_{i,j}^{n+1} = \frac{1}{2}\left[h_{i,j}^{n} + h_{i,j}^{n+1/2} - \frac{\Delta t_2}{\Delta x}(U_{i+1,j}^{n+1/2} - U_{i,j}^{n+1/2})\right] \tag{3.5}$$

$$U_{i,j}^{n+1} = \frac{1}{2}\left[U_{i,j}^{n} + U_{i,j}^{n+1/2} - \frac{\Delta t_2}{\Delta x}\left(F_{i+1,j}^{n+1/2} - F_{i,j}^{n+1/2}\right)\right] + g\Delta t_2 \left(\frac{h_{i+1,j}^{n+1/2} + h_{i,j}^{n+1/2}}{2}\right)$$

$$\left(- \left(\frac{Z_{fi+1,j} - Z_{fi,j}}{\Delta x}\right) - S_{fxi,j}^{n+1/2} \right) + \Delta t_2 \left(f V_{i,j}^{n+1/2} - \frac{\tau_{sxi,j}^{n+1/2}}{\rho}\right) + \varepsilon \frac{\Delta t_2}{\Delta x^2}$$

$$\left(U_{i-1,j}^{n+1/2} - 2 U_{i,j}^{n+1/2} + U_{i+1,j}^{n+1/2} \right)] \qquad (3.6)$$

$$V_{i,j}^{n+1} = \frac{1}{2}\left[V_{i,j}^{n} + V_{i,j}^{n+1/2} - \frac{\Delta t_2}{\Delta x}\left(G_{i+1,j}^{n+1/2} - G_{i,j}^{n+1/2}\right) + \right.$$

$$\left. \varepsilon \frac{\Delta t_2}{\Delta x^2}\left(V_{i-1,j}^{n+1/2} - 2 V_{i,j}^{n+1/2} + V_{i+1,j}^{n+1/2}\right)\right] \qquad (3.7)$$

The L'x, Ly and L'y operators are descritized in a similar manner.

3.1.3 McCormack Stability Criteria

As with any finite difference scheme the question of stability must be addressed. The stability criteria is determined from the Courant-Friedrich-Levy criterion. The maximum time step in the modified McCormack scheme is given by [Baldwin, McCormack & Diewart 1975]:

$$\Delta t \le \left(\frac{2\,\Delta x}{(u + C_{el})_{max}}, \frac{2\,\Delta y}{(v + C_{el})_{max}} \right)_{MIN} \qquad (3.8)$$

where Δy is the grid spacing in the y direction. The celerity C_{el} is defined as:

$$C_{el} = \sqrt{g\,h} \tag{3.9}$$

where C_{el} is the celerity velocity in m s^{-1}.

The modified McCormack scheme allows a time step twice as large as the standard McCormack scheme when equal grid spacings are used in the x and y directions. Therefore the introduction of the extra operator, actually reduces overall computations.

3.2 Energy Equation

A numerical scheme is required to model the temperature distribution in the river flow, for determining the melting of the river ice cover due to a thermal effluent. The scheme must solve the two-dimensional temperature equation including convection and dispersion.

A one-dimensional example will be used to show the difficulties in the development of a numerical scheme for the energy equation [Patankar 1980]:

$$\frac{\partial uT}{\partial x} = \frac{d}{dx}\left(D_x \frac{\partial T}{\partial x}\right) \tag{3.10}$$

from which the following symbols are defined:

$$FF = u \tag{3.11}$$

$$DD = \frac{D_x}{\Delta x} \tag{3.12}$$

where both terms have the same dimension. The FF term indicates the strength of convection and the DD term indicates the dispersion conductance. The value of DD

always remains positive but FF may be positive or negative. The central difference in space discritization equation may be written using the new terms:

$$A_i T_i = A_{i+1} T_{i+1} + A_{i-1} T_{i-1} \tag{3.13}$$

where:

$$A_{i+1} = DD_{i+1} - \frac{FF_{i+1}}{2} \tag{3.14}$$

$$A_{i-1} = DD_{i-1} + \frac{FF_{i-1}}{2} \tag{3.15}$$

$$A_i = DD_{i+1} + \frac{FF_{i+1}}{2} + DD_{i-1} - \frac{FF_{i-1}}{2} \tag{3.16}$$

$$A_i = A_{i+1} + A_{i-1} + (FF_{i+1} - FF_{i-1}) \tag{3.17}$$

If an example is taken where:

$DD_{i+1} = DD_{i-1} = 1$ and $FF_{i+1} = FF_{i-1} = 4$

solving the one-dimensional equation using

$T_{i+1} = 200$ and $T_{i-1} = 100$ the result is $T_i = 50$

and using

$T_{i+1} = 100$ and $T_{i-1} = 200$ the result is $T_i = 250$.

The unrealistic results obtained are caused by negative coefficients for A_{i-1} or A_{i+1} depending on the sign of FF. When the value of $|FF|$ exceeds 2DD this is possible. The ratio is known as the Peclet number:

$$P = \frac{u\Delta x}{D} \tag{3.18}$$

where P is the dimensionless Peclet number. In cases where convection dominates, that is, the Peclet number is greater than 2, central difference schemes do not give usable results.

The modified McCormack finite difference scheme is actually a central difference scheme due to the use of forward and backward differences. Use of this scheme for the river water temperature distribution gave temperature values outside of the range of the neighbouring points. An increase in the dispersion coefficient in regions of large temperature gradients eliminated this problem However, excessive dispersion occurred, especially in the upstream direction.

The introduction of Leonard's quadratic upstream interpoleration is a possible scheme for river temperature distribution modelling [Leonard 1979b]. This scheme uses an upstream weighted normal curvature term to calculate the wall temperature of each finite difference cell.

Use of the normal curvature term however causes behaviour similar to that of the modified McCormack scheme, including when extra dispersion is employed.

The use of an upwinding scheme was adopted to overcome these difficulties.

3.2.1 Upwinding Scheme

The use of the upwinding scheme may be illustrated by the tanks shown in Fig. 3.2, which represent finite difference cells. Fluid flow from one stirred tank to another through short tubes represents convection. Heat transfer through the tank walls represents dispersion. Fluid flowing from one tank to the next is at the temperature of the previous tank and unaffected by the fluid in the tank it is entering or the next

upstream tank. This represents the essence of the upwind scheme. The dispersion term heat flow occurs between the tank and the two adjacent tanks. The use of a central difference scheme is therefore appropriate for the dispersion term [Patankar 1980].

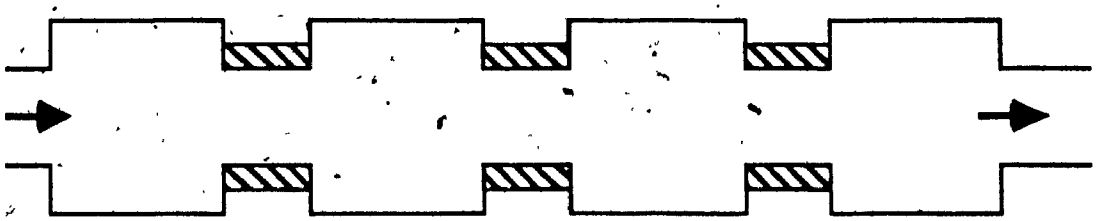

Fig. 3.2 Tank Model

Use of an upwinding scheme is correct according to Raithby [Raithby 1976] when steady or near steady convection is dominate in the development of the temperature field and either the flow is closely aligned with the grid lines or no strong cross flow gradients are present. If flow moves along the grid lines the Peclet number should be of the order of 10 or larger. In the case of river temperature distribution, flow is often oriented along grid lines with large Peclet numbers. The flow velocity varies little and no strong cross flow gradients exist, such as shock waves. The use of an upwinding scheme is therefore justified in this work.

3.2.2 Discritization of the Energy Equation

The upwind scheme is an explicit forward time method. This scheme takes into account the direction of the convecting velocity. The development of the convecting term discritization is shown, using Fig. 3.3 as a reference [Roache 1976].

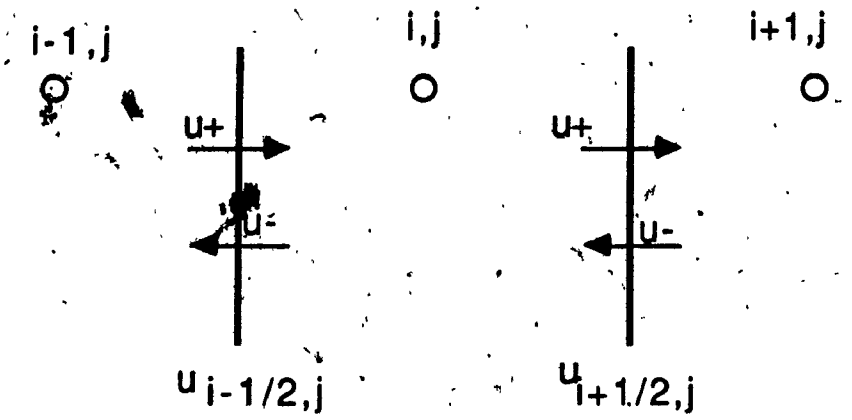

Fig. 3.3 Convecting Velocity Directions

$$U_{i-(1/2),j} = \frac{U_{i-1,j} + U_{i,j}}{2} \tag{3.19}$$

$$U_{i+(1/2),j} = \frac{U_{i,j} + U_{i+1,j}}{2} \tag{3.20}$$

$$\frac{\partial UT}{\partial x} = \frac{U_{i+(1/2),j}\,T_{i,j} - U_{i-(1/2),j}\,T_{i-1,j}}{\Delta x} \quad U_{i-(1/2),j} \text{ and } U_{i+(1/2),j} > 0 \tag{3.21}$$

$$\frac{\partial UT}{\partial x} = \frac{U_{i+(1/2),j}\,T_{i+1,j} - U_{i-(1/2),j}\,T_{i,j}}{\Delta x} \quad U_{i-(1/2),j} \text{ and } U_{i+(1/2),j} < 0 \tag{3.22}$$

In the case of velocity reversal or converging velocities within a cell, a combination of the formulas is used. A similar derivation is employed for derivatives in the y direction.

The time term of energy equation is evaluated using forward differences. A central difference formulation is used for the dispersion term employing the cell wall water

depth and dispersion coefficient. The discritization of the two-dimensional energy equation is given by equation (3.23).

$$h_{i,j}^{n+1} T_{i,j}^{n+1} = T_{i,j}^{n} h_{i,j}^{n+1} - \Delta t \left(\frac{\partial UT}{\partial x} + \frac{\partial VT}{\partial y} \right) +$$

$$\frac{\Delta t}{\Delta x^2} \left(D_{x\, i+(1/2),j}^{n+1} h_{i+(1/2),j}^{n+1} (T_{i+1,j}^{n} - T_{i,j}^{n}) - D_{x\, i-(1/2),j}^{n+1} h_{i-(1/2),j}^{n+1} (T_{i,j}^{n} - T_{i-1,j}^{n}) \right) +$$

$$\frac{\Delta t}{\Delta y^2} \left(D_{y\, i,j+(1/2)}^{n+1} h_{i,j+(1/2)}^{n+1} (T_{i,j+1}^{n} - T_{i,j}^{n}) - D_{y\, i,j-(1/2)}^{n+1} h_{i,j-(1/2)}^{n+1} (T_{i,j}^{n} - T_{i,j-1}^{n}) \right) +$$

$$\Delta t \, (h_{i,j}^{n+1} \Phi_{i,j}^{n+1}) \qquad (3.23)$$

where the convection terms are calculated using the appropriate upwinding formula and the cell wall water depth is calculated in a similar manner to the wall velocities.

The energy equation is solved using a one step approach for x and y derivatives to allow conservation of temperature at river boundaries.

3.2.3 Cell Wall Dispersion Coefficients

The cell wall dispersion coefficient is determined by use of the harmonic mean of the adjacent cell values [Patankar 1980].

$$D_{x\, i-(1/2),j} = \frac{2 D_{x\, i-1,j} D_{x\, i,j}}{D_{x\, i-1,j} + D_{x\, i,j}} \qquad (3.24)$$

$$D_{x\, i+(1/2),j} = \frac{2 D_{x\, i+1,j} D_{x\, i,j}}{D_{x\, i+1,j} + D_{x\, i,j}} \qquad (3.25)$$

Similar formulas are used in the y direction.

The use of the harmonic mean as opposed to the simple arithmetic mean yields more realistic results. If one cell has a dispersion coefficient of zero, the harmonic mean sets the wall dispersion coefficient to zero, as opposed to the arithmetic mean which would give an average wall dispersion coefficient, not zero heat flux. In a second case where one cell dispersion coefficient has a much higher value than the neighbouring cell, the heat transfer is controlled by the cell with low dispersion. The arithmetic mean would use an average of the cell walls as the controlling dispersion value.

3.2.4 Upwinding Stability Criterion

The stability requirement of the two-dimensional upwinding scheme is given by:

$$\Delta t \leq \frac{1}{2(D_x,D_y)_{max}\left(\frac{1}{\Delta x^2}+\frac{1}{\Delta y^2}\right)+\frac{|u|}{\Delta x}+\frac{|v|}{\Delta y}} \qquad (3.26)$$

3.3 Boundary Conditions

Solution of the equations governing the melting of river ice by thermal effluent, requires a complete and appropriate set of boundary conditions for each boundary type and equation.

Open boundaries are locations where flow may enter or leave the computational zone. The required boundary conditions for the hydrodynamic equations are dependent on the flow regime and are summarized in Table 3.1. In the case of subcritical flow which is most frequently encountered on natural rivers, the inflow velocity in the longitudinal and transverse direction is specified from the river flow quantity and river

geometry. At the outflow boundary, the water depth is imposed with particular care being taken to account for the increase or decrease in water depth at points on the outflow cross section, due to ice thickness changes.

Table 3.1 Required Boundary Conditions at Open Boundaries [after Garcia 1983]

	SUBCRITICAL FLOW		SUPERCRITICAL FLOW	
	INFLOW B.C.'S	OUTFLOW B.C.'S	INFLOW B.C.'S	OUTFLOW B.C.'S
2 - D PROBLEMS	2	1	3	0

At inflow boundaries the energy equation requires specification of the water temperature. The outflow boundary condition is $(\partial T)/(\partial x) = 0$ for boundaries in the longitudinal direction and $(\partial T)/(\partial y) = 0$ for boundaries in the transverse direction.

Closed boundaries are locations where solid walls, such as the river banks, limit the flow field. This requires that the velocity perpendicular to the wall be zero at all times. For the case when ϵ is not zero, non slip boundary conditions are required. This is accomplished by the specification of fictitious points outside the computational region. As seen in Fig. 3.4 the boundary occurs at the cell face. At the fictitious points the velocity components are set equal to the magnitude of the inside point, but opposite in sign.

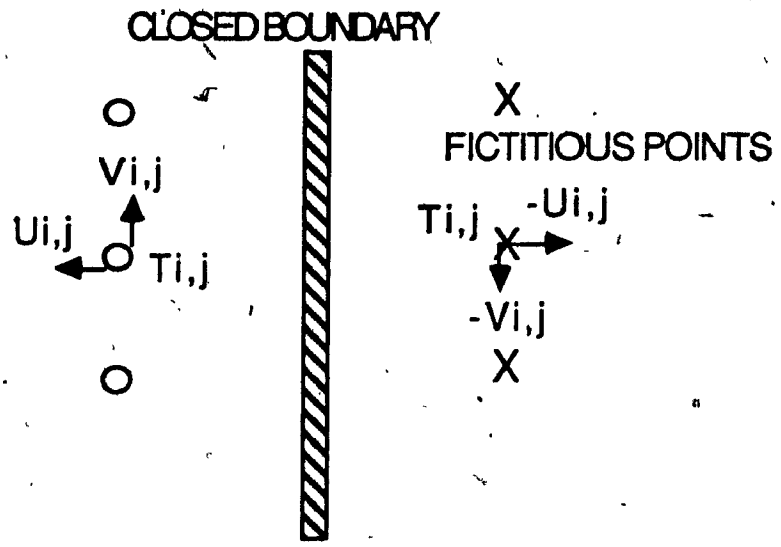

Fig. 3.4 Boundary Conditions at Closed Boundaries

The energy equation boundary condition for temperature, is the requirement of setting the temperature at the inside and the temperature of the fictitious point to be equal. The heat flux at the river shore becomes zero. This originates from no convection at the boundary, due to zero wall velocity and no dispersion at the boundary due to zero temperature gradient across the boundary.

3.4 Initial Conditions

To begin modelling a solution to river ice melting by a thermal effluent, a complete set of initial conditions is required.

The water velocity components are initially set to zero everywhere on the computational domain. The inflow velocities are increased over a short time period to their steady state values. The movement of the flow downstream occurs at the flow

celerity velocity. The water depth at all points is initially specified to the outflow boundary water depth or level pool depth.

Temperature at all points in the computational domain is set to the inflow temperature.

Ice thickness is set to the average prevailing thickness present over the river reach for all computational points.

CHAPTER 4
MODEL APPLICATIONS AND DISCUSSIONS

Two sets of tests have been performed using the model for the melting of river ice cover due to a thermal effluent. A series of results is presented to show the variation in ice cover melting caused by varying effluent discharge temperatures, air temperatures, flow velocities, dispersion constants, channel geometrics and turbulent viscosity coefficients. A comparison is also carried out with a set of field data.

4.1 Model Tests

The model in this work has been used for a number of parameter combinations, to illustrate the behaviour of the river ice cover near the source of a thermal effluent.

A simple river geometry has been chosen for these tests as is shown in Fig. 4.1. The river has a flat bed and an outflow depth of 3 m. Transverse width of the river is 750 m. The flow enters the river at the left boundary and flows to the right. The entrance velocity is 0.2 m s^{-1} in the longitudinal direction only. Manning's roughness coefficient for the river bed is 0.030 and 0.020 for the ice cover underside. The coefficient of turbulent viscosity is 0.25 m^2s^{-1}. A value of 10.0 is used for the dispersion constants. Thermal effluent enters the river flow at the shore on the lower side of the figure with a flow rate of 4.5 m^3s^{-1}. Initial ice thickness is set to 0.10 m. The prevalent meteorological conditions are summarized in Table 4.1.

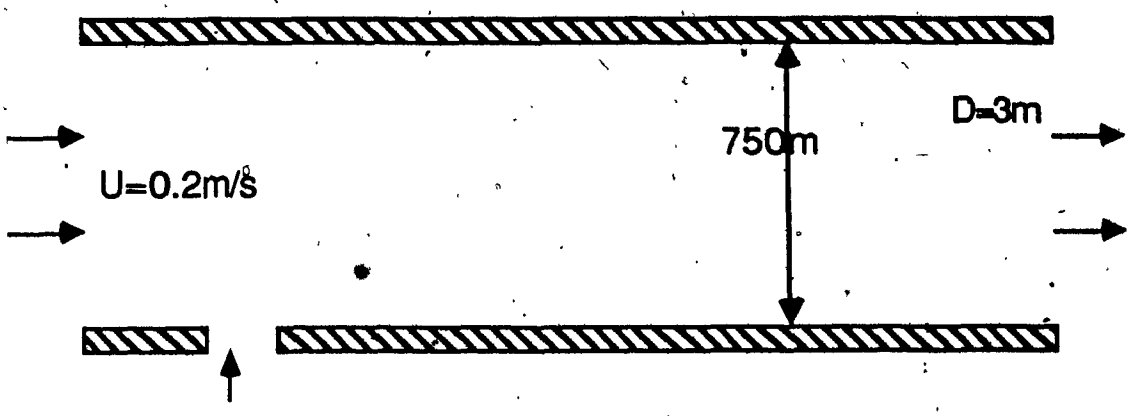

Fig. 4.1. Test River Geometry

Table 4.1. Meteorological Conditions

Parameter	Value & Unit
Cloud Cover	5 tenths
Latitude	45°
Month	February
Wind Velocity	20 km hr^{-1}
Relative Humidity	60%

The set of figures and the table which follow give the results obtained in the tests. The effluent temperature and air temperature is indicated on each figure. The series of figures from Fig. 4.3 to Fig. 4.8 illustrates the ice cover thickness distribution on the river. A contour interval of 0.025 m is employed on all the figures. The transverse scale is exaggerated to better show the melting of the ice cover. Table 4.2 summarizes the

lengths of the downstream ice free reaches.

Results were obtained by first using the hydrodynamic equations to establish the steady state flow field of the river. Thermal effluent was then introduced. Continued use of the hydrodynamic equations allowed variation in the flow pattern of the river, due to changes in ice thickness, to be considered. A grid spacing of 500 m is used in the x direction and a grid spacing of 50 m is used in the y direction, with a time step of 15.0 s.

4.1.1 Discussion of the Model Tests

Fig. 4.9 shows the transverse ice thickness at two sections, for an air temperature of -20° C and an effluent temperature of 10°C. The hydrodynamic results indicated an increase in the flow depth of the river, in regions of ice melting, as shown on Fig. 4.10 which is for the same test and sections as the previous figure. This increase in flow depth was equal to 90% of the decrease in the ice cover thickness. Fig. 4.11 and Fig. 4.12 shows a similar behaviour in the longitudinal direction at the shore of the effluent discharge. At the discharge location the ice cover thickness is reduced by 0.24 m and the water depth increases 0.22 m. Testing with an ice cover present caused an increase in the friction slope of 80 to 90% in the longitudinal direction, compared to when no ice cover is present on the river. Field studies show rivers have a higher stage when ice covered, due to the increased flow resistance [Burrel & Davar 1982]. An increase in flow velocity also occurred in regions of ice cover suppression. The transverse velocity profile at two sections is shown on Fig. 4.13. Near the shores some reduction in velocity occurs, but the ice cover melting causes an increase in the flow velocity of 25% as compared to the other shore, at the discharge cross section where the water is ice free. The mid-reach section where ice thickness is reduced, shows a 5% velocity increase between shores. A check of inflow and outflow quantities shows an agreement within 2% of the flow quantity.

Tests have been done using different values for the turbulent viscosity coefficient in the hydrodynamic equations. As seen on Fig. 4.14 a doubling of this value caused only a slight effect on the ice cover thickness, for the -20°C air temperature and 10°C effluent temperature case. The ice cover thickness was increased by 3 to 4 mm. The use of a zero turbulent viscosity coefficient and slip boundary conditions also has little effect on ice thickness as illustrated on Fig. 4.15, with only a 2 mm change. Symmetry has been checked by introducing the effluent at both shores of the river and having the main flow direction oriented along the y axis. The results of these tests for longitudinal ice thickness is illustrated on Fig. 4.16. As seen on the figure the model produces symmetrical results within 1 cm of ice cover thickness at all points, with exact agreement in the x direction.

As expected, ice cover melting increased with an increase in air temperature and effluent temperature. The contour line figures illustrate well the long downstream ice free reaches which occur due to a thermal effluent discharge. The ice melting occurs predominately downstream, near the shore, on the side of the effluent discharge. A slight reduction in ice thickness occurs upstream of the point of discharge over a distance of 500 m. In the transverse direction the ice cover quickly thickens to the undisturbed thickness over a distance of about 150 m, as one moves across the river from the effluent source. An increasing effluent temperature or air temperature results in a wider opening in the ice cover. The ice cover thickens much more slowly in the longitudinal direction over a distance of 10 km, downstream of the ice free reach. This is caused by a lower temperature gradient than in the transverse direction. These results are in agreement with what Ashton observed during the field study [Ashton 1980; Ashton 1981]. In the case of low air temperature and a low effluent discharge temperature no ice free region occurs, only a reduction in thickness, as shown on Fig. 4.8..

The ice cover thickness in areas unaffected by the thermal effluent was influenced

by a change in air temperature. As expected a lower air temperature produced a greater ice cover thickness.

A comparison has been carried out with an analytical solution for the length of the downstream ice free reach using a water depth of 3.2 m, a flow velocity of 0.23 ms^{-1} and mixing the effluent over a width of 100 m [Al-Saleh, Sarraf & Kahawita 1987]. This comparison is shown in Table 4.2 and on Fig. 4.2. The analytical solution used a linear heat transfer relation between the water and air, dependant on air temperature. The 0°C isotherm was used as the location of the end of the downstream ice free reach. The lengths of the downstream ice free reaches predicted by the numerical model, are shorter due to the complete ice cover heat transfer relation used in this model. This model does not employ the 0°C isotherm criteria, but rather the heat transfer to the underside of the ice cover. This permits ice cover to exist on water above 0°C. The ice cover edge therefore occurs upstream of the 0°C isotherm with the location depending on the heat transfer within the ice cover, from the top surface and the underside heat transfer.

A series of tests have also been performed to verify the behaviour of the temperature equation calculation. Fig. 4.17 shows the temperature profile at the entrance to the channel cross section which was used in the tests. The tests were performed at a Peclet number of 100 and a Peclet number of infinity or the zero diffusion case. The theoretical comparison from Leonard [Leonard 1979a] is included on the figure. On Fig. 4.18 and Fig. 4.19 a similar comparison is carried out for the mid-reach and exit cross sections of the channel. In the infinite Peclet number case perfect agreement exists at all sections and a close comparison exists in the other case. There is perfect symmetry of the temperature plume about the central axis. It is also found that temperature is conserved within 0.33%, between the inflow and outflow boundaries.

Tests have also been performed using a different river geometry with an irregular boundary as seen on Fig. 4.22. In this river geometry the width has been changed to 500 m and the effluent is introduced with a mixed temperature of 1.50 °C over a width of 100m from the shore. The other parameters are unchanged including the grid spacing, but the time step is decreased to 10.0 s at the velocities of 0.4 and 0.6 ms^{-1}. Three velocity values of 0.2, 0.4 and 0.6 ms^{-1} are used. The development of the velocity field is shown on Fig. 4.20 for the water depth and Fig. 4.21 for the velocity profile at the mid-reach sections, for a velocity of 0.2 ms^{-1}. The velocity field develops a near steady state with no oscillations and an uniform friction slope over the channel length of 0.0021%. The figures are for the time before ice melting begins to occur. The velocity fields for the three test velocities are shown on Fig. 4.22, Fig. 4.23 and Fig. 4.24. The velocity increases downstream due to the reduced water depth. This velocity increase on Fig. 4.19 is 14%.

Temperature contour lines at the three test velocities are given on Fig. 4.25, Fig. 4.26 and Fig. 4.27. As expected an increase in velocity caused an increased movement of the heated water downstream. The development of the temperature distribution at three cross sections for a velocity of 0.4 m/s is shown on Fig. 4.28, Fig. 4.29 and Fig. 4.30. The temperature profile is most quickly established near the effluent source, within 4 hours, and more slowly at downstream sections, within 32 hours. Especially at sections downstream of the ice free reach, a slight decrease in water temperature of 0.01° C occurs, due to increased heat transfer to the atmosphere at open water reaches. At the effluent source cross section, away from the shore, the water temperature decreases up to 0.1° C due to movement of the heated water to the increased flow velocity region in the ice free reach. Fig. 4.31 shows the temperature profile at several sections at a velocity of 0.2 ms^{-1}.

The increase is stream velocity caused an increase in the length of the downstream ice free reach as shown on Fig. 4.32. A linear relationship was found to exist between the length of the ice free reach and the velocity, as was used in previous analytical models [Al-Saleh, Sarraf & Kahawita 1987]. Fig. 4.33, Fig. 4.34 and Fig. 4.35 show the ice thickness profiles at various cross sections at the three velocities. The higher velocities caused a decrease in ice thickness at all downstream sections. The largest changes occurred near the shore of the effluent discharge.

Tests have been performed using different values for the dispersion constant. Fig. 4.36 shows the temperature distribution at a dispersion constant of 20.0 and Fig. 4.37 shows the zero dispersion test. Only small differences exist in the width and length of the increased temperature region. The ice thickness profiles are shown for two cross sections at various dispersion constants on Fig. 4.38 and Fig. 4.39. A slight reduction in ice thickness of up to 1.0 cm occurs away from the shore of the effluent source and a slight increase in ice thickness of up to 1.0 cm at this shore in the main flow location, as the dispersion constant was increased from 0 to 20.

The dispersion coefficient and velocity profiles at two sections are compared for a dispersion constant of 10.0 on Fig. 4.40 and Fig. 4.41. An increase in velocity of 15% and a large increase of 100% in the dispersion coefficient is seen in ice free regions in the figures. A doubling in dispersion is expected in ice free regions as well as a direct link between velocity and dispersion.

Changing the grid spacing had no effect within the grid increment, on the length of the ice free reach as is shown on Fig. 4.42 for the 0.6 ms^{-1} case.

Table 4.2 Downstream Ice Free Reaches

Air Temperature °C	Effluent Temperature °C	Downstream Ice Free Reach km	
		Model	Analytical Solution
- 5	20	16.0	17.9
- 5	10	9.5	11.8
- 5	5	1.5	2.7
- 20	20	8.0	8.2
- 20	10	1.0	2.7
- 20	5	0.0	0.9

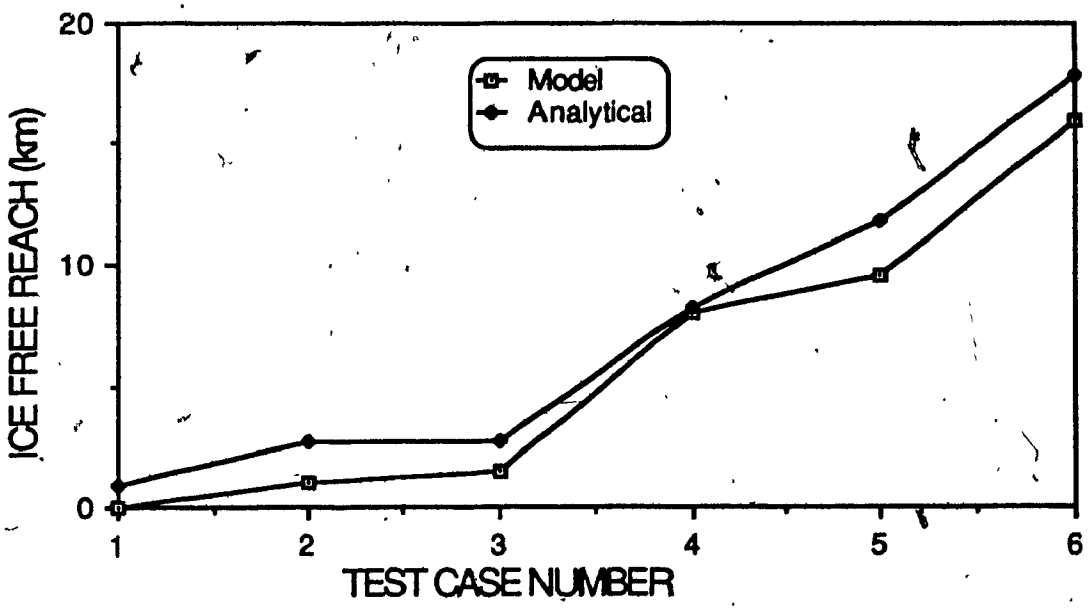

Fig. 4.2 Comparison of Model Results

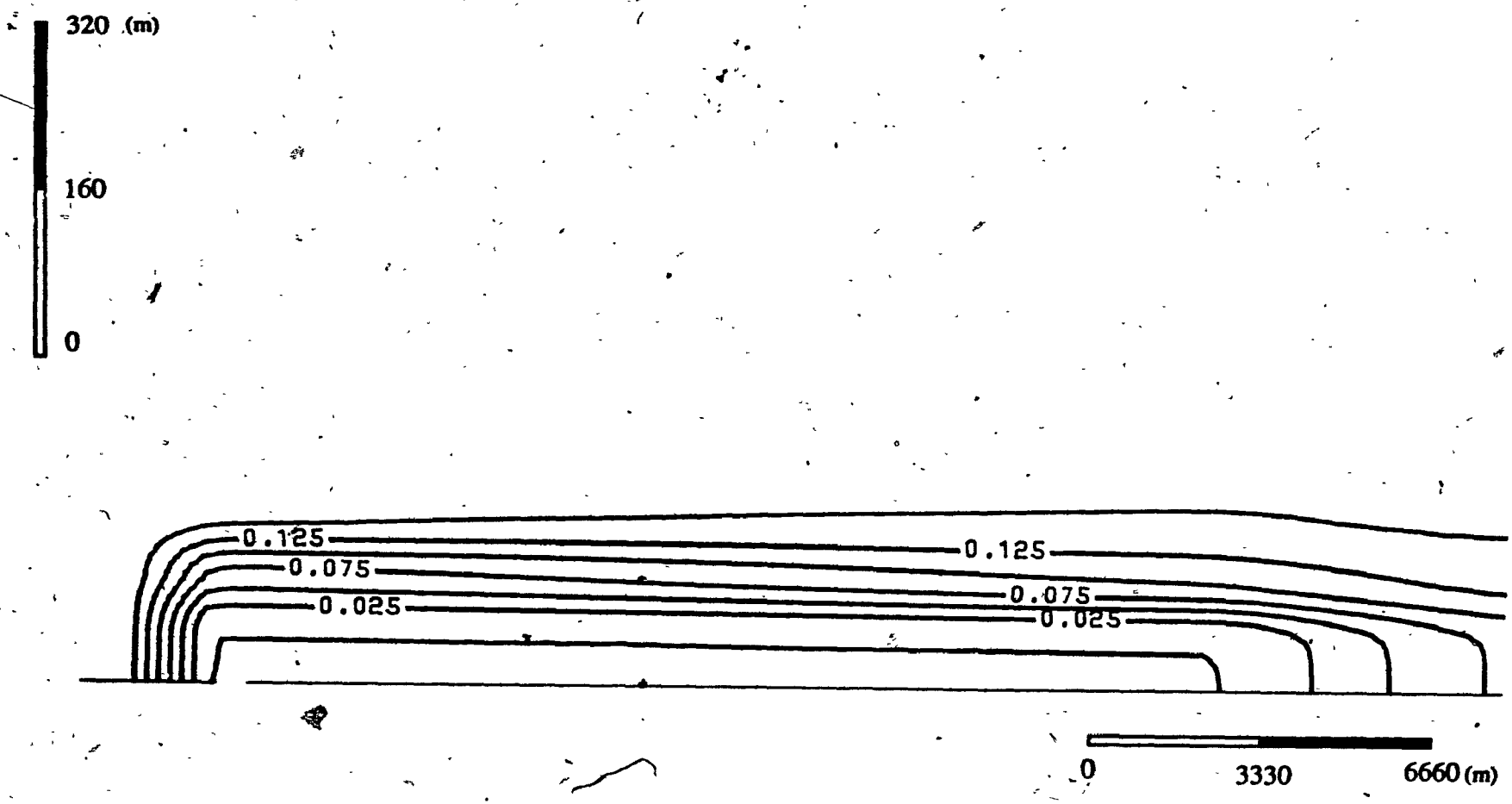

Fig.4.3 Ice Thickness Distribution at an Air Temperature of-5°C and an Effluent Temperature of 20°C

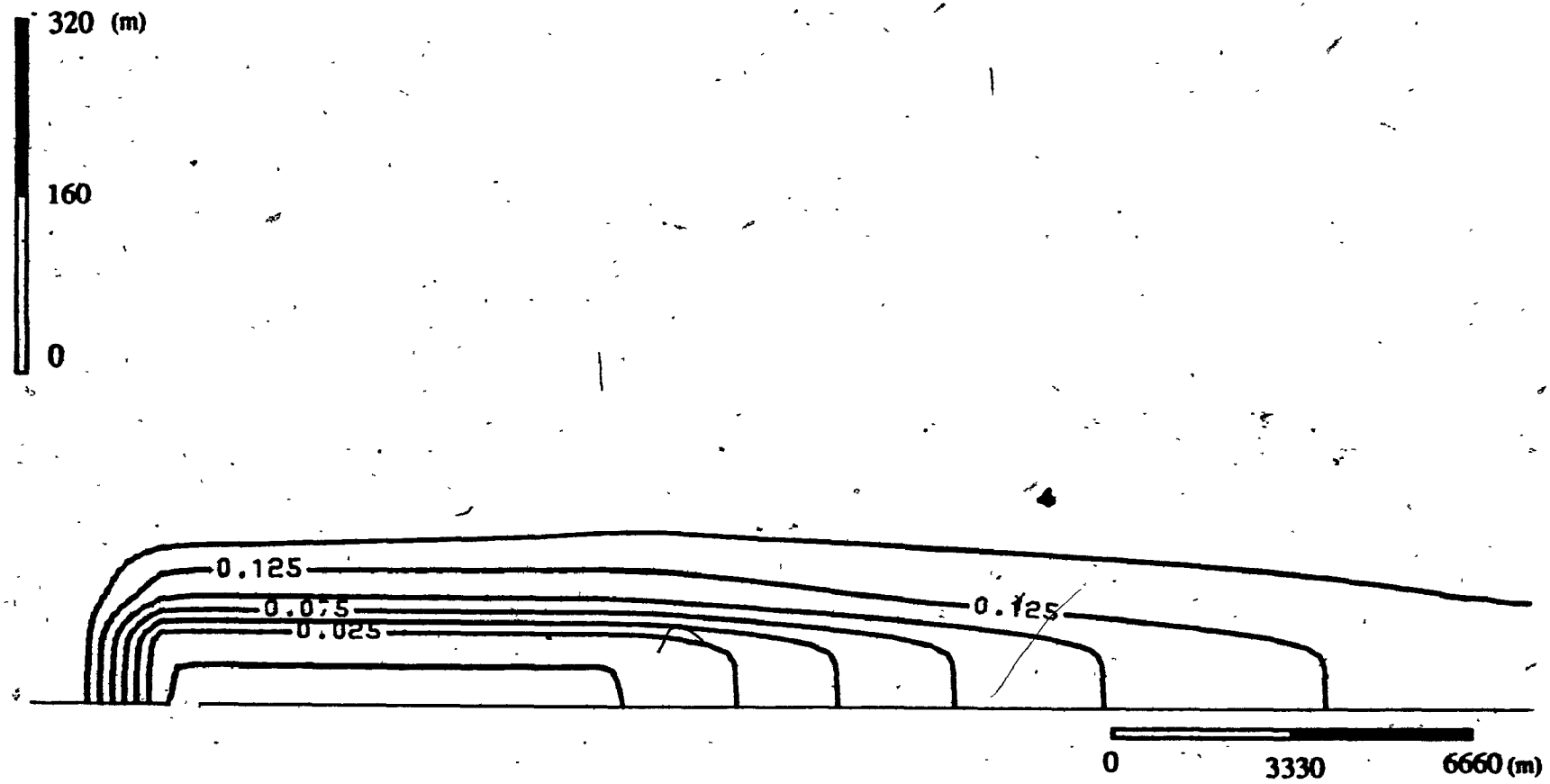

Fig.4.4 Ice Thickness Distribution at an Air Temperature of-5°C and an Effluent Temperature of 10°C

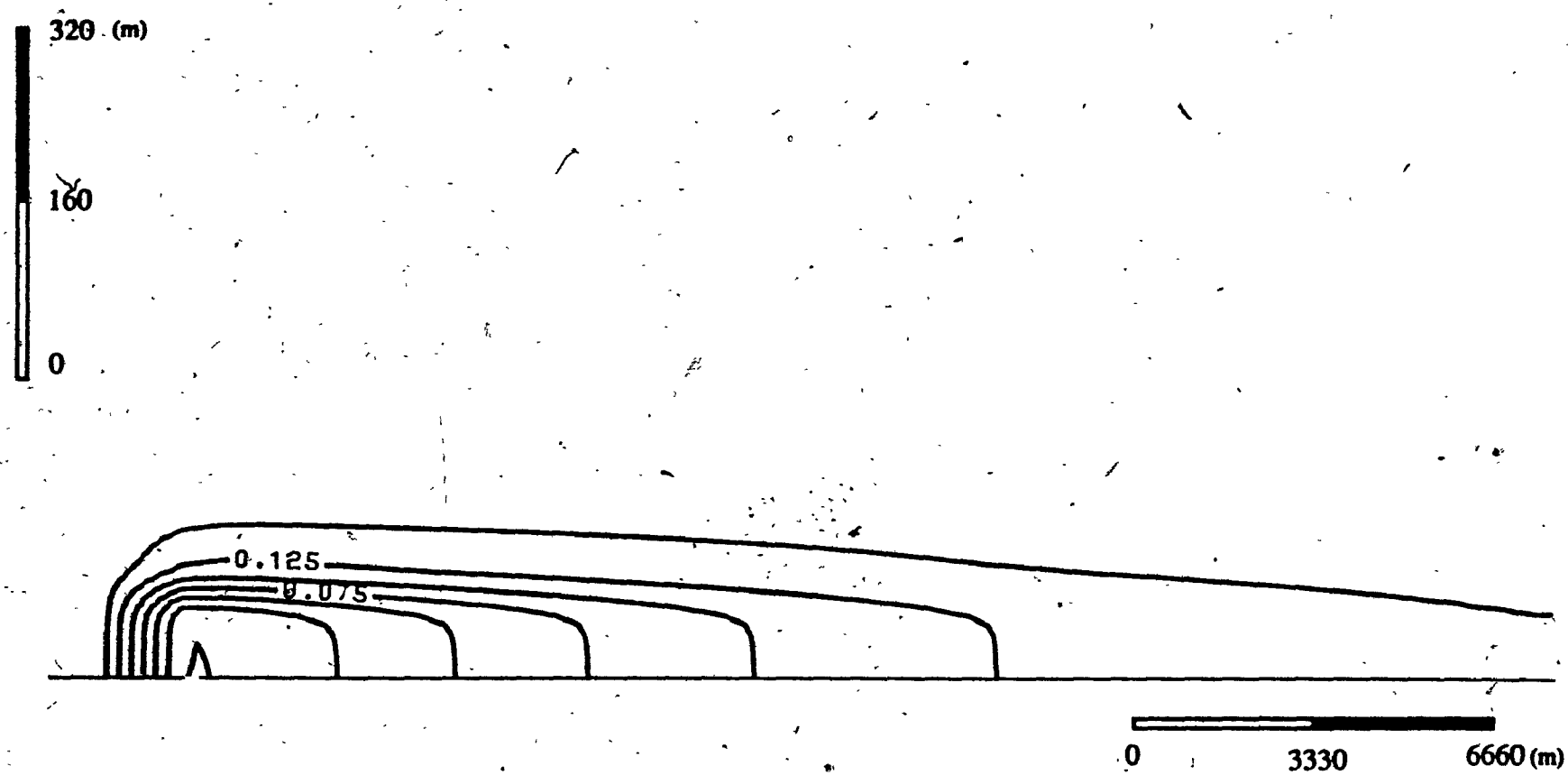

Fig.4.5 Ice Thickness Distribution at an Air Temperature of -5°C and an Effluent Temperature of 5°C

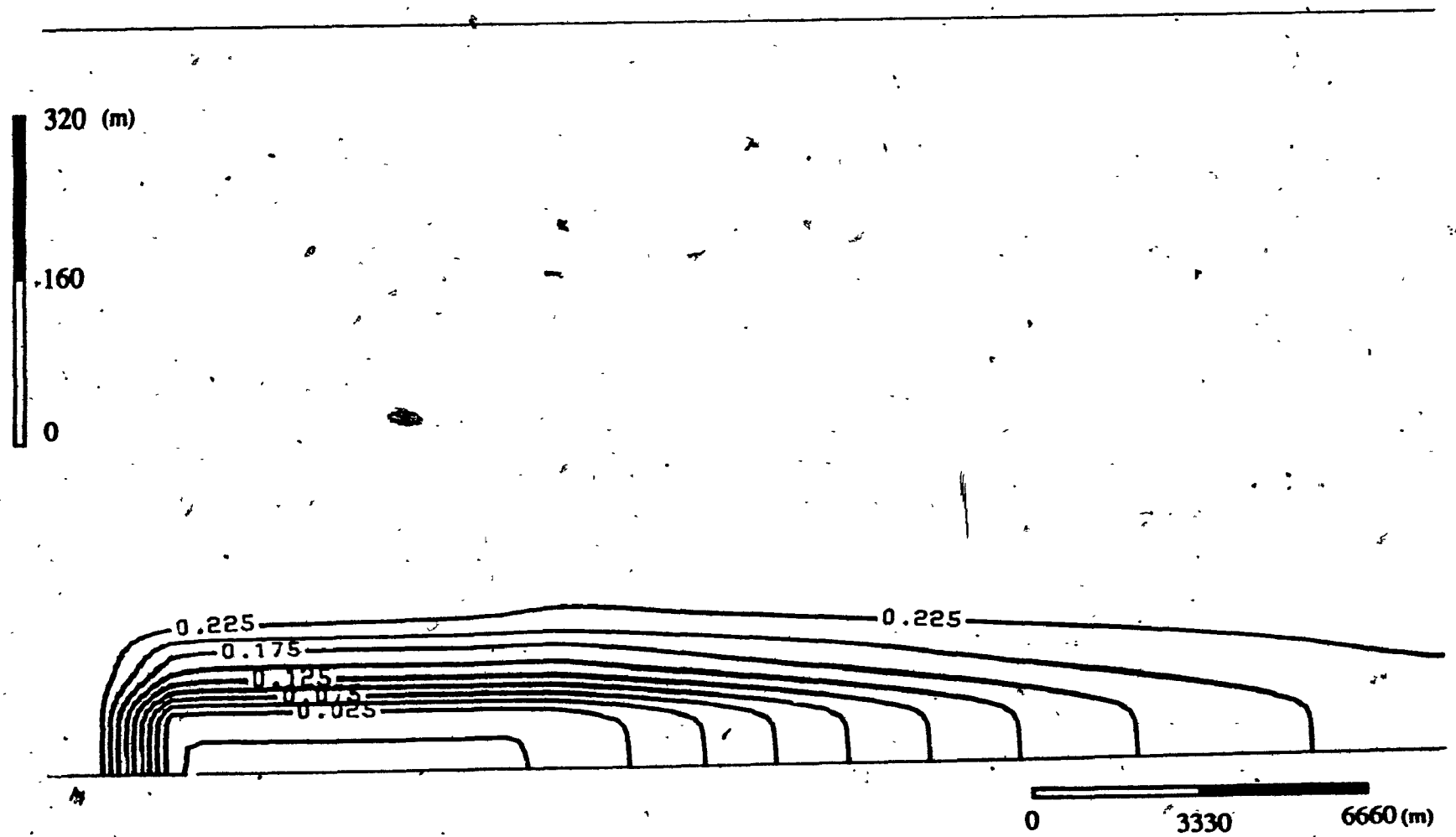

Fig.4. 6 Ice Thickness Distribution at an Air Temperature of-20°C and an Effluent Temperature of 20°C

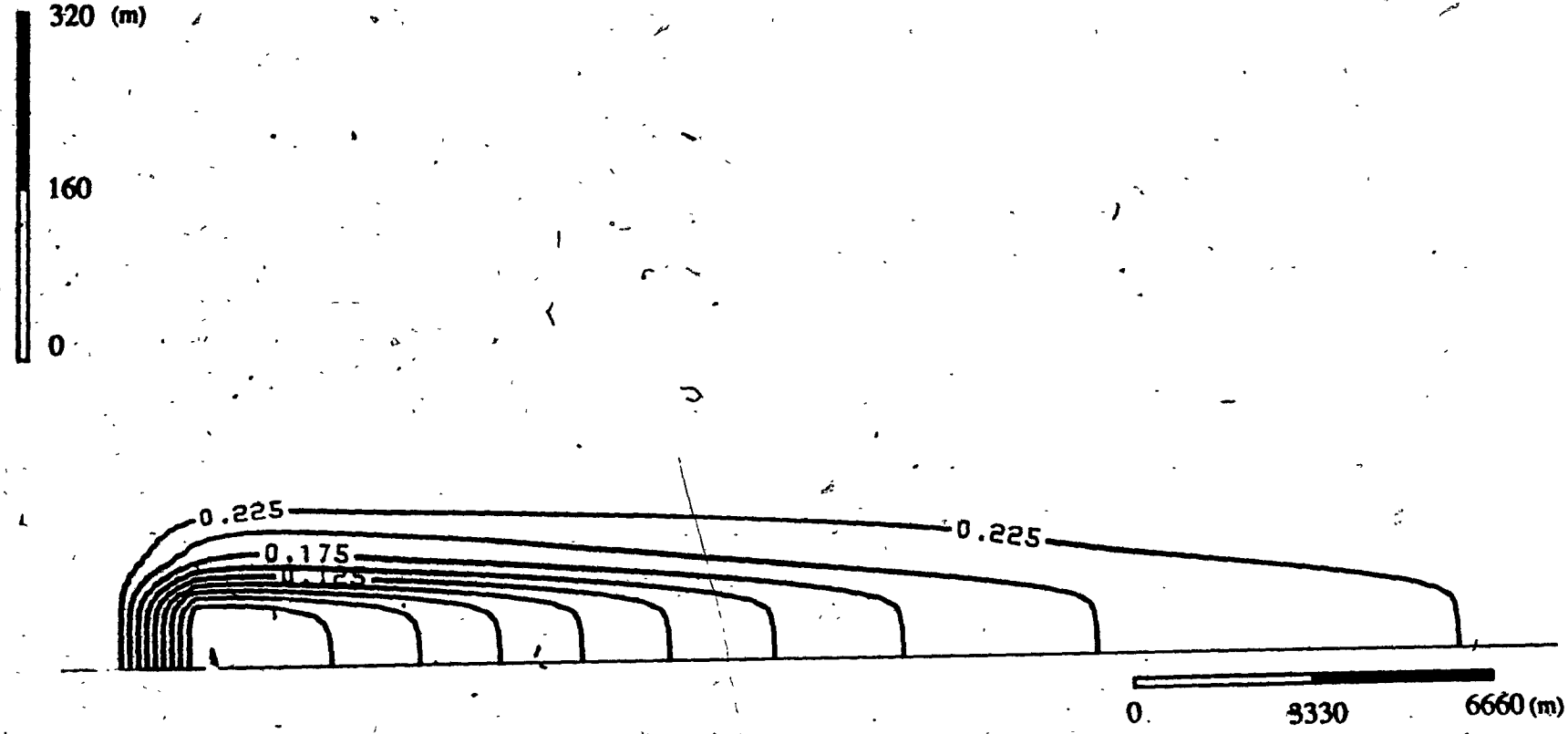

Fig.4. 7 Ice Thickness Distribution at an Air Temperature of-20°C and an Effluent Temperature of 10°C

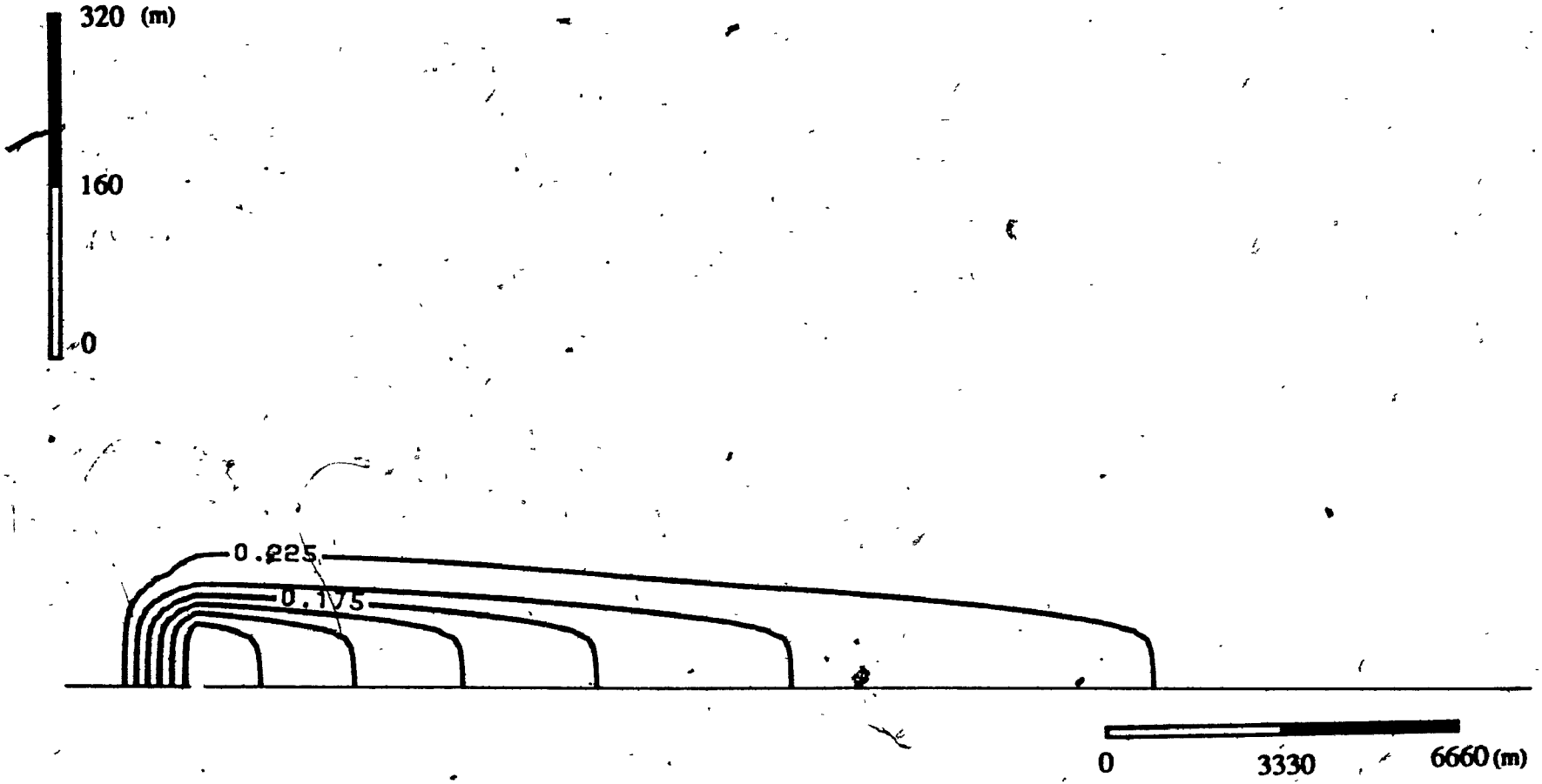

Fig.4. 8 Ice Thickness Distribution at an Air Temperature of-20°C and an Effluent Temperature of 5°C

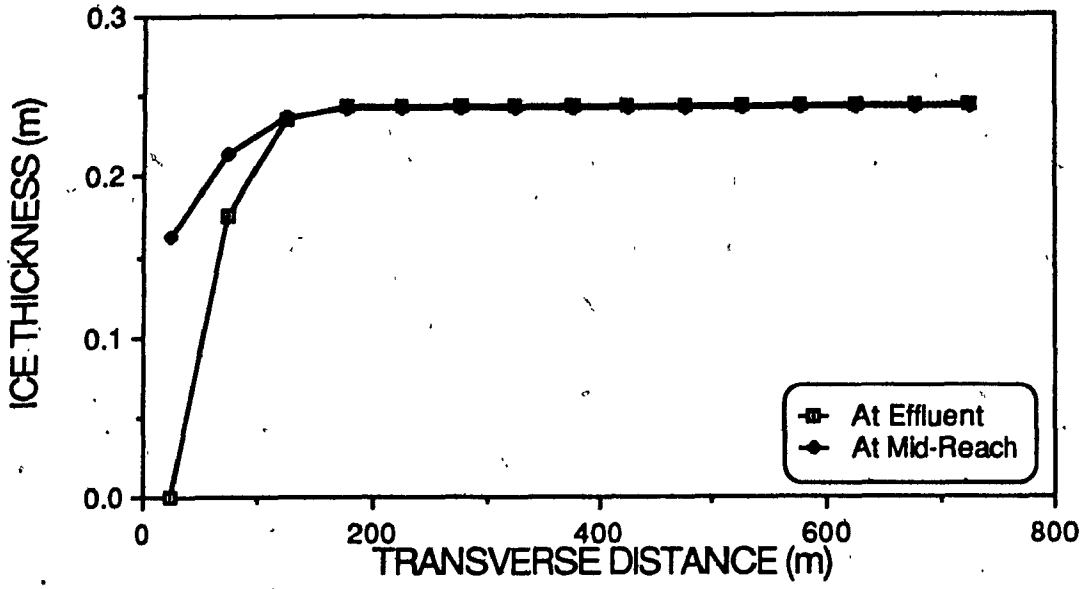

Fig. 4.9 Transverse Ice Thickness Variations

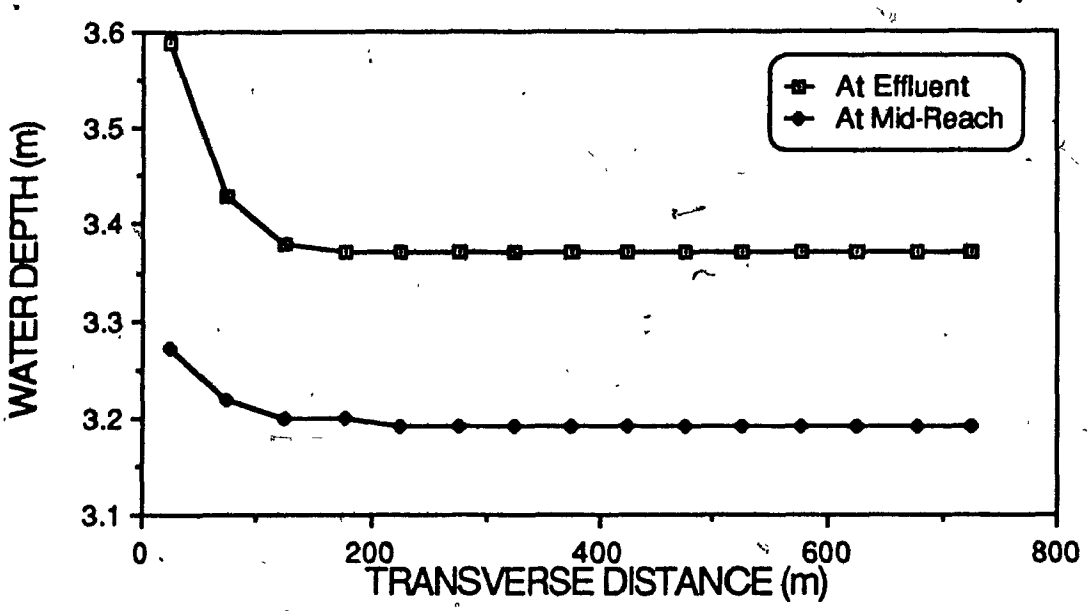

Fig. 4.10 Transverse Water Depth Profiles

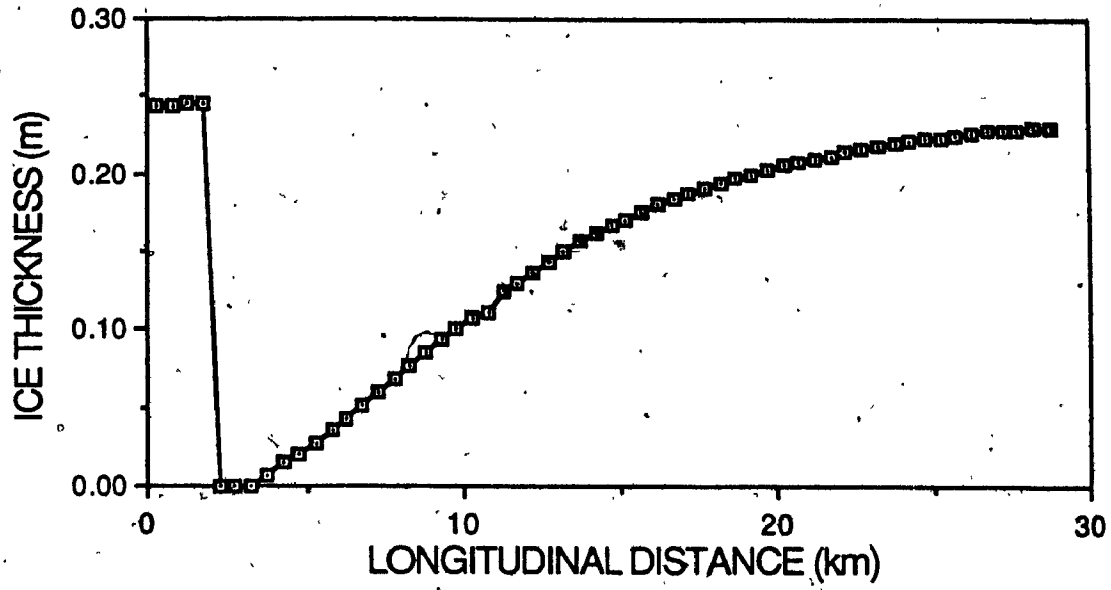

Fig. 4.11 Longitudinal Ice Thickness Variation

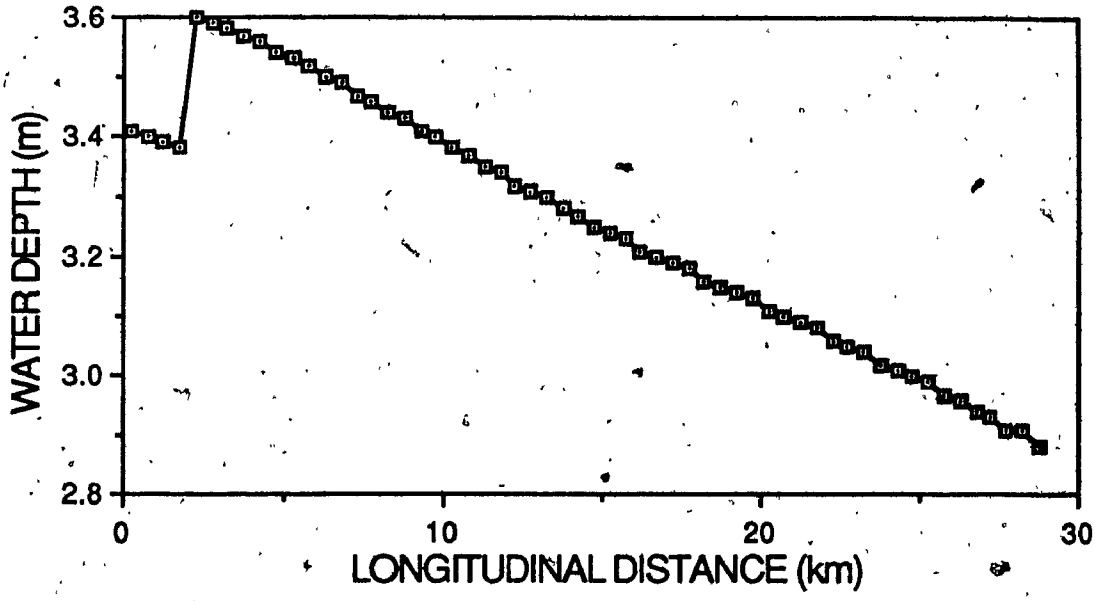

Fig. 4.12 Longitudinal Water Depth Profile

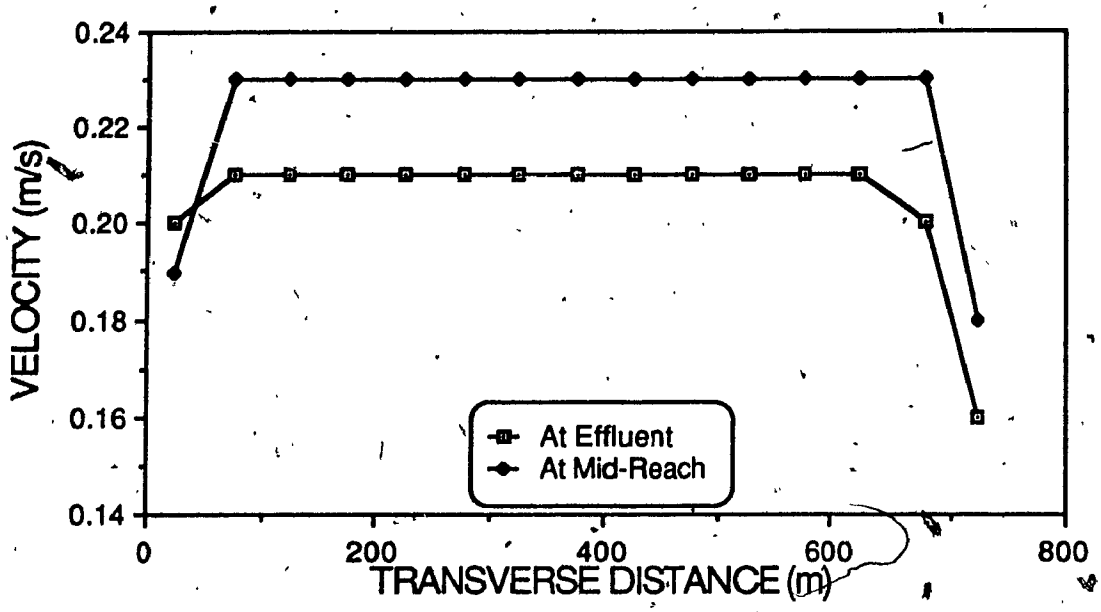

Fig. 4.13 Transverse Velocity Profiles

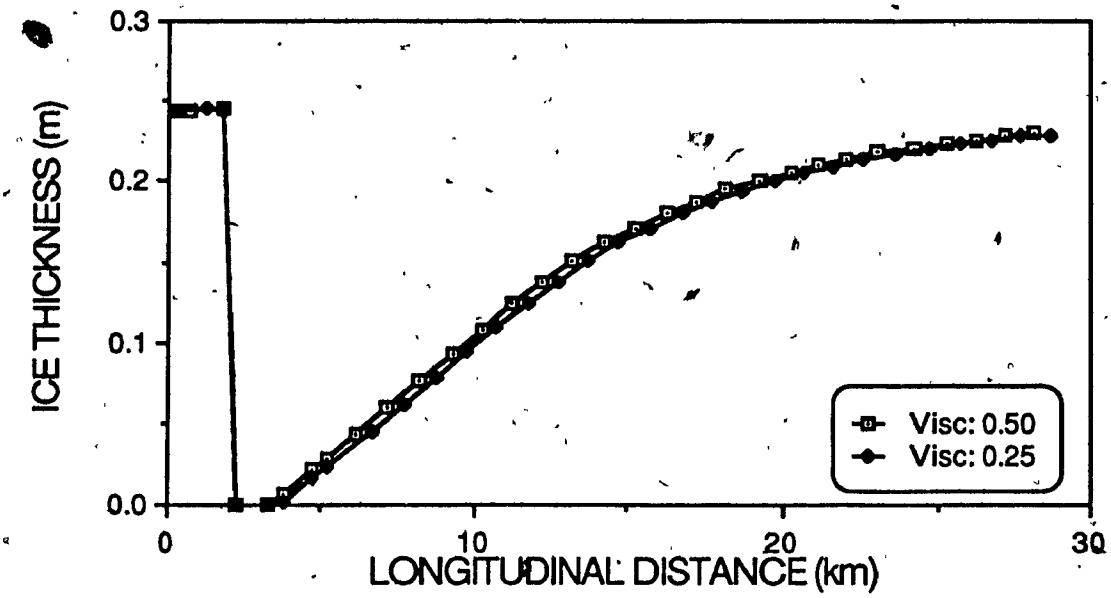

Fig. 4.14 Viscosity Coefficient Comparison

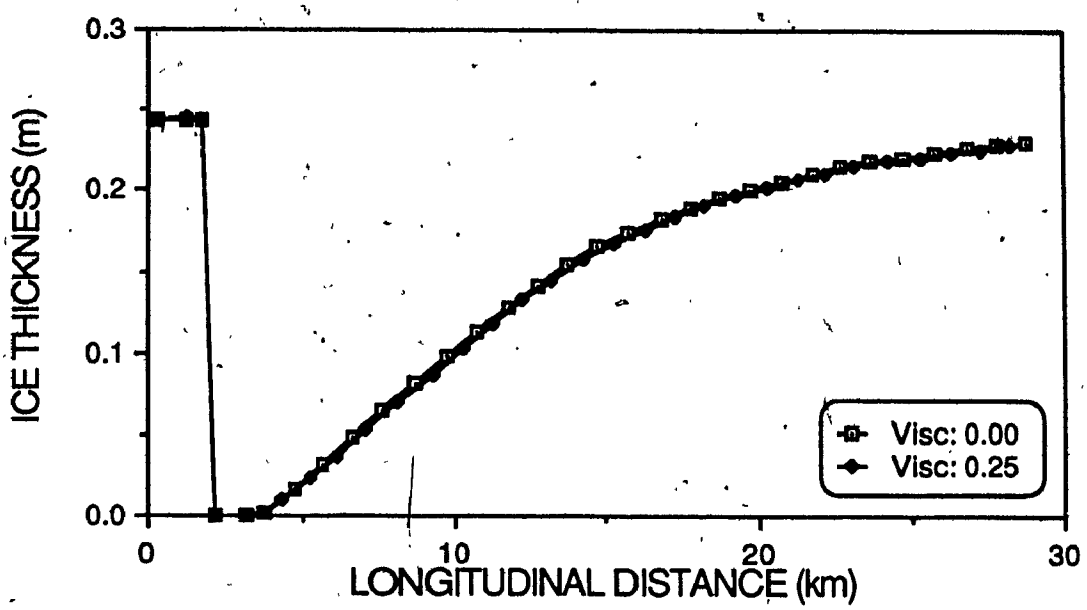

Fig. 4.15 Boundary Conditions Comparison

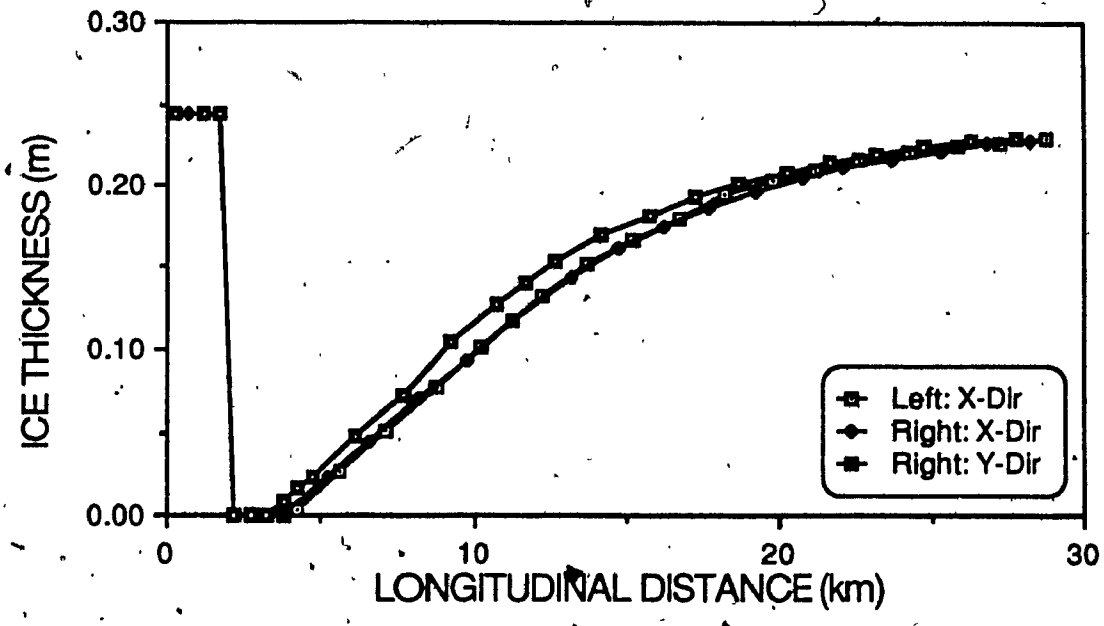

Fig. 4.16 Solution Symmetry Check Graph

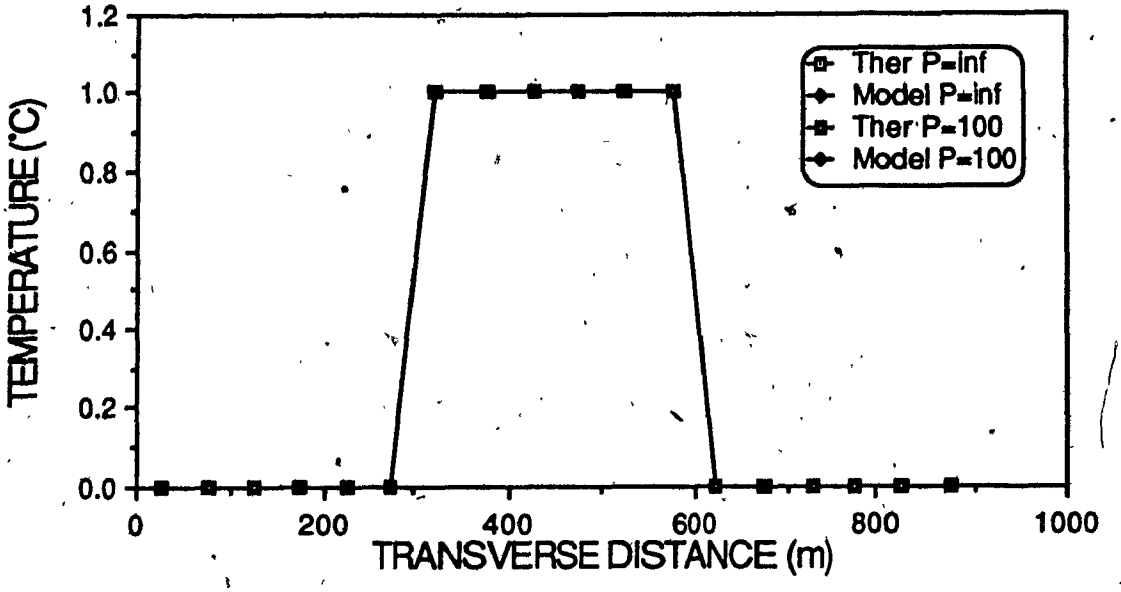

Fig. 4.17 Transverse Temperature at Entrance Cross Section

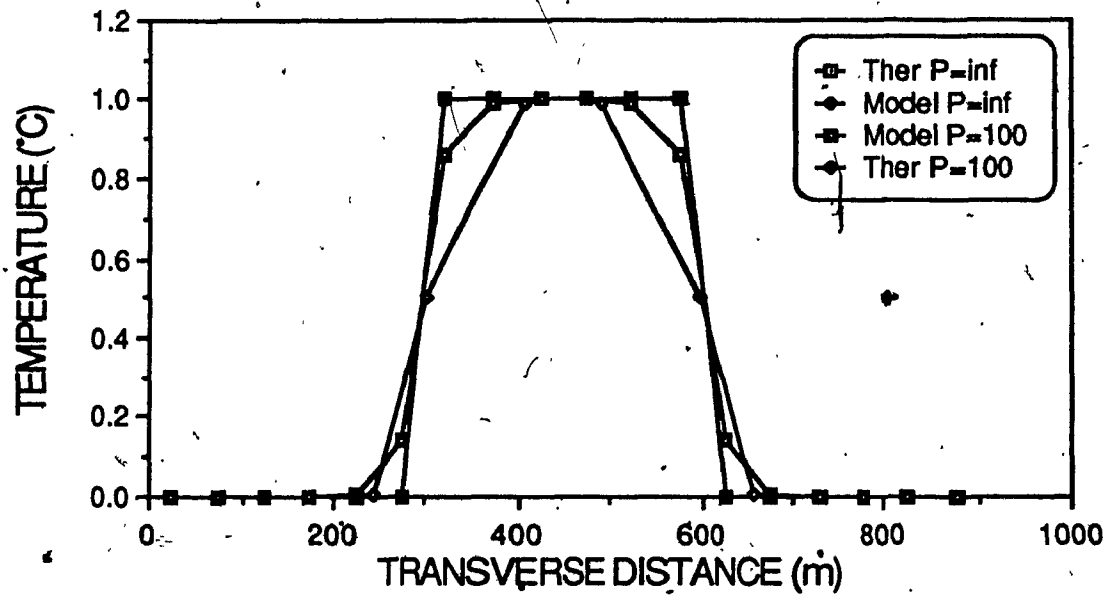

Fig. 4.18 Transverse Temperature at Mid-Reach Cross Section

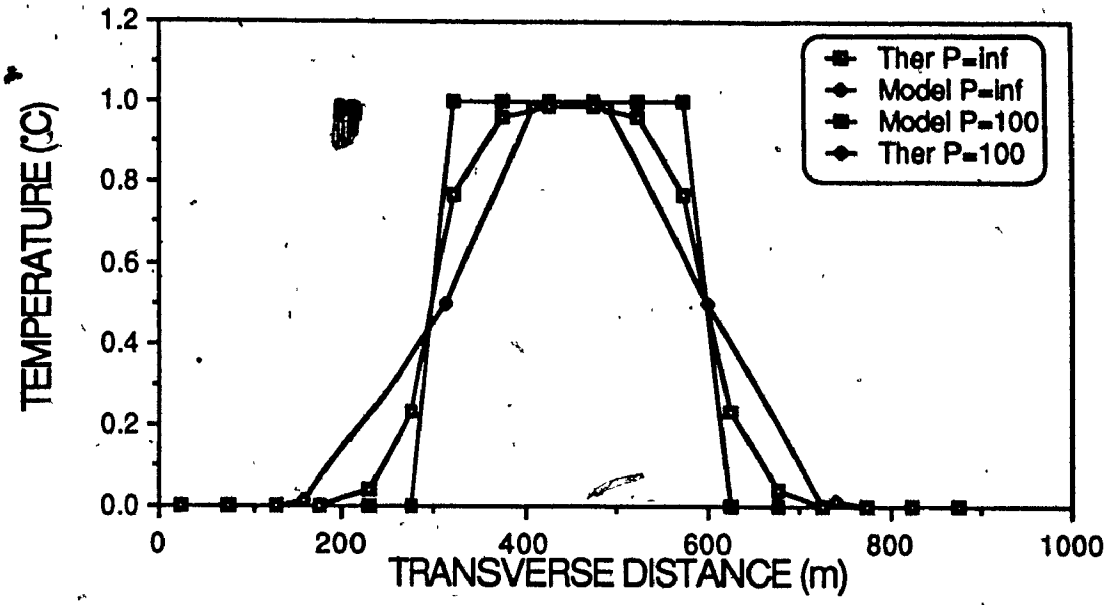

Fig. 4.19 Transverse Temperature at Exit Cross Section

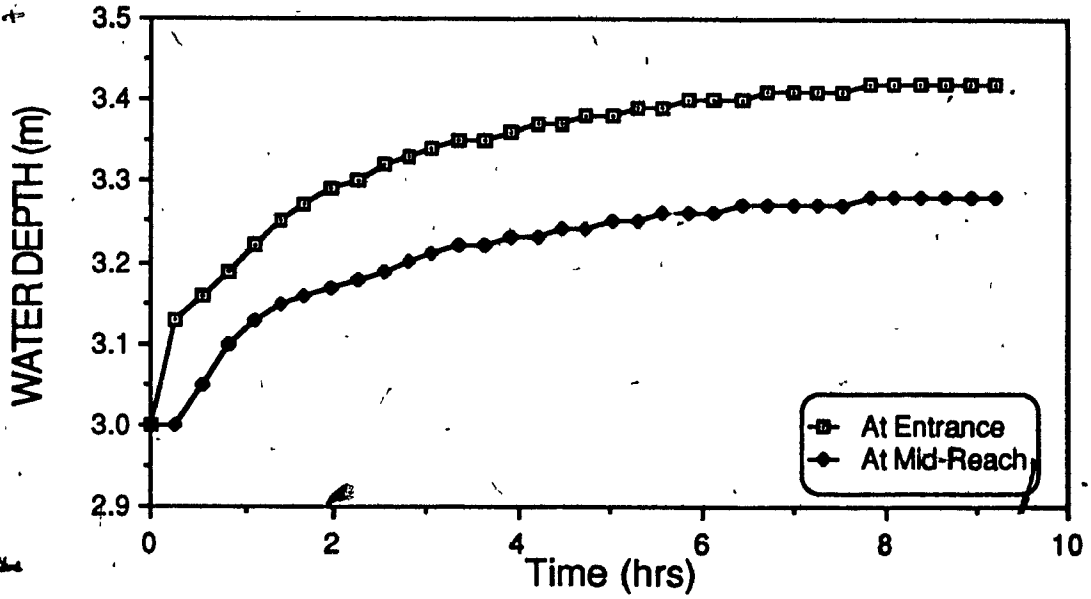

Fig. 4.20 Water Depth Development

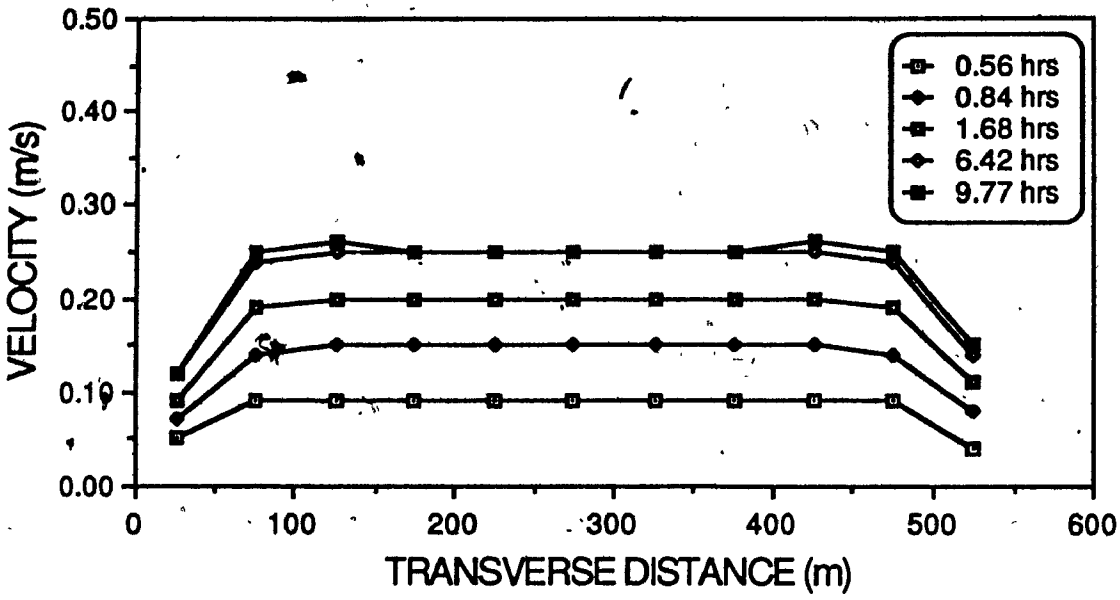

Fig. 4.21 Velocity Profile Development at Mid-Point

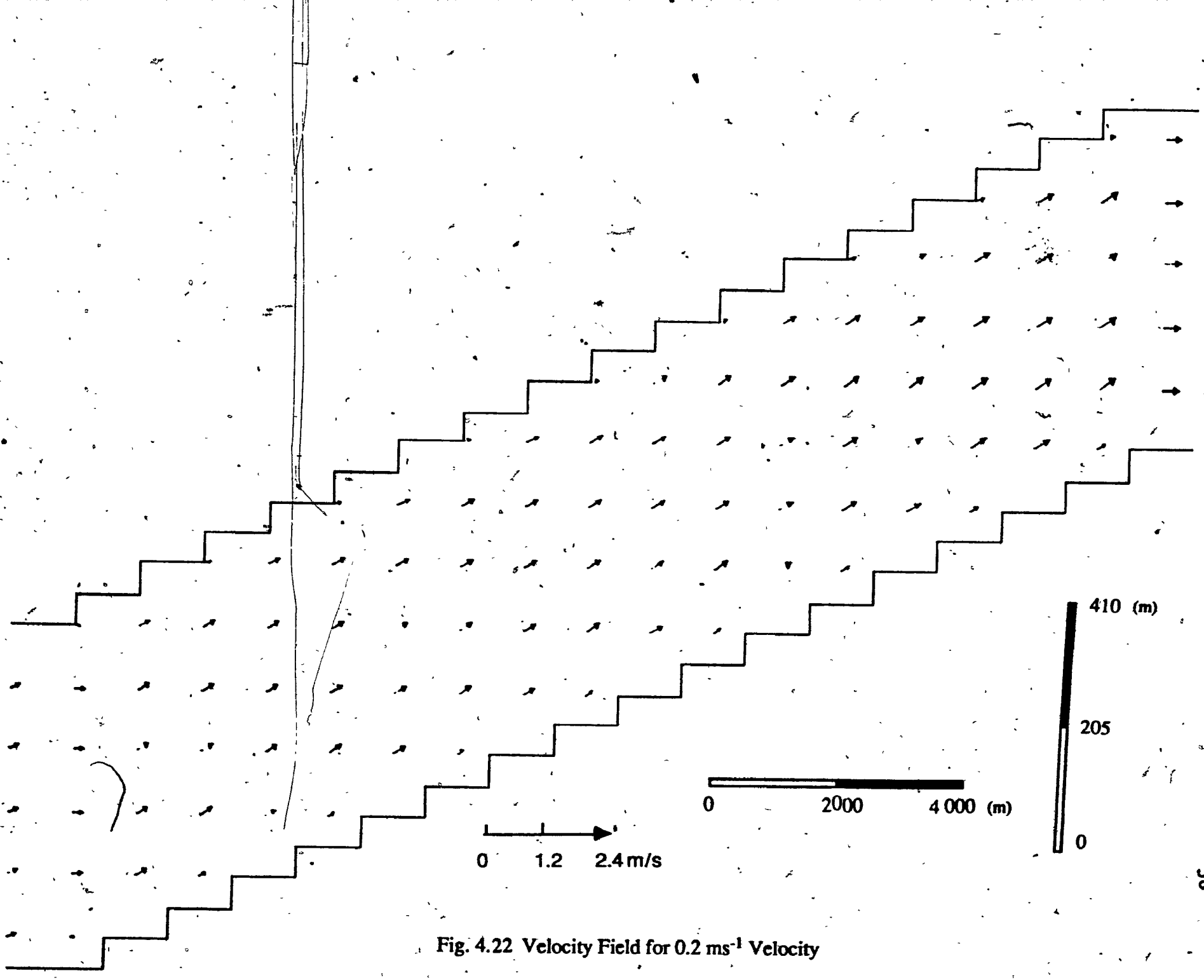

Fig. 4.22 Velocity Field for 0.2 ms^{-1} Velocity

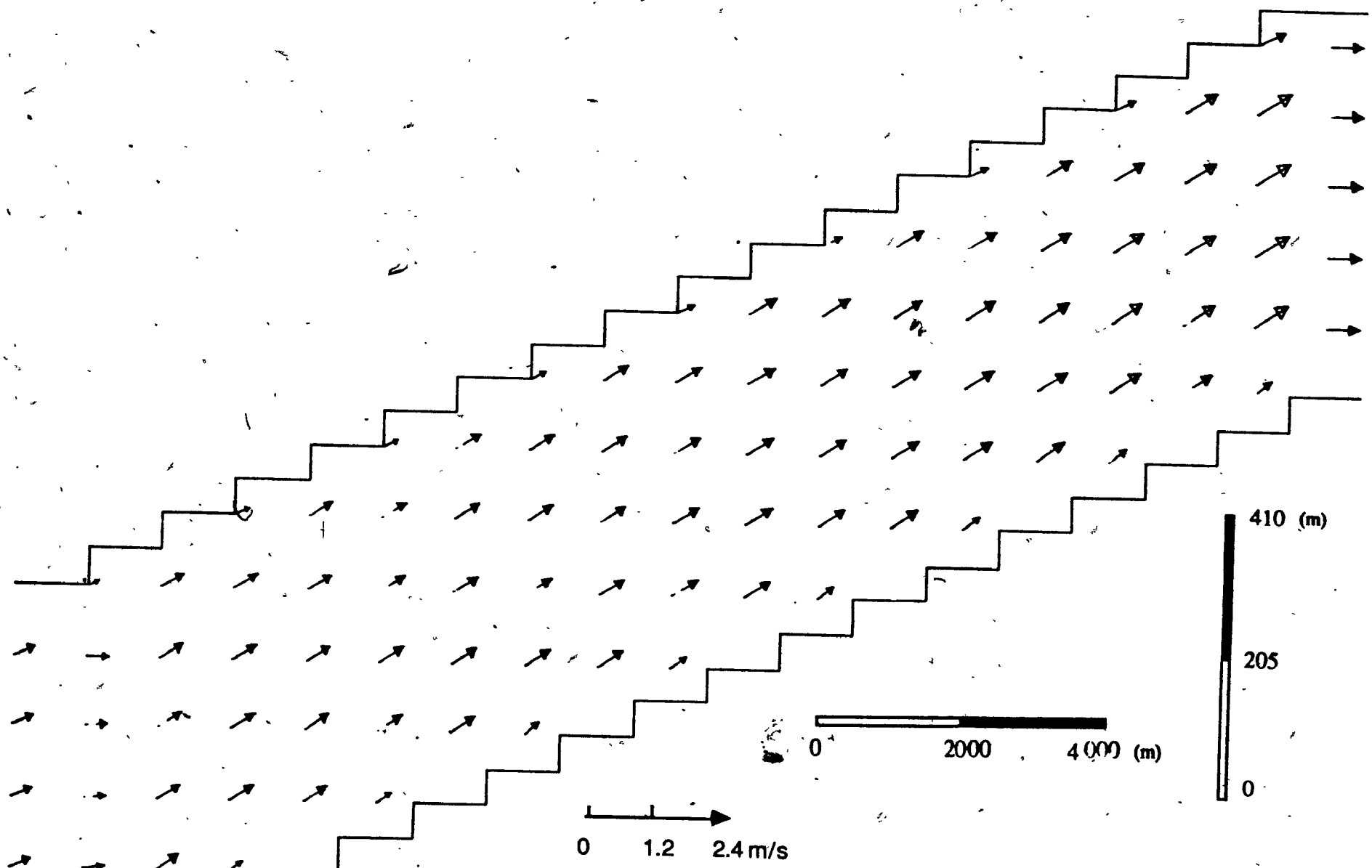

Fig. 4.23 Velocity Field for 0.4 ms^{-1} Velocity

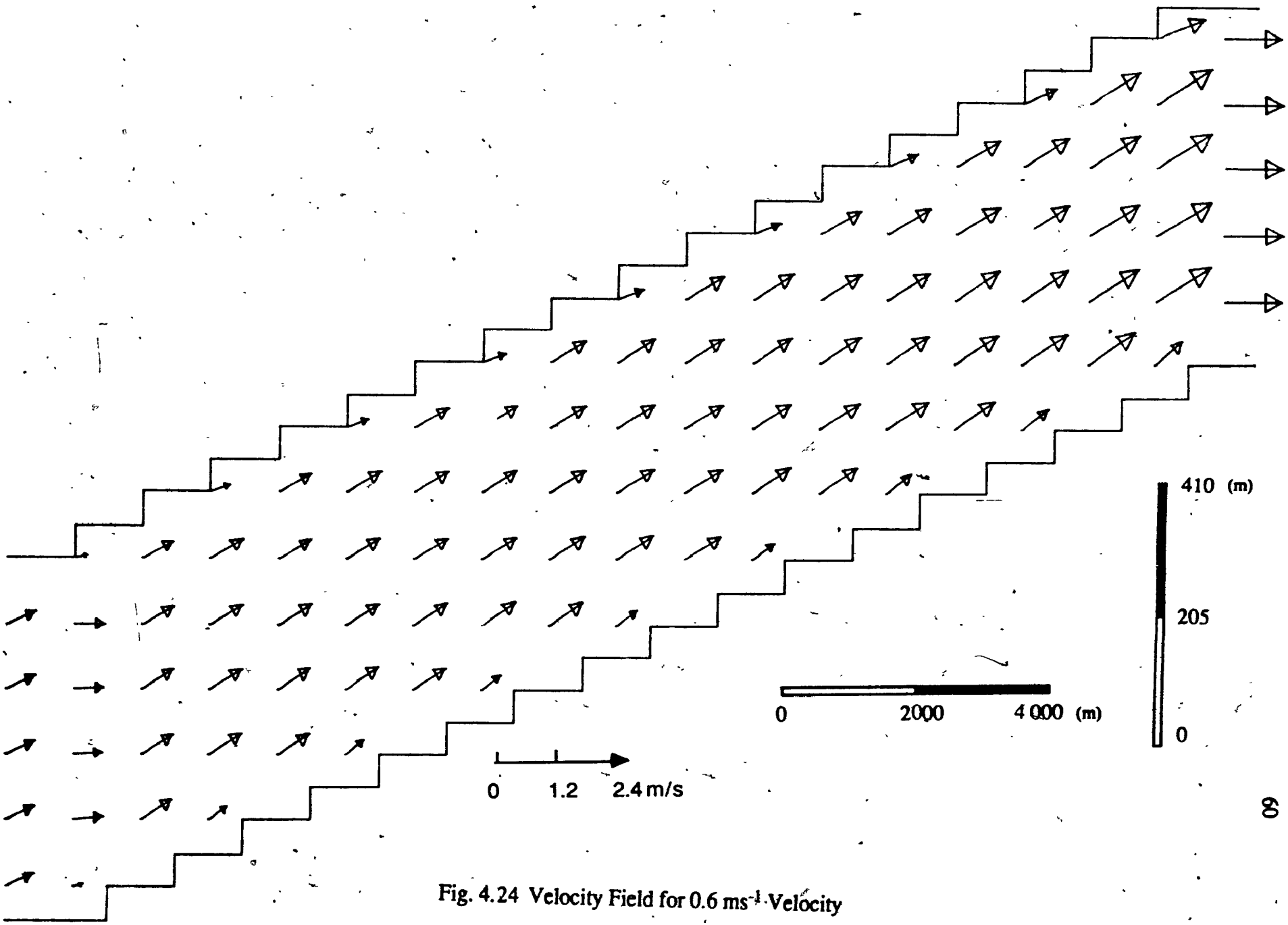

Fig. 4.24 Velocity Field for 0.6 ms^{-1} Velocity

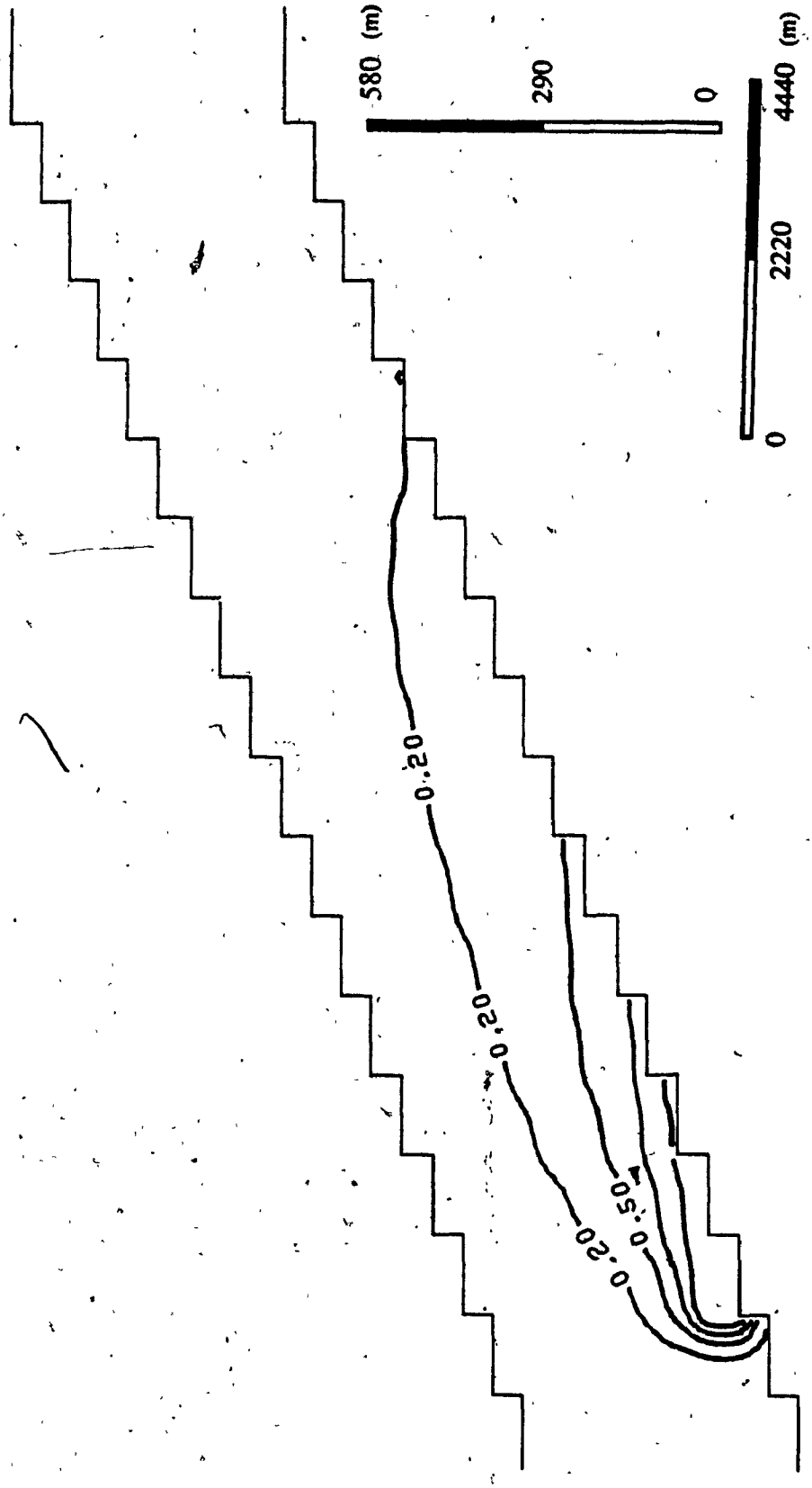

Fig. 4.25 Temperature Distribution at 0.2 ms^{-1}

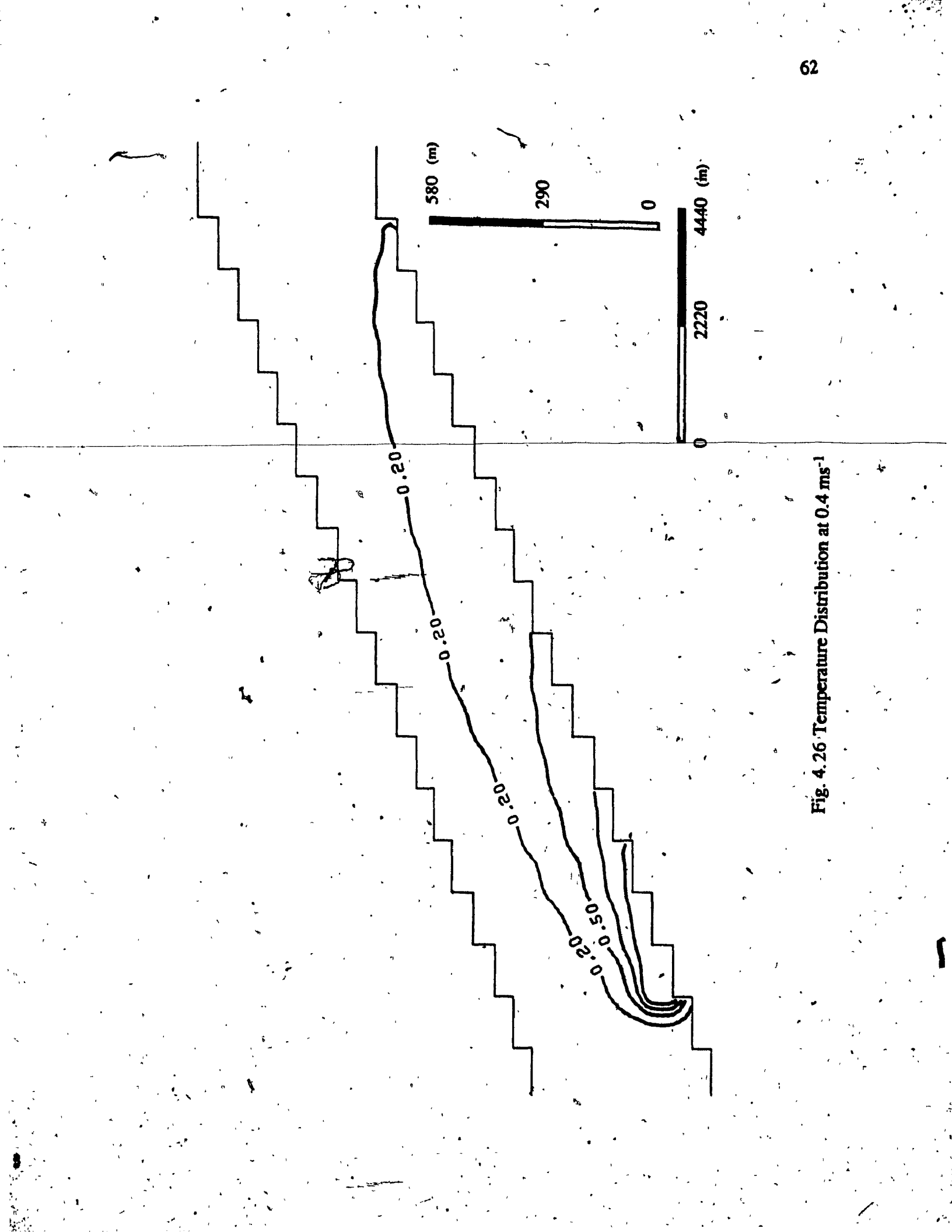

Fig. 4.26 Temperature Distribution at 0.4 ms^{-1}

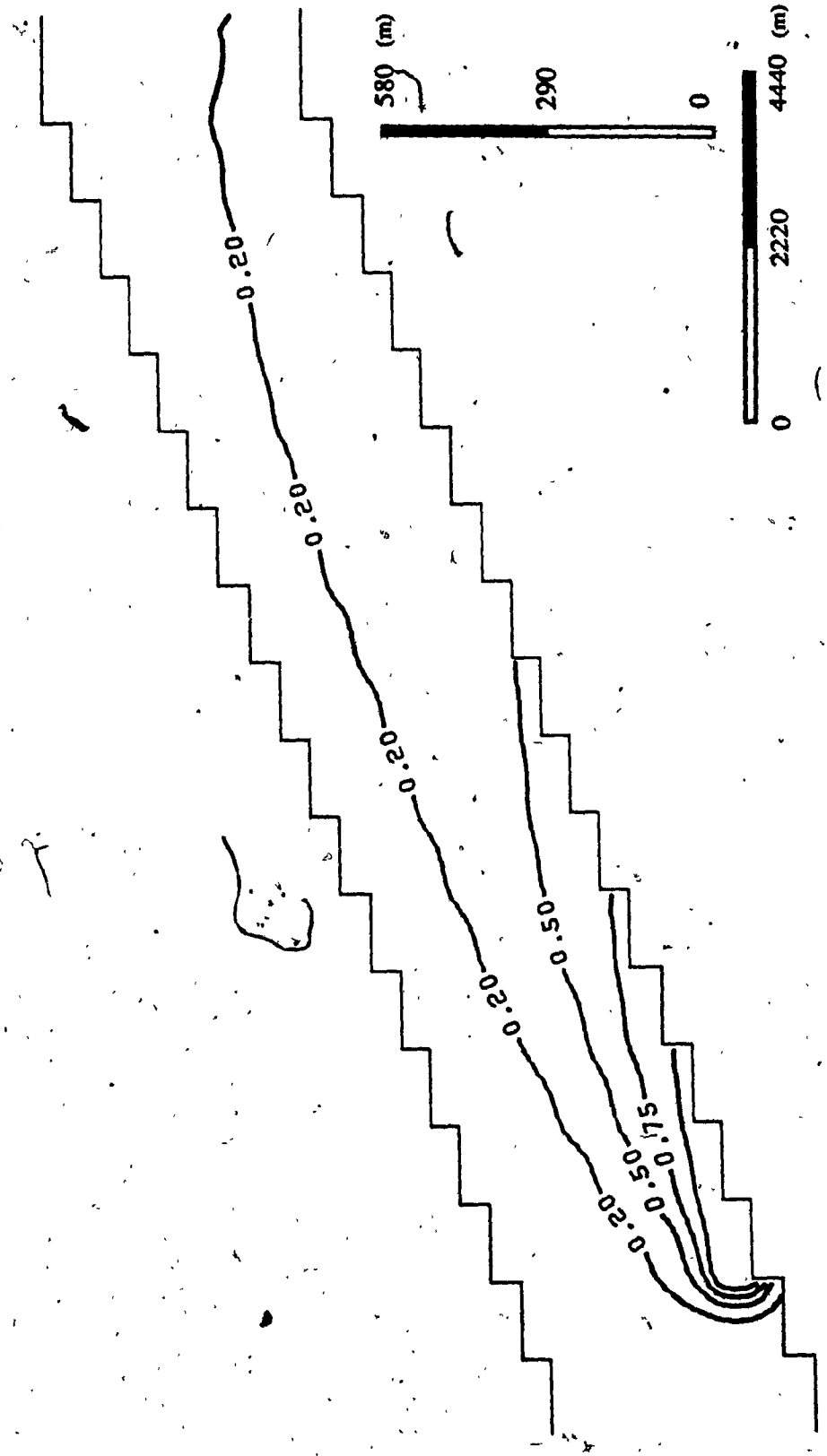

Fig. 4.27. Temperature Distribution at 0.6 ms^{-1}

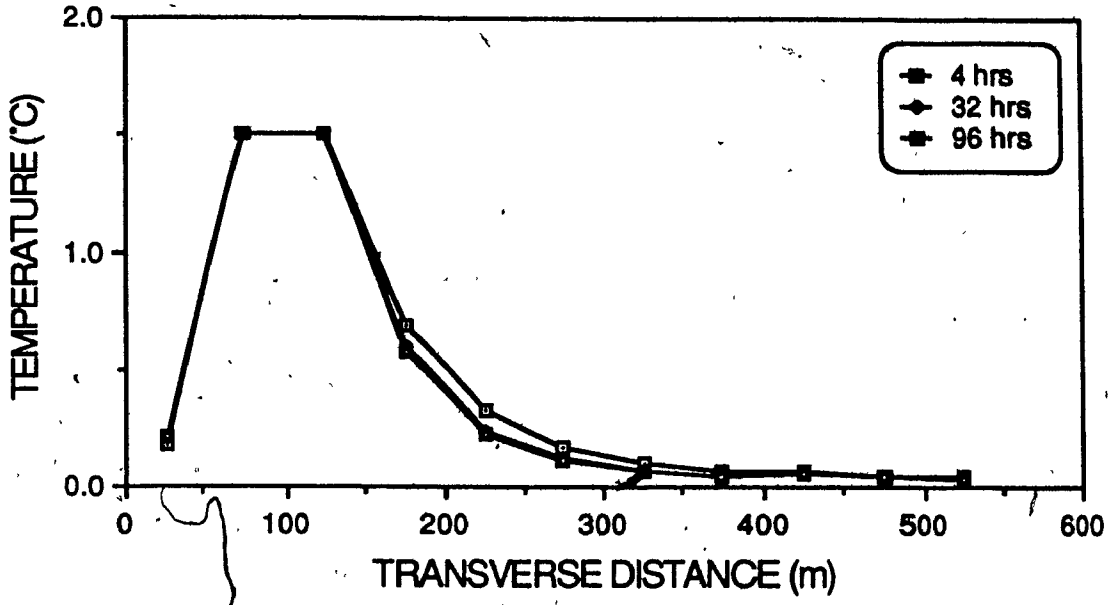

Fig. 4.28 Temperature Profile Development at the Effluent Source Cross Section

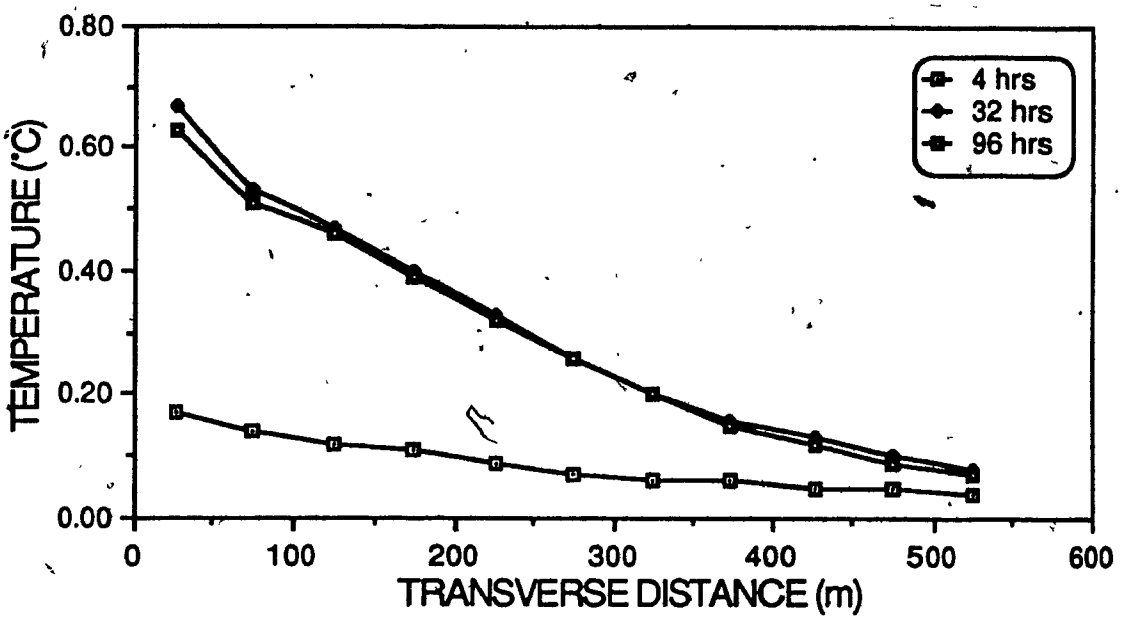

Fig. 4.29 Temperature Profile Development at the Mid-Reach Cross Section

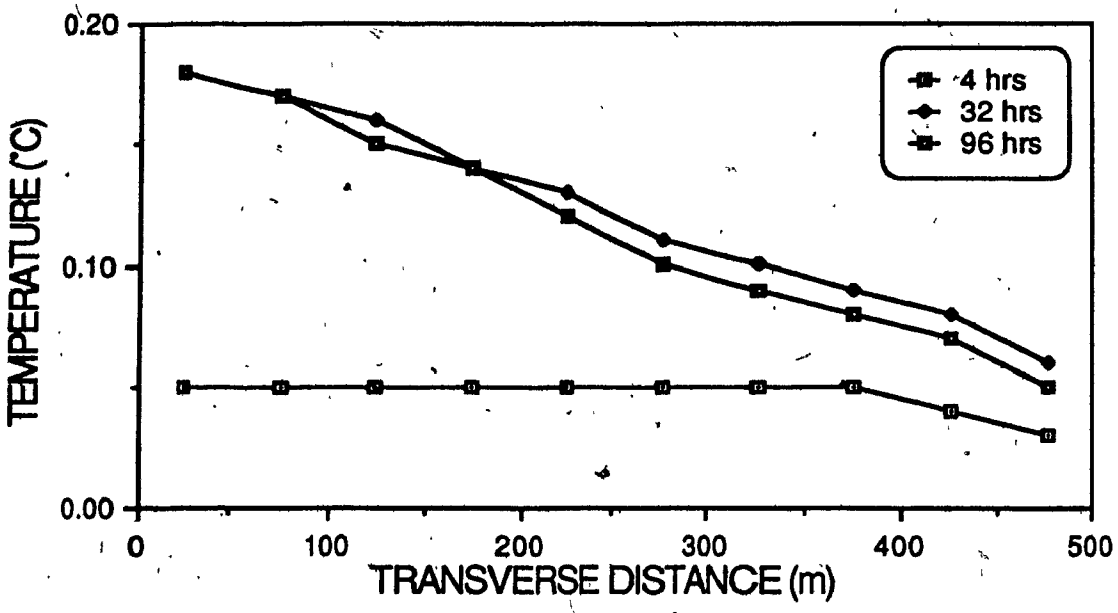

Fig. 4.30 Temperature Profile Development at the Exit Cross Section

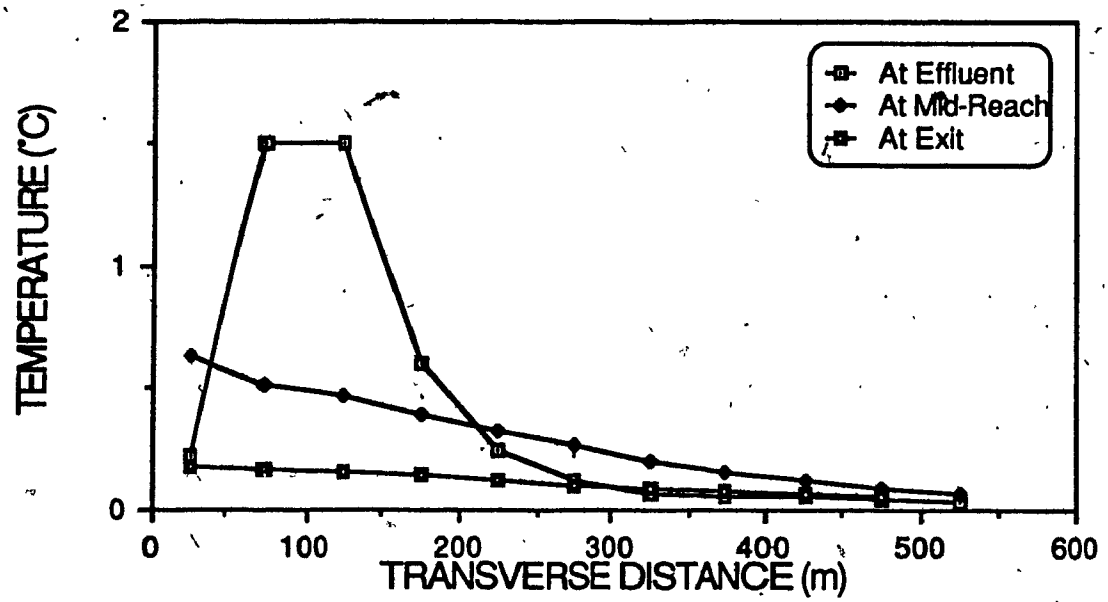

Fig. 4.31 Temperature Profiles

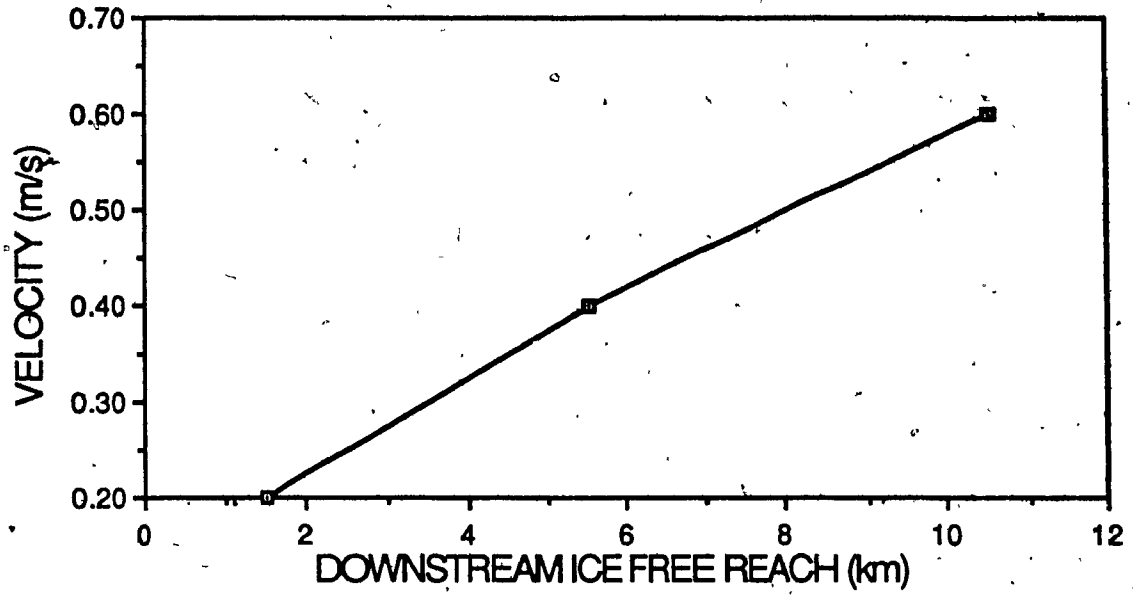

Fig. 4.32 Downstream Ice Free Reach at Variable Velocity

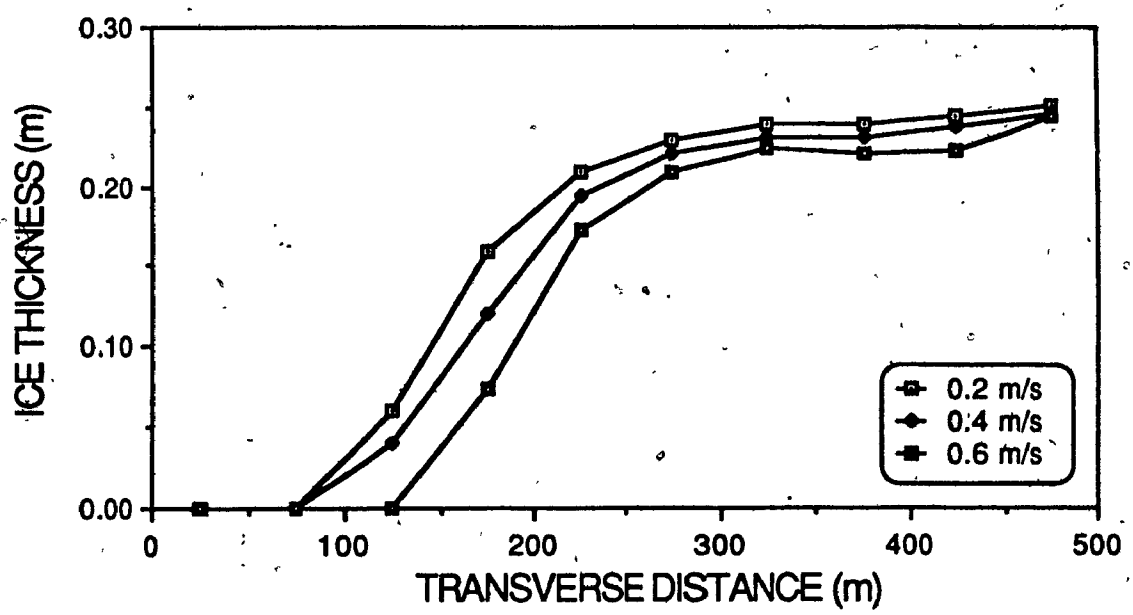

Fig. 4.33 Ice Thickness Profile at 500 m Below Effluent Source

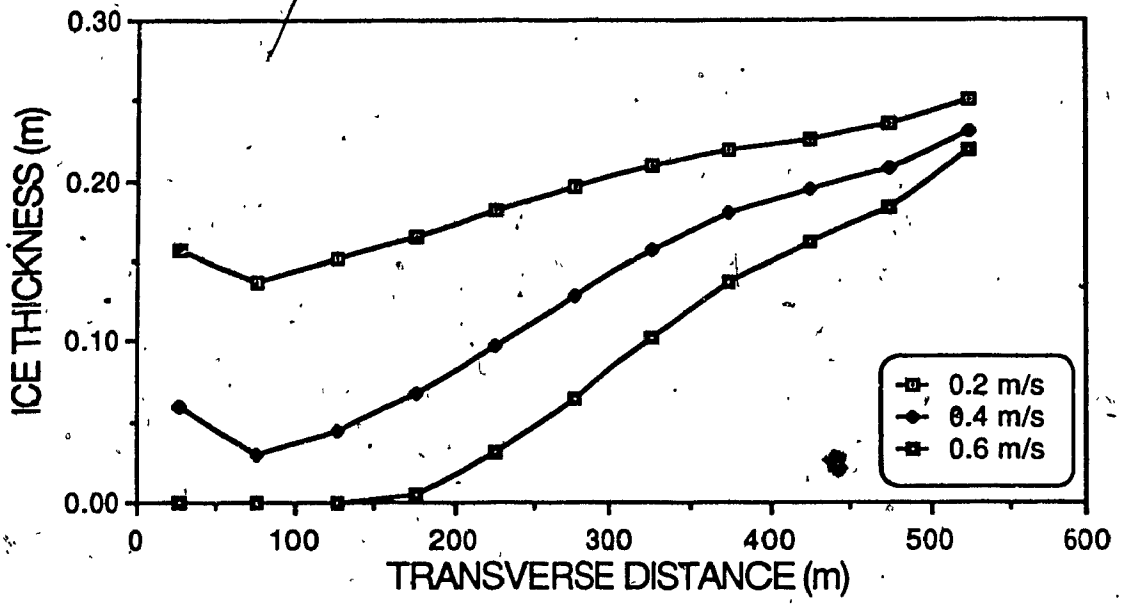

Fig. 4.34 Ice Thickness Profile at Channel Mid-Reach for Three Velocities

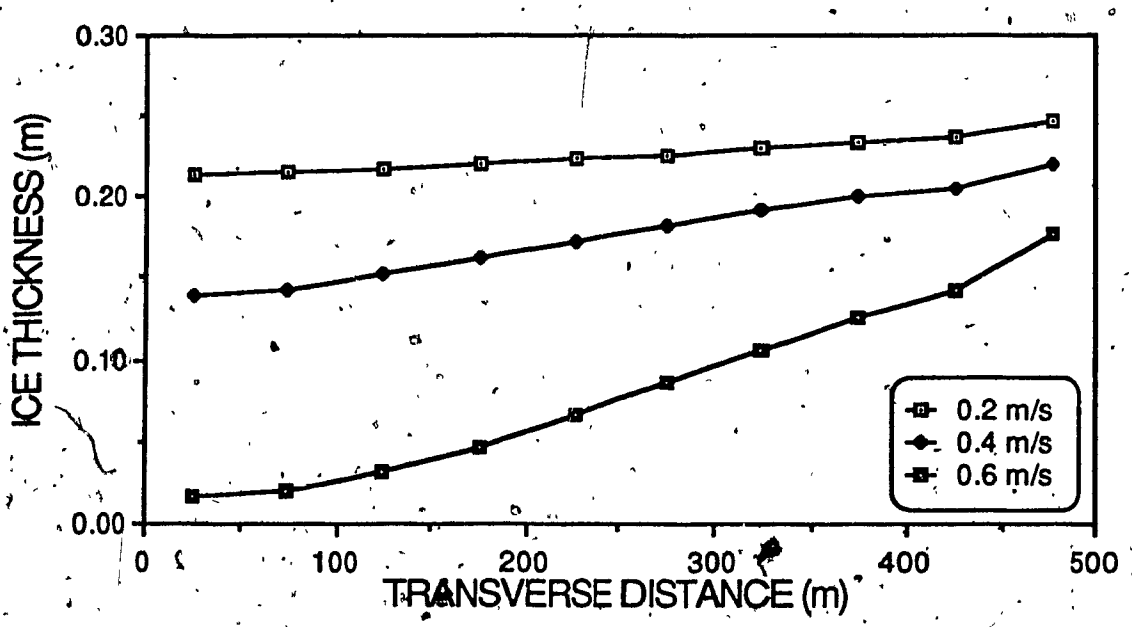

Fig. 4.35 Ice Thickness Profile at Channel Exit for Three Velocities

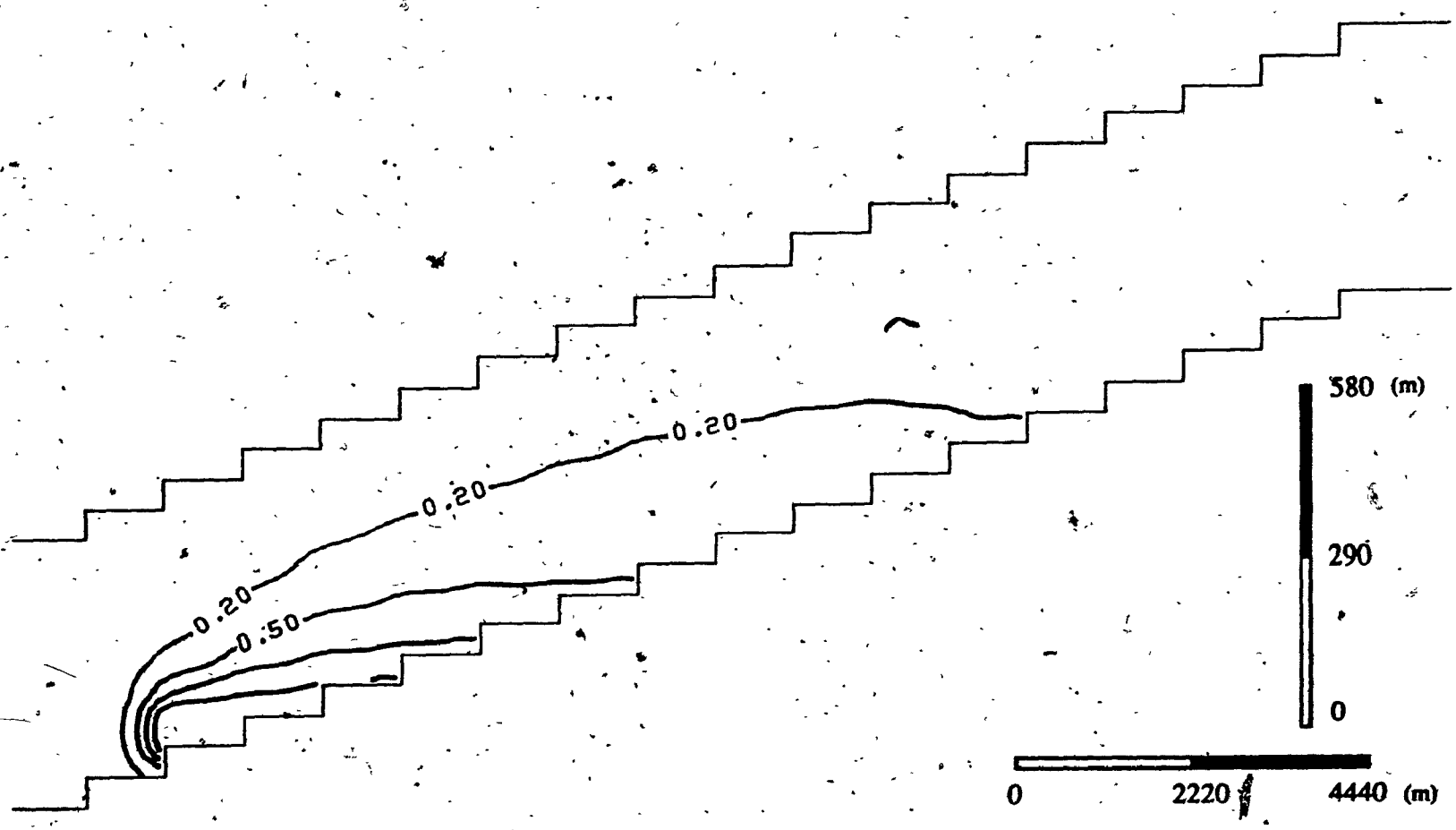

Fig. 4.36 Temperature Distribution at a Dispersion Constant of 20.0

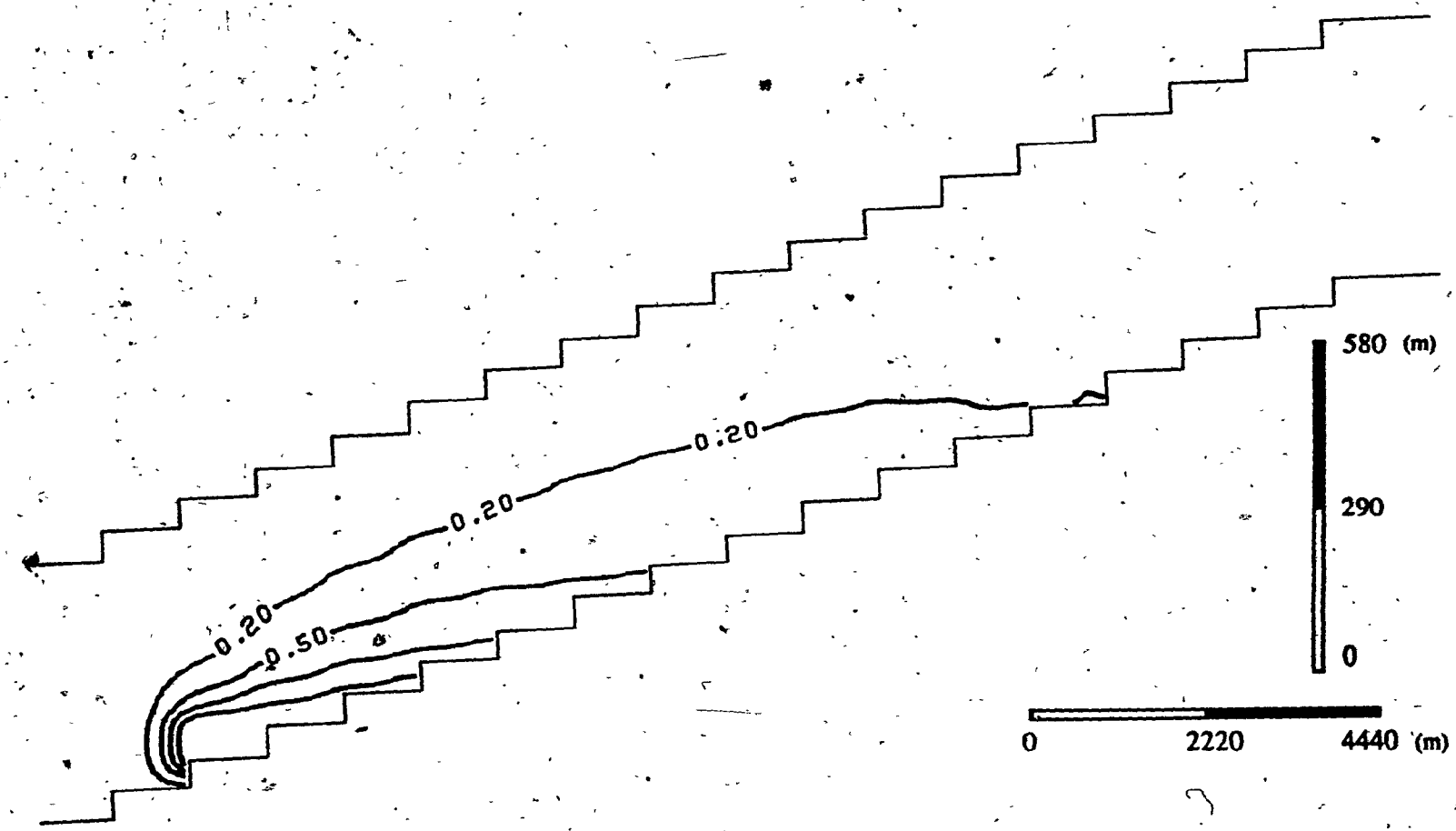

Fig. 4.37 Temperature Distribution at a Dispersion Constant of 00.0

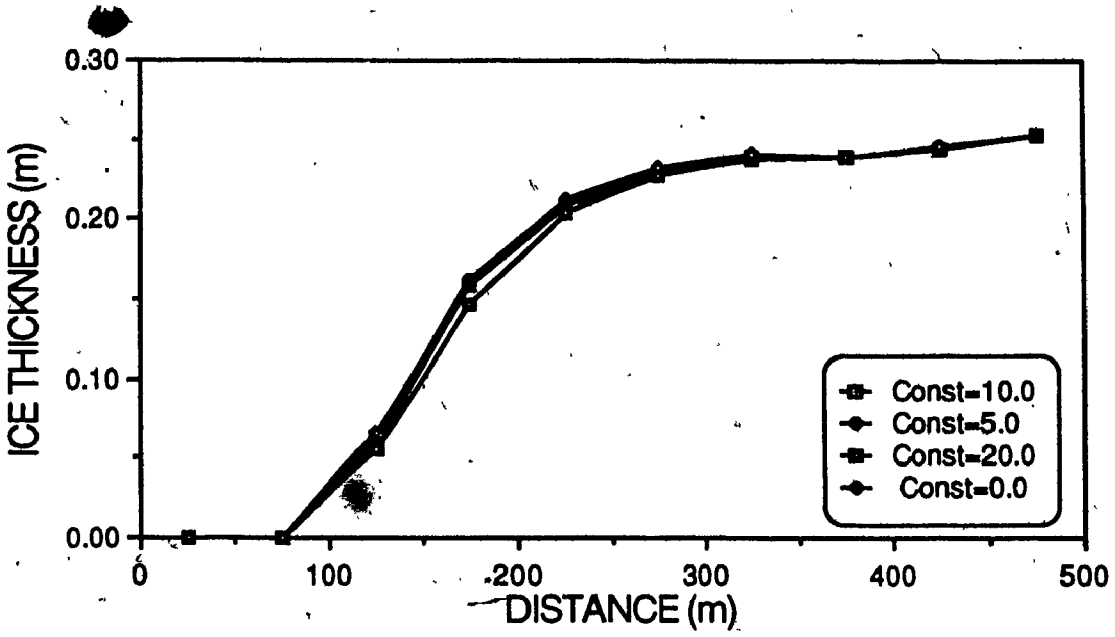

Fig. 4.38 Ice Thickness Dispersion Comparison at 500 m Below Effluent Source

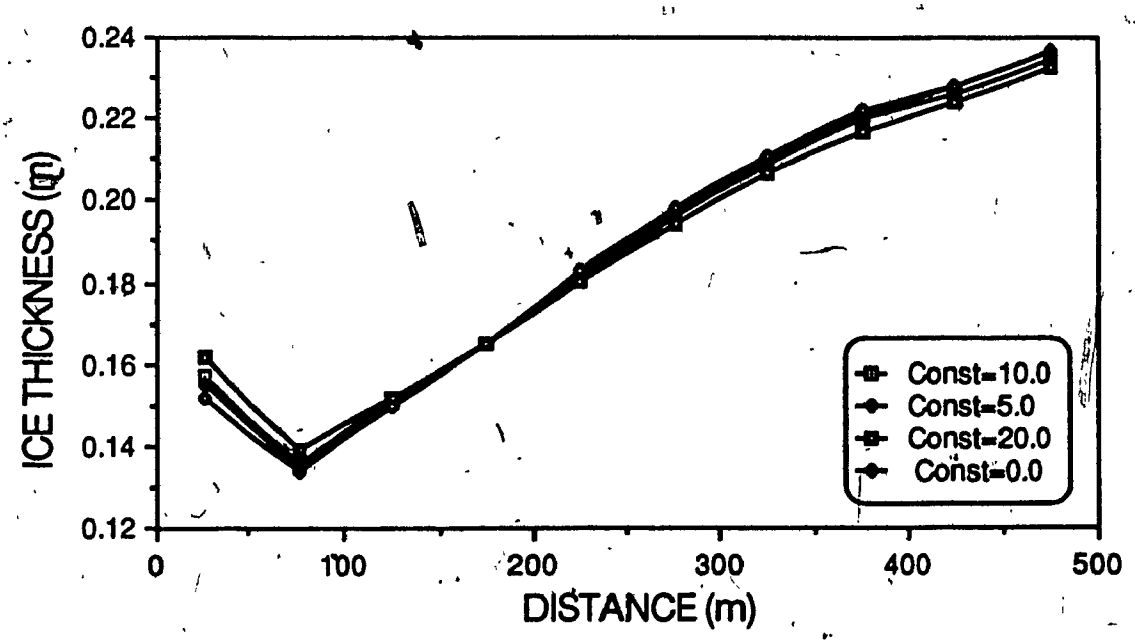

Fig. 4.39 Ice Thickness Dispersion Comparison at Mid-Reach

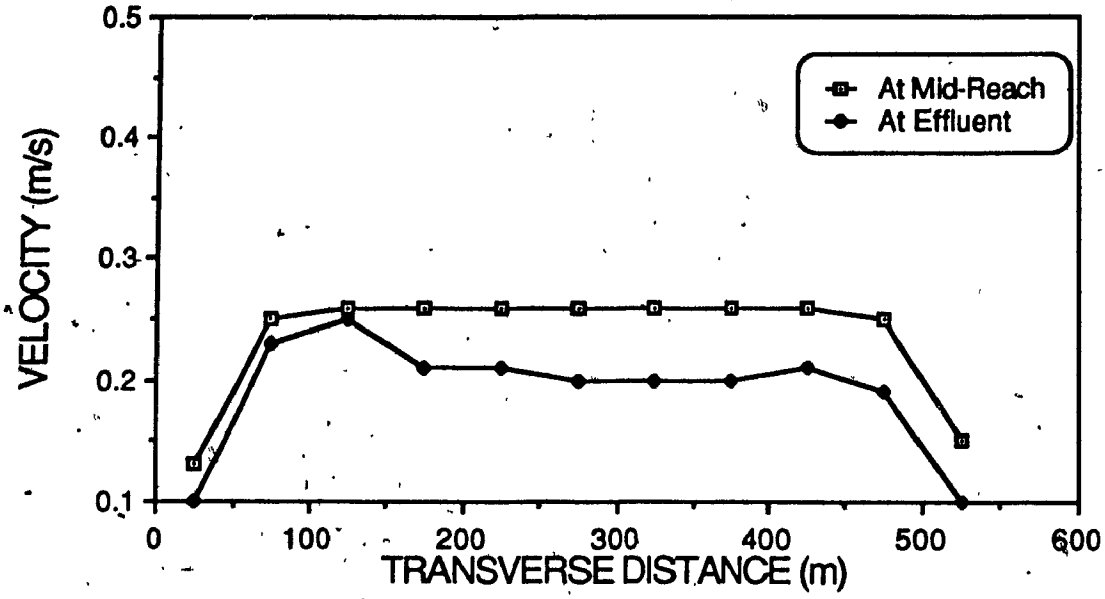

Fig. 4.40 Convection Dispersion Comparison Velocity Profiles

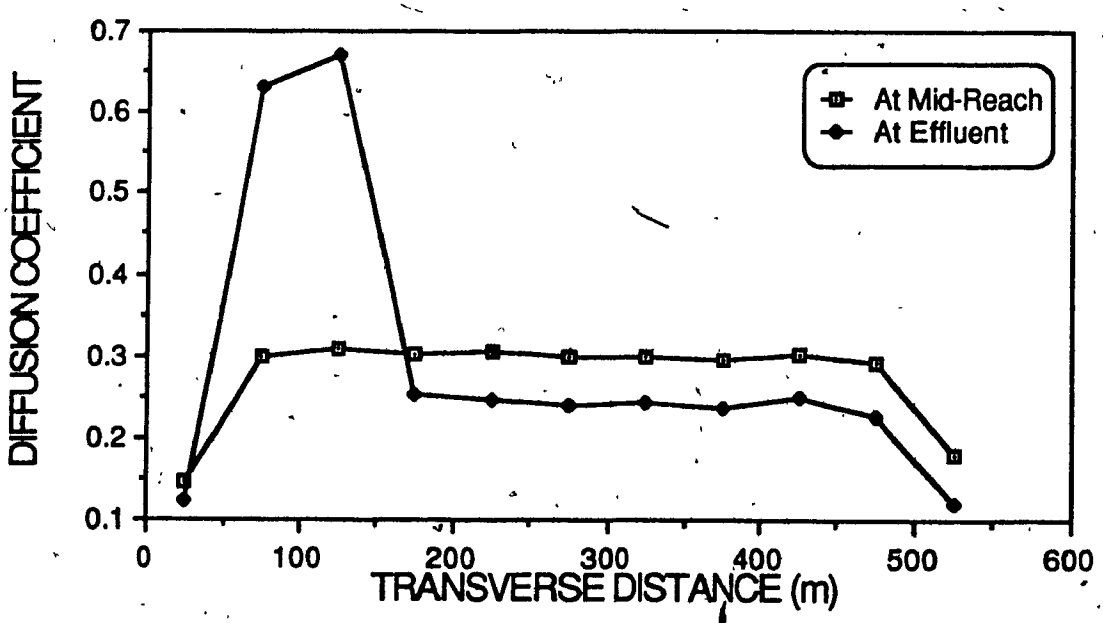

Fig. 4.41 Convection Dispersion Comparison Diffusion Profiles

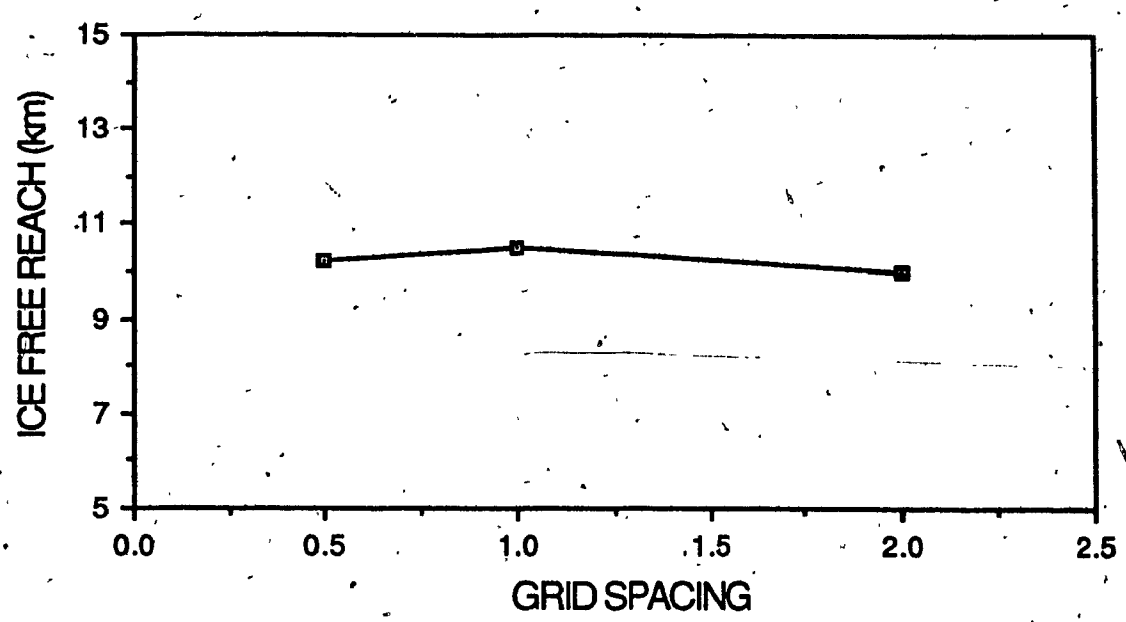

Fig. 4.42 Influence of Grid Spacing Comparison

4.2 Field Comparison

In February 1980 the U.S. Army Cold Regions Research and Engineering Laboratory carried out a field study on the melting of river ice by a side discharge thermal effluent. The study was performed on the Mississippi River near Bettendorf, Iowa, under the direction of Dr. G.D. Ashton [Ashton 1980; Ashton 1981].

At the field study site the Mississippi River is approximately 1 km in width, narrowing in the downstream direction. The discharge during the study period was almost constant at 850 m^3s^{-1}. The water depth varies from 2 m near the shore to a maximum of 10 m in the main channel. Average velocity of the flow is 0.25 m s^{-1}. The river bathymetry was determined from river sounding charts obtained from the Rock Island Corps of Engineers. The geometry and bottom elevation of this section of the

river is shown on Fig. 4.43. The direction of the river flow is from right to left with a gradual increase in depth, in the downstream direction. Lock & Dam 14 is located approximately 3 km upstream of the reach shown and Lock & Dam 15 is located approximately 1 km downstream of the reach shown. The river bed consists of sandy clay material with no rocks and few sudden changes in elevation. A Manning's coefficient of 0.030 is used in the hydrodynamic equations. The geometry of the river valley looking upstream from the outflow boundary is illustrated by Fig. 4.44.

A complete meteorological record of 3 hour readings is available from the Moline, Illinois airport weather office located 6 miles from the study site. Air temperature, wind velocity, humidity, cloud cover and precipitation records are given. During the study period, from February 14 to February 17 the air temperature was initially warm and then became cold. There was only a short period of light snowfall during the study period. In the computations, the daily averaged meteorological values up to the time of the ice edge determination was employed. The meteorological variables for the dates of February 14 and February 17 are summarized in Table 4.3.

Table 4.3 Field Study Meteorological Conditions

Parameter & unit	February 14	February 17
Air temperature °C	- 2.13	-18.75
Cloud Cover tenths	9.8	0.0
Latitude degrees	41.5	41.5
Wind Velocity m s^{-1}	4.20	3.99
Vapour Pressure mb	2.10	1.05

The side discharge thermal effluent originates from the Riverside thermal power plant. The thermal discharge characteristics were determined from plant operating records. During the study period the daily average discharges were almost constant. A complex intake and outfall arrangement caused mixing of the discharge over a width of 30 m from the shore, with a mixed temperature of 2.97°C.

Temperature readings of the water were taken at a few locations during the field study. These readings indicated no constant variation of temperature with depth, indicating complete mixing in the vertical direction. At the entrance to the study reach an inflow water temperature of slightly above 0°C was found. The value of 0.05°C is used for the inflow water temperature in the model. A value of 10.0 is used for the dispersion constants, due to the gentle flow of the river.

Ice cover edge locations were determined from oblique aerial photographs, taken during overflights of the river. The cold weather during the study period caused a reduction in the length of the open water reach. A thin ice covering formed over previously open water on February 17. The ice cover areas not affected by the thermal effluent increased in thickness during the study period, from an initial average channel thickness of 0.25 m. The ice cover underside was relatively smooth with a few ripples. A Manning coefficient of 0.020 was used in the model for the ice cover underside. Snow accumulation on the river ice cover was negligible. No significant amounts of frazil ice was present in the river flow, due to a complete ice cover upstream of the study reach. A grid spacing of 125 m in the x direction, 25 m in the y direction and a time step of 4.5 s is used in the calculations.

4.2.2 Discussion of Field Comparison

Fig. 4.45 shows the velocity field with a complete ice cover and Fig. 4.46 shows

the velocity field for the ice cover condition on February 14. Slight changes have occurred due to the ice cover melting with an increase in flow velocity in the ice free regions and a decrease elsewhere.

On Fig. 4.47 and on Fig. 4.48 the model temperature distributions of the river for February 14 and February 17 respectively are shown. The colder air temperature on February 17 and the different ice cover conditions caused changes in the temperature profile. The downstream length of the 0.5°C and 0.7°C contour line is reduced for February 17 due to the faster cooling of the open water areas. The downstream position of the 0.2°C contour line is relatively unchanged. This is due to the presence of an ice cover over a larger extent of the channel, reducing water cooling as compared to open water areas. The heated water has moved in the downstream direction mainly, with a slight temperature difference upstream, caused by dispersion. In areas near the shore, outside the main river flow, lower water temperatures are present. This results from cooling of the stationary water.

The ice thickness contours are shown on Fig. 4.49 and Fig. 4.50 for Febraury 14 and February 17 respectively. A comparison of the field study findings and model results is given in Table 4.4.

Table 4.4 Comparison of Ice Free Reaches

	February 14		February 17	
	Field Study	Model	Field Study	Model
Ice Free Reach	yes	yes	yes	yes
Downstream Length km	8.0	6.6	4.3	1.9

As seen in Table 4.4 the model correctly predicts whether suppression of the river ice will occur. The length of the downstream reach calculated by model especially on February 14, compares well with the field study findings. This type of modelling often has discrepancies of several km [Hayes & Ashton 1985]. Much of the difference in the findings may be a result of a number of small thermal effluent discharges not accounted for in the field study data and therefore not included in the model calculations. These discharges would have the effect of lengthening the ice free reach. The two most significant of these discharges is located approximately 1.5 km downstream of the power plant and therefore would likely by the cause of the discrepancy on February 17.

The width of the downstream ice free reach, increases initially, becomes constant and then narrows. A similar behaviour is demonstrated by the field data. Upstream of the effluent discharge, a slight reduction in ice thickness occurs, especially on February 14.

On Februay 17 a much greater undisturbed ice thickness is present on the channel, following the cold weather period. As seen, especially on Fig. 4.49, a greater ice thickness was present in bays with low flow velocity. This is commonly found in field studies of river ice. Furthermore a small area of thin ice is present on the shoreline on the side of the effluent discharge. This was noted during the field study.

As experienced during the model tests, the ice thickened much more quickly in the transverse direction than the longitudinal or main flow direction. The field study found this to be true.

The relationship between river flow temperature and ice presence depends on air temperature. The heat exchange between the atmosphere and the ice top surface depends on a number of weather variables, most importantly air temperature. This heat exchange must balance with the heat exchange at the water-ice interface to maintain ice thickness

equilibrium. Therefore as noted on the temperature and ice thickness figures, the colder air temperature permits ice cover on a warmer river flow.

Fig. 4.51 shows a comparison of the river flow temperature at the mid-point of the ice free reach for February 17. The mid-depth temperature readings are used. Good agreement initially occurs within 2% but then some divergence of up to 30%, again likely caused by the minor effluent sources. No field water temperature data is available for February 14. Fig. 4.52 shows a comparison of transverse section temperature profiles for February 17. The comparison is for the width of the ice free reach from the shore. The maximum water temperature occurs a short distance from the shore. The discrepancy at the downstream section is again likely cauased by the minor effluent sources. On Fig. 4.53 the time development of the water temperature profiles at 0.5 km below the effluent source for February 17 are shown. The water temperature profile is quickly established at near steady state values. The water temperature profiles at several x-direction sections are shown on Fig. 4.54 for Feburary 17. As one moves downstream the profiles become less sharp as expected, due to mixing. Fig. 4.55 shows a comparison between the ice free width predicted and measured on Feburary 17 with agreement within 12%. The ice thickness for several x-direction sections are shown on Fig. 4.56 for February 14, again with less sharp profiles downstream. Fig. 4.57 shows the time widening of the ice free reach at three sections on February 17 with a maximum time of 660 hours. As expected the steady state is reached first near the effluent source and then at downstream sections.

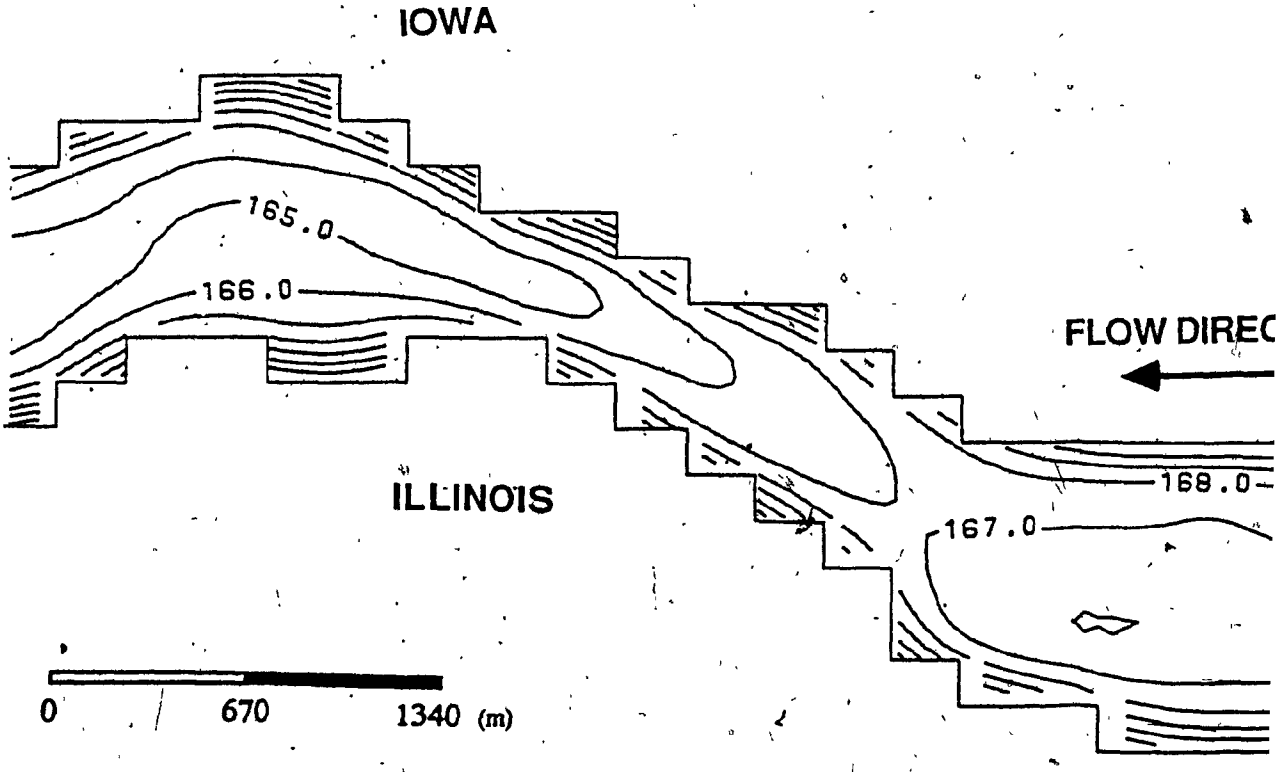

Fig

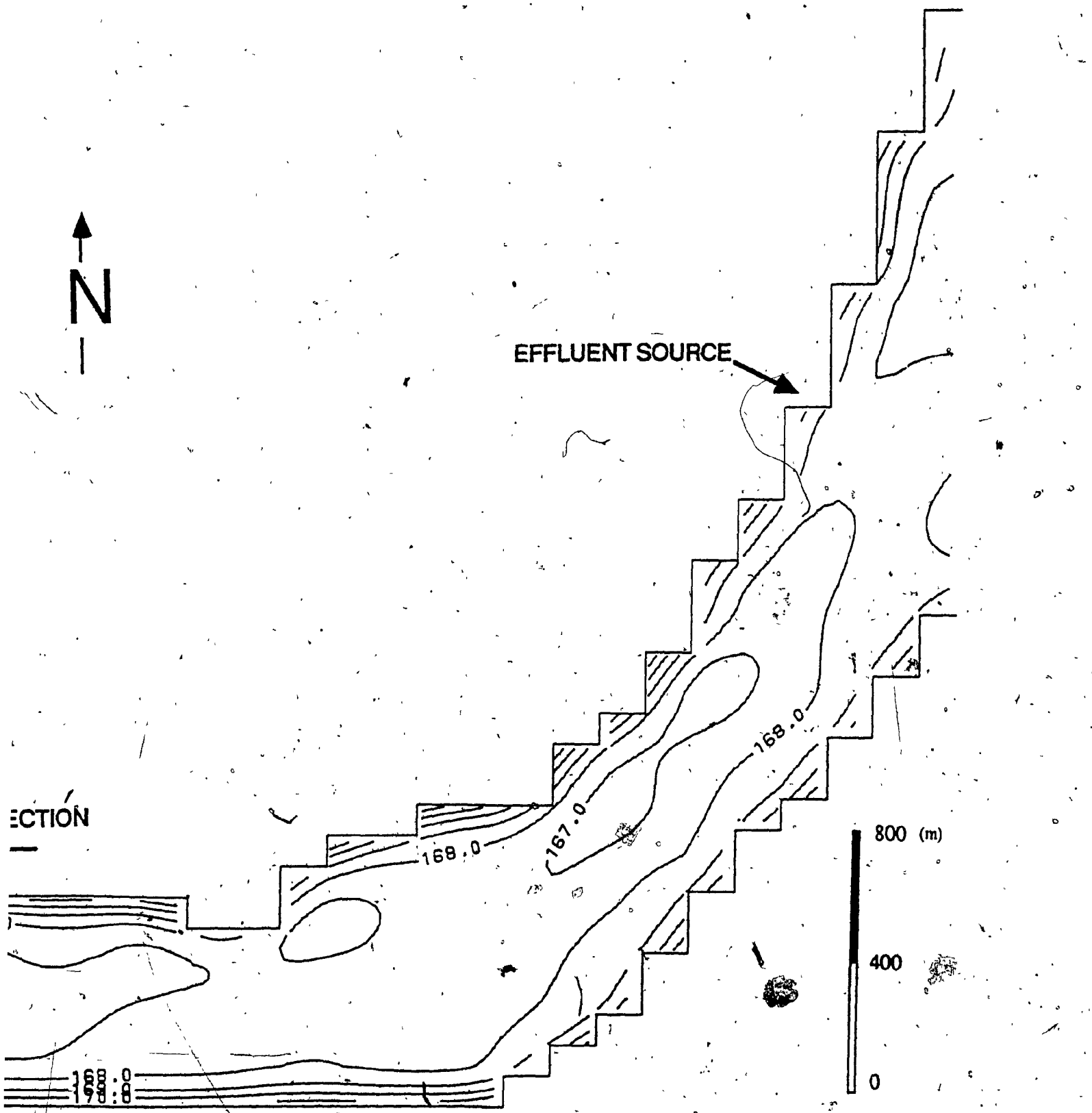

Fig.4.43 Mississippi River Bathymetry

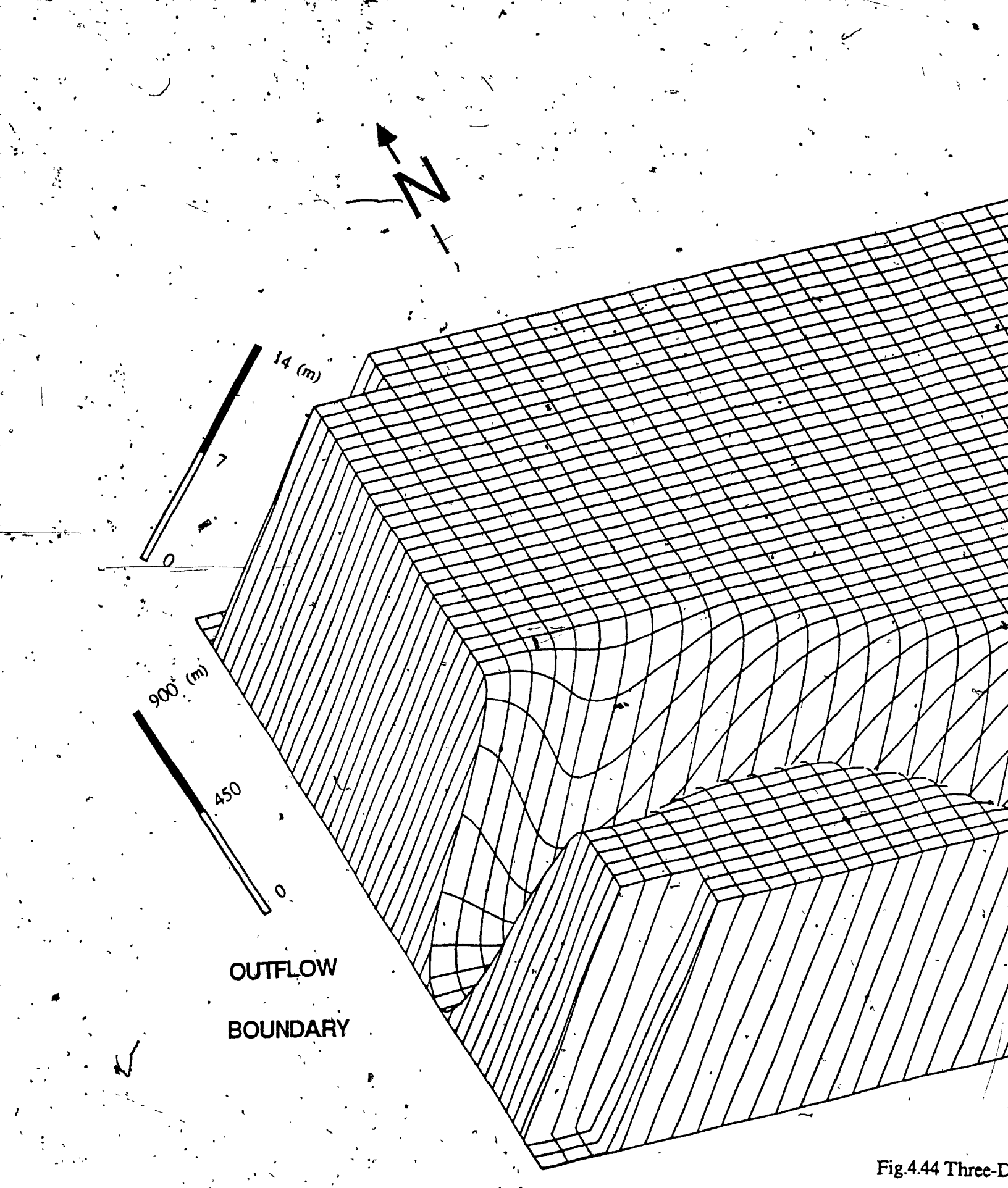

Fig.4.44 Three-D

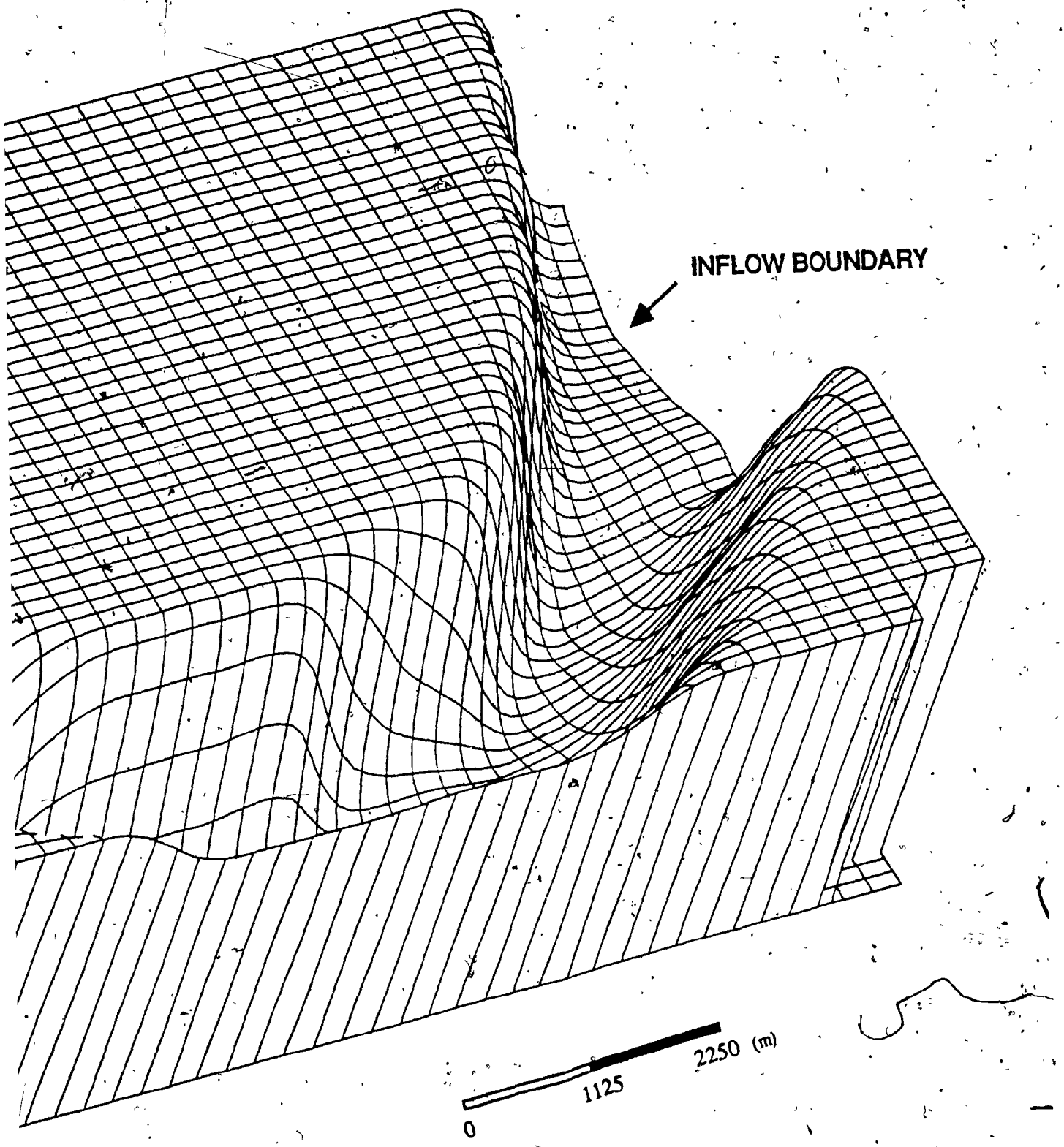

Dimensional View of River Bed

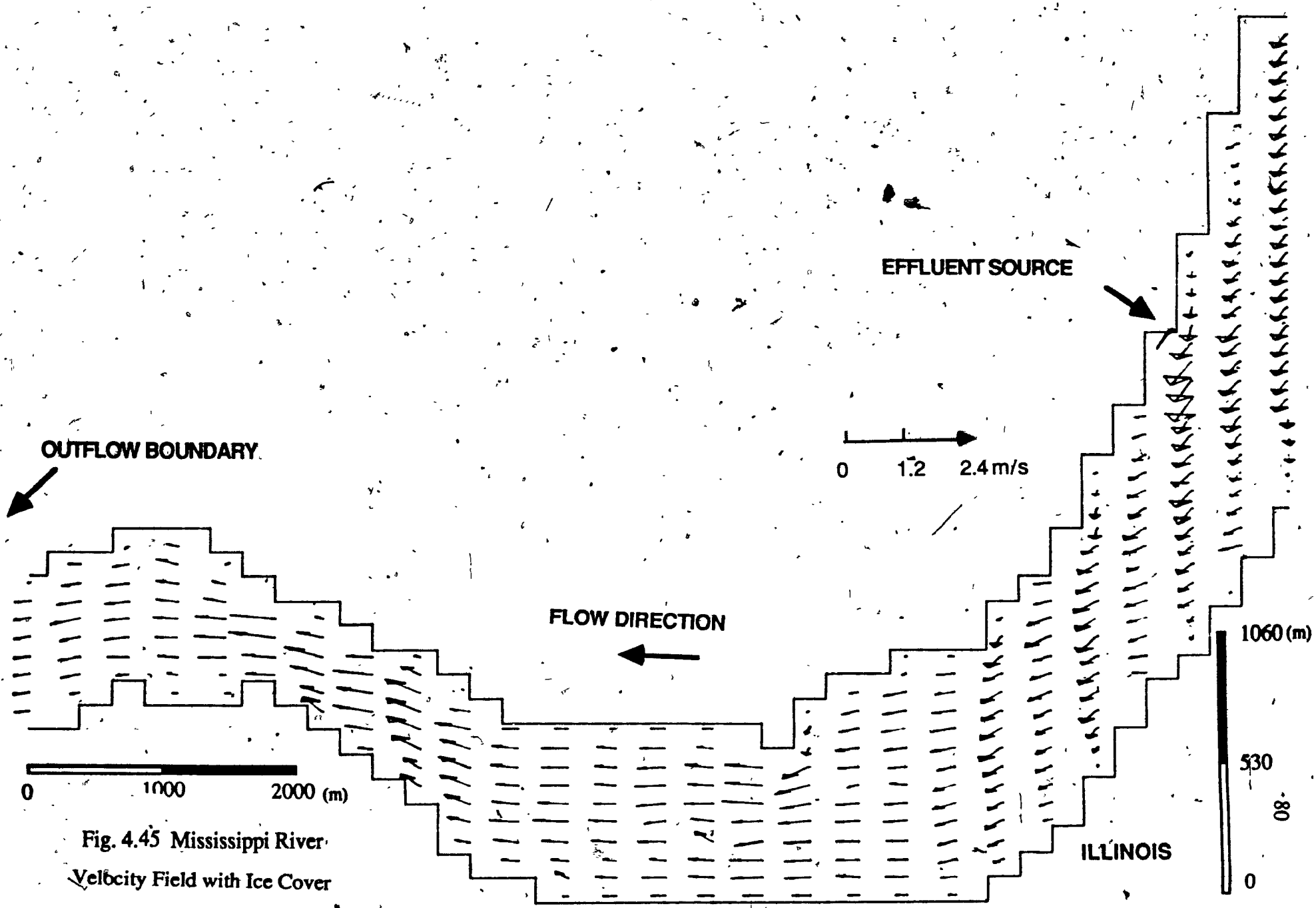

Fig. 4.45 Mississippi River Velocity Field with Ice Cover

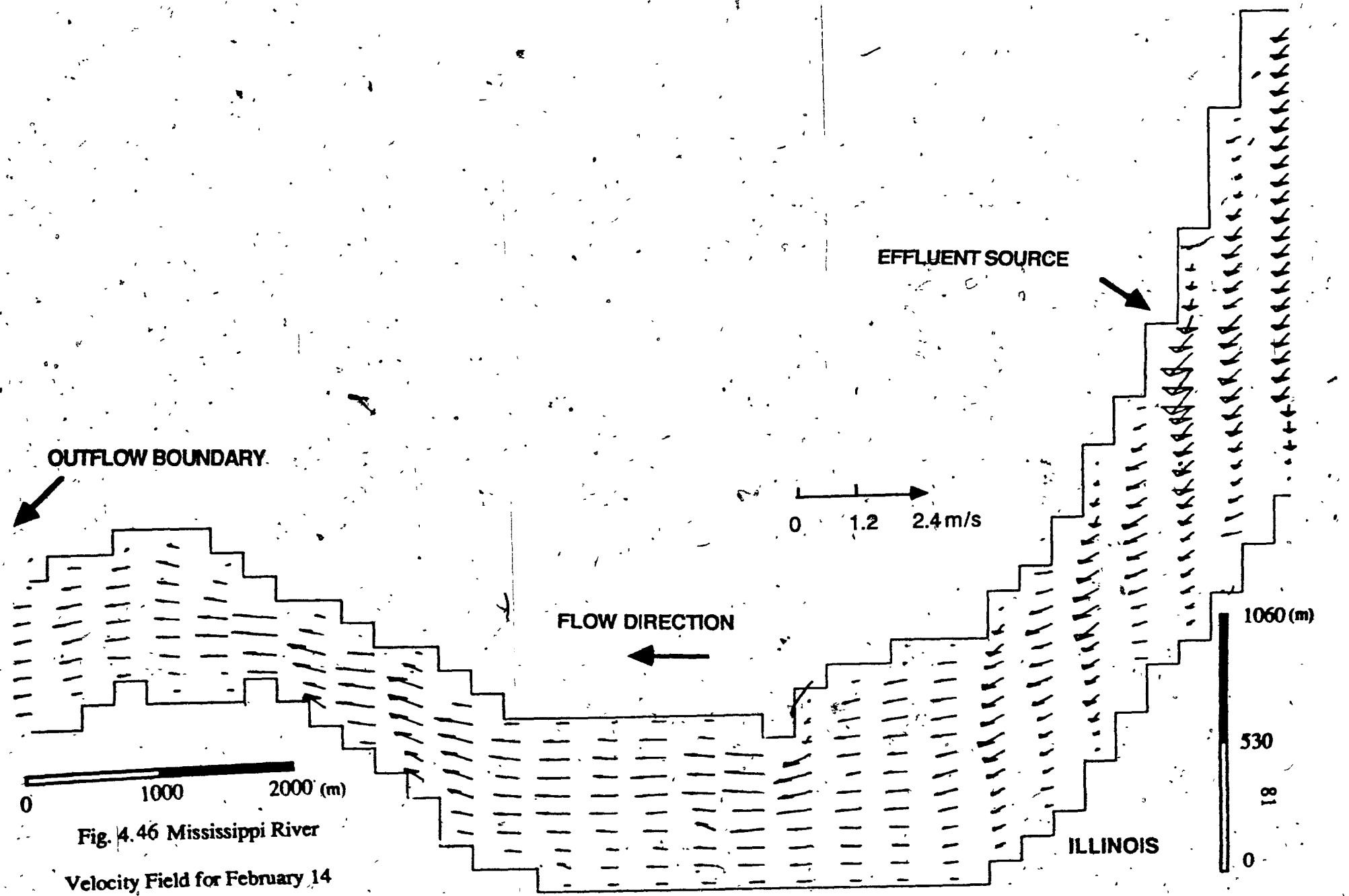

Fig. 4.46 Mississippi River

Velocity Field for February 14

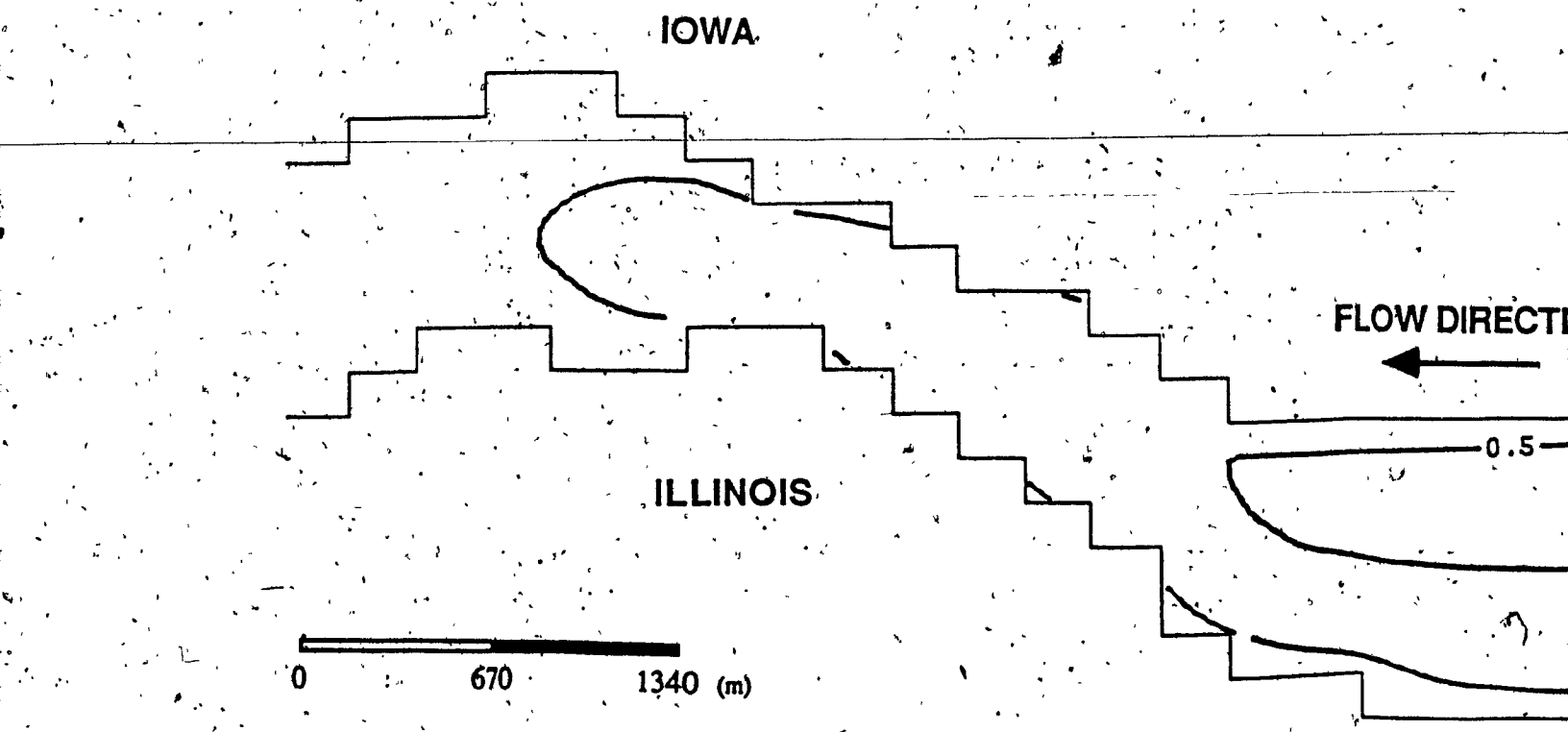

Fig.4.47 Mississippi River Tem

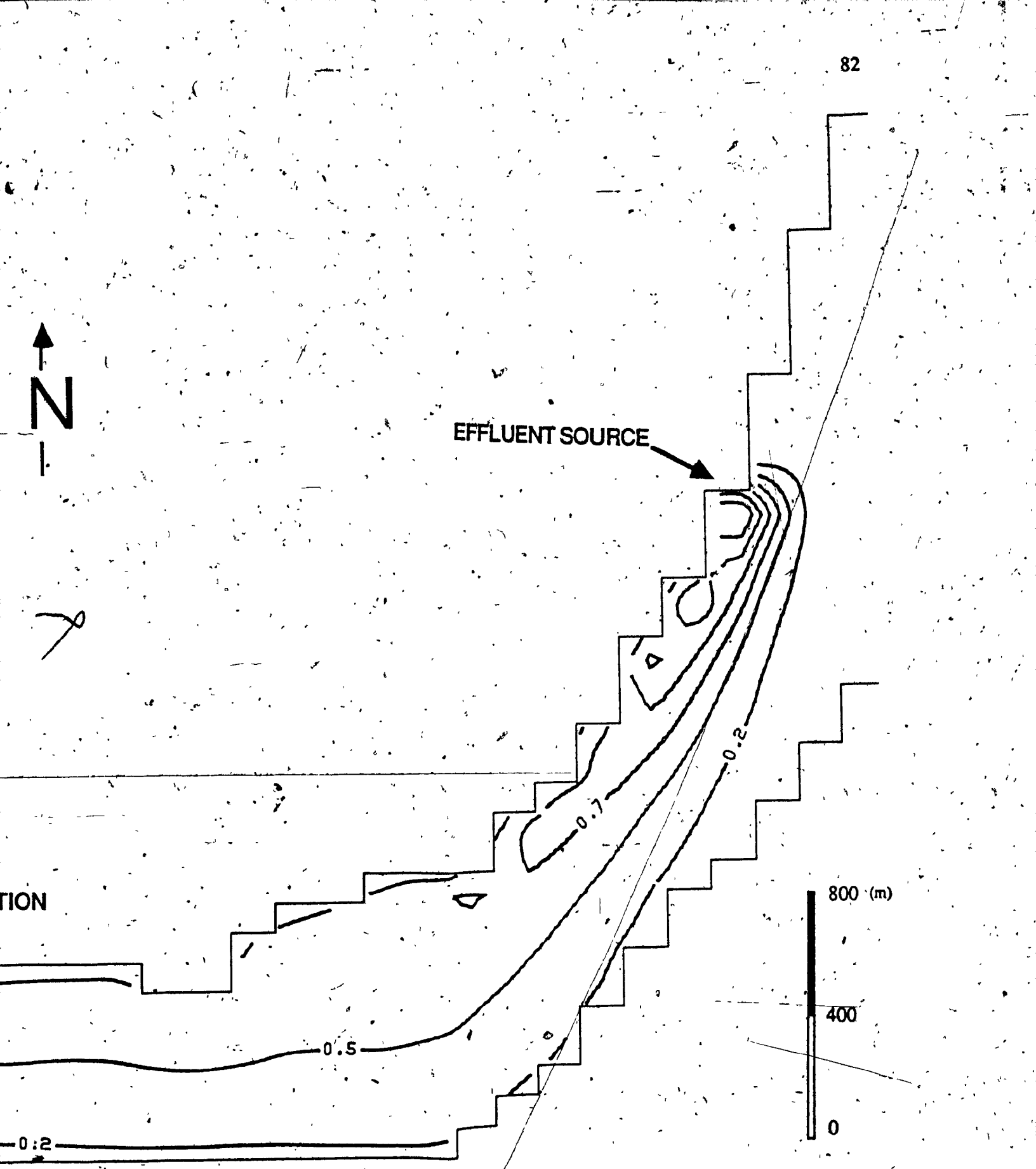

TION

mperature Distribution for Februrary 14

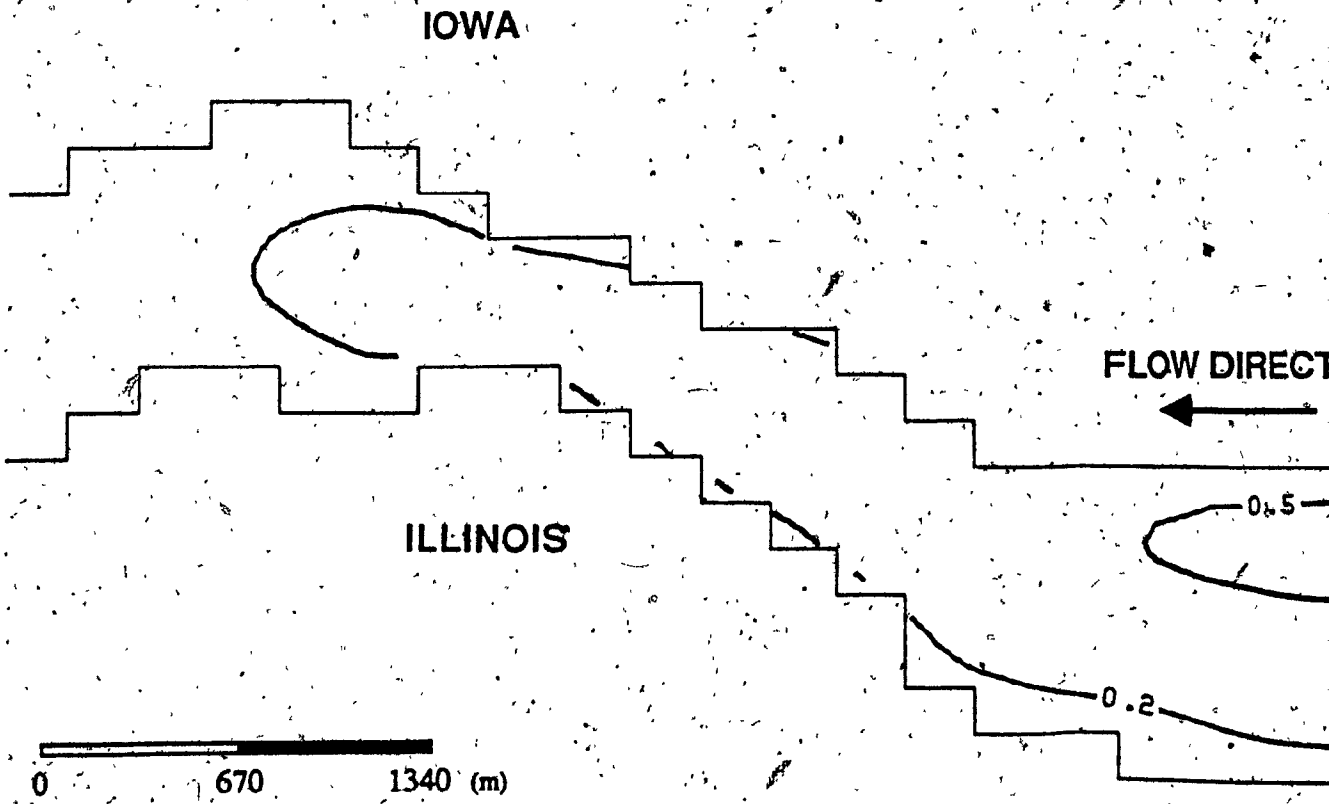

Fig.4.48 Mississippi River Ten

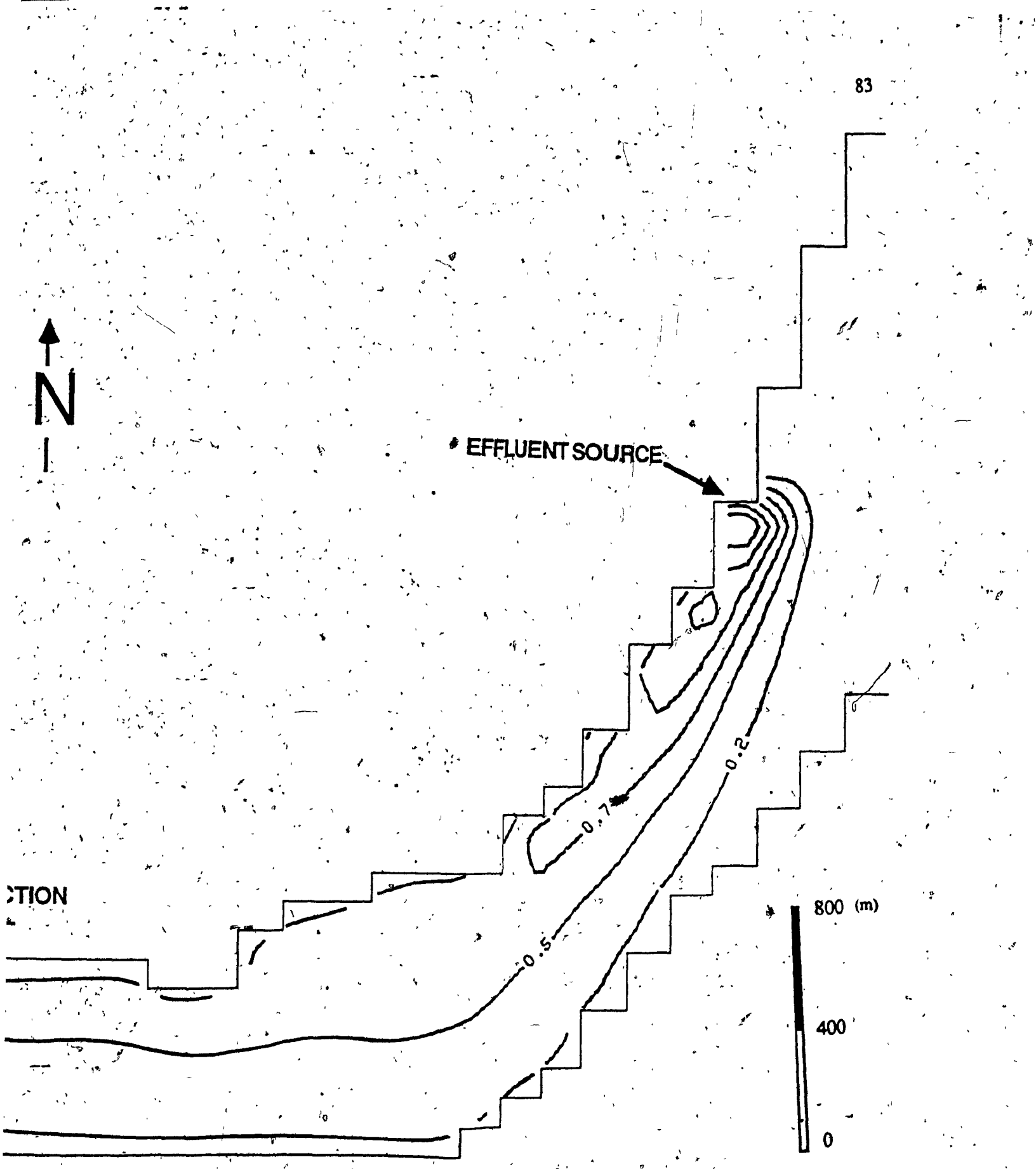

CTION

emperature Distribution for Februrary 17

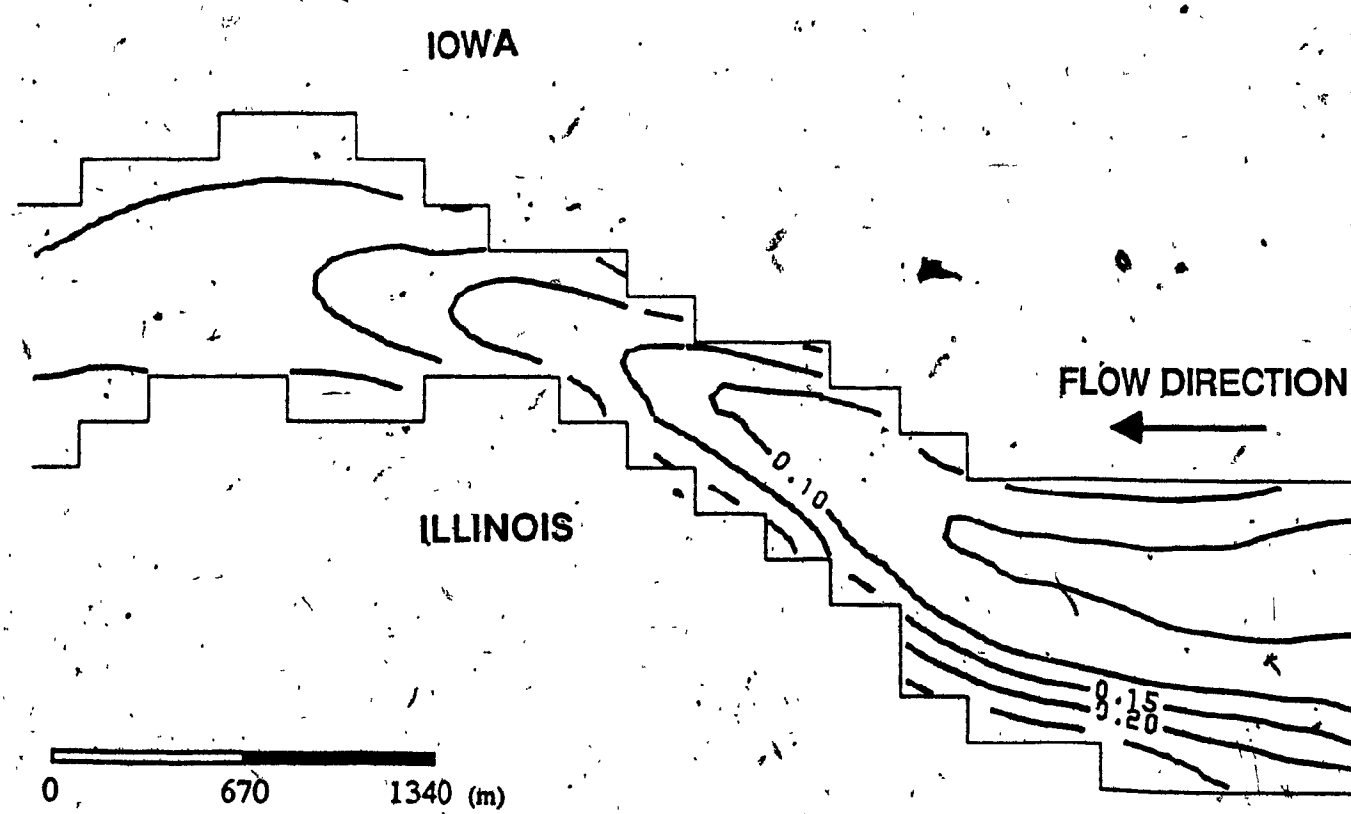

Fig.4.49 Mississippi River Ice T

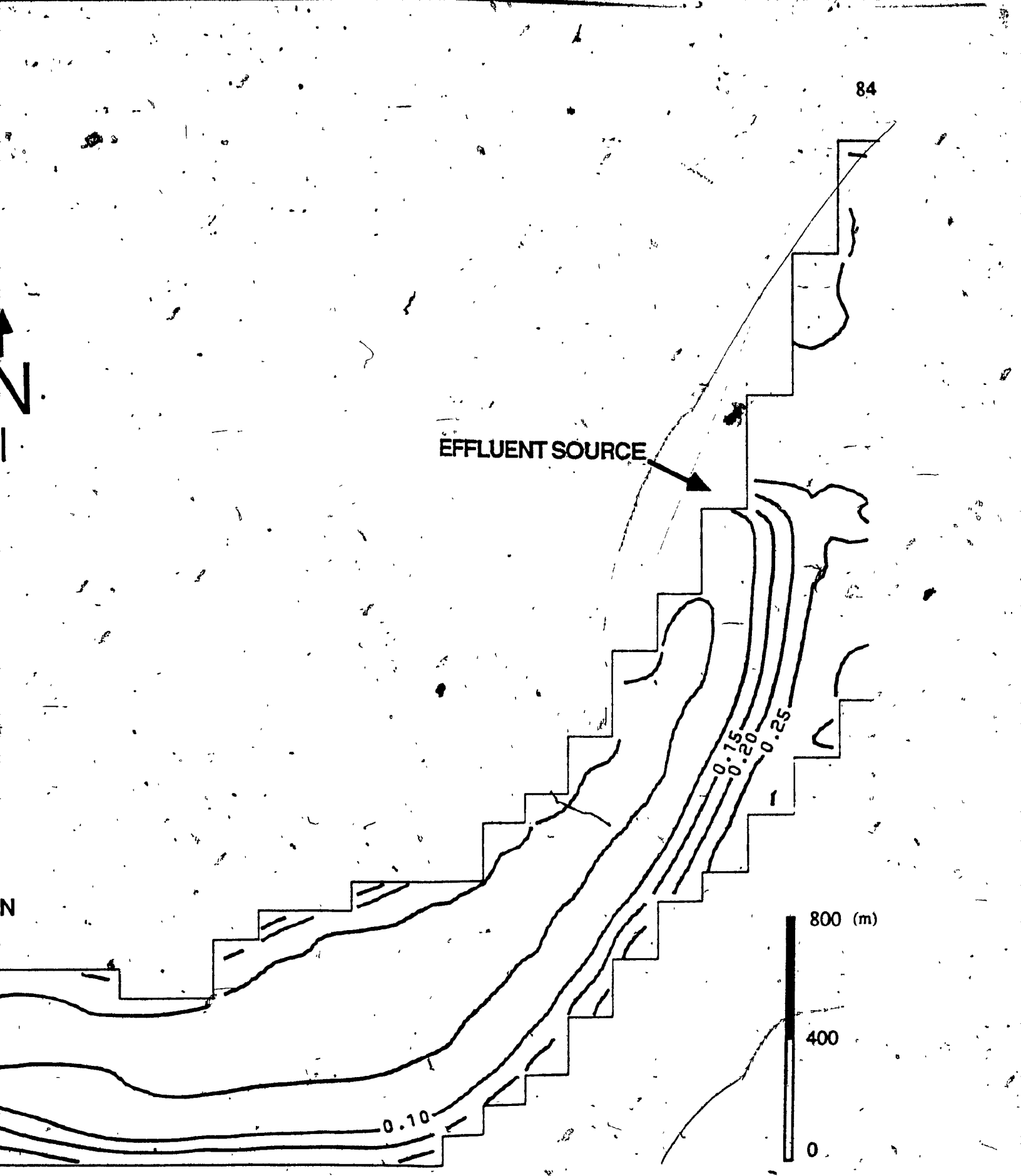

Thickness for Februrary 14

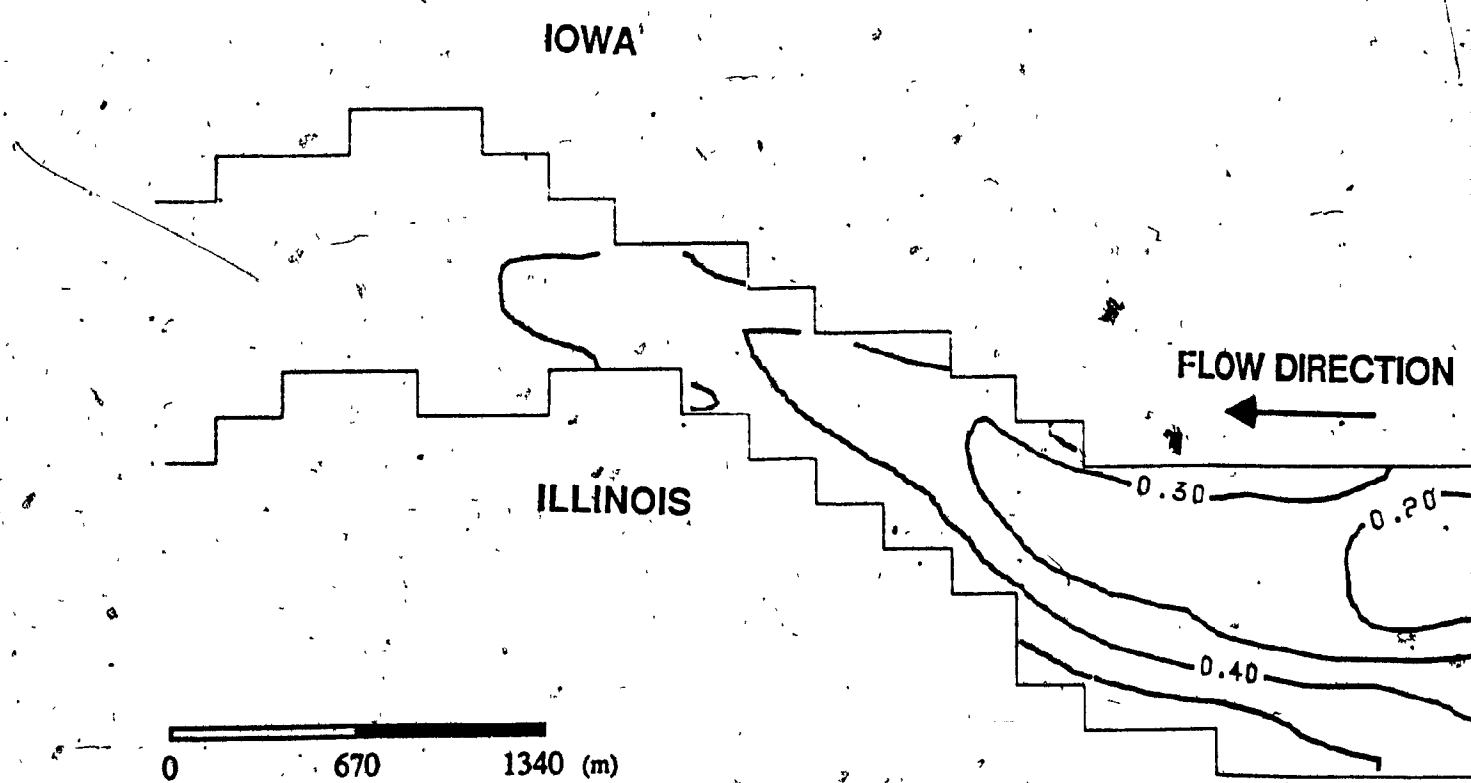

Fig.4.50 Mississippi River Ice Th

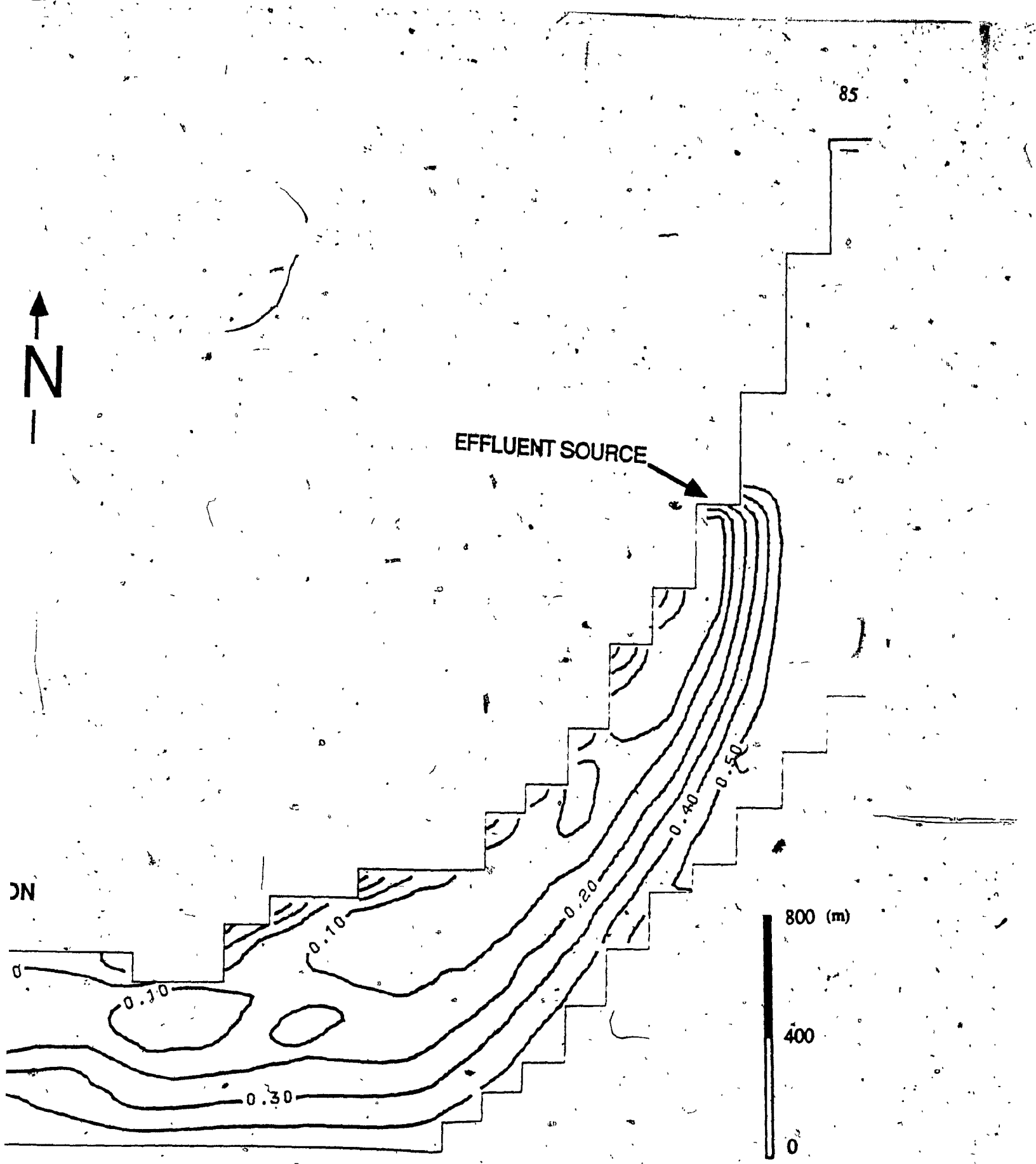

ce Thickness for Februrary 17

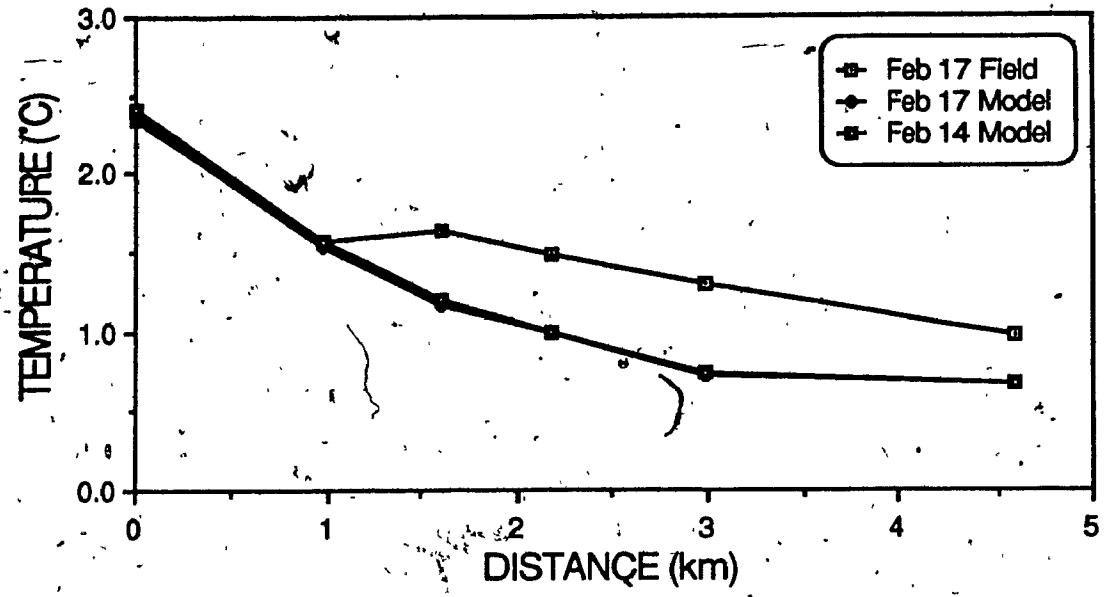

Fig. 4.51 Longitudinal Temperature Comparison

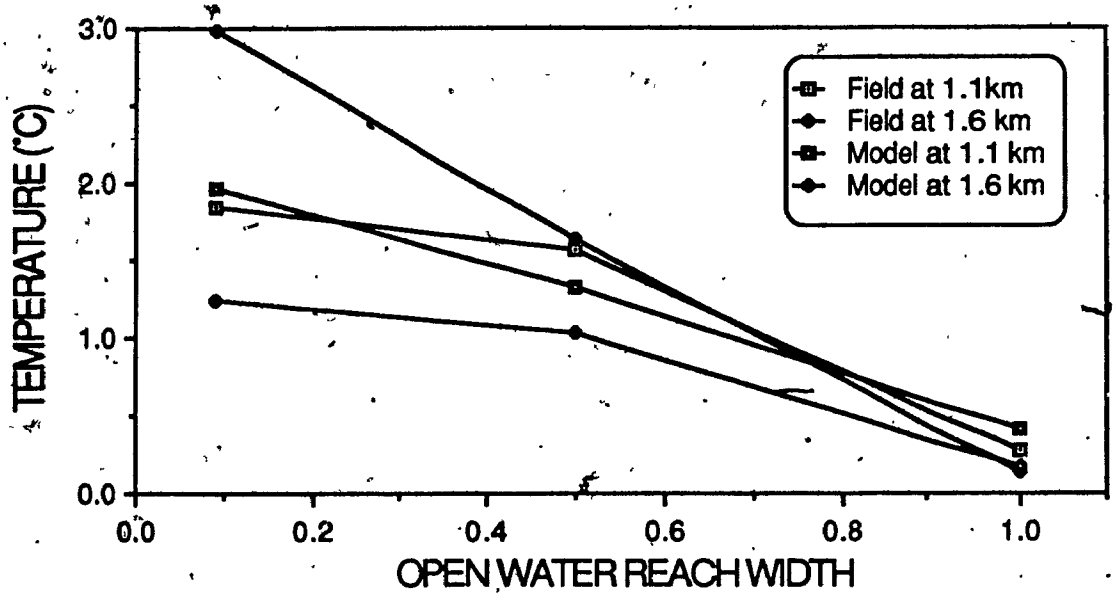

Fig. 4.52 Transverse Temperature Comparison

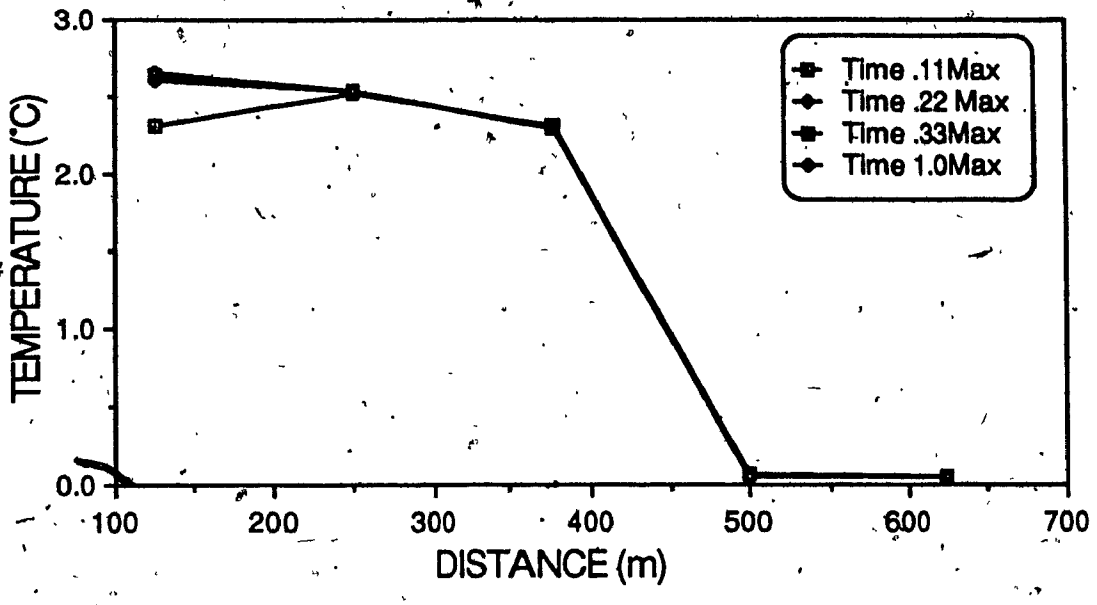

Fig. 4.53 Time Water Temperature Graph of Model

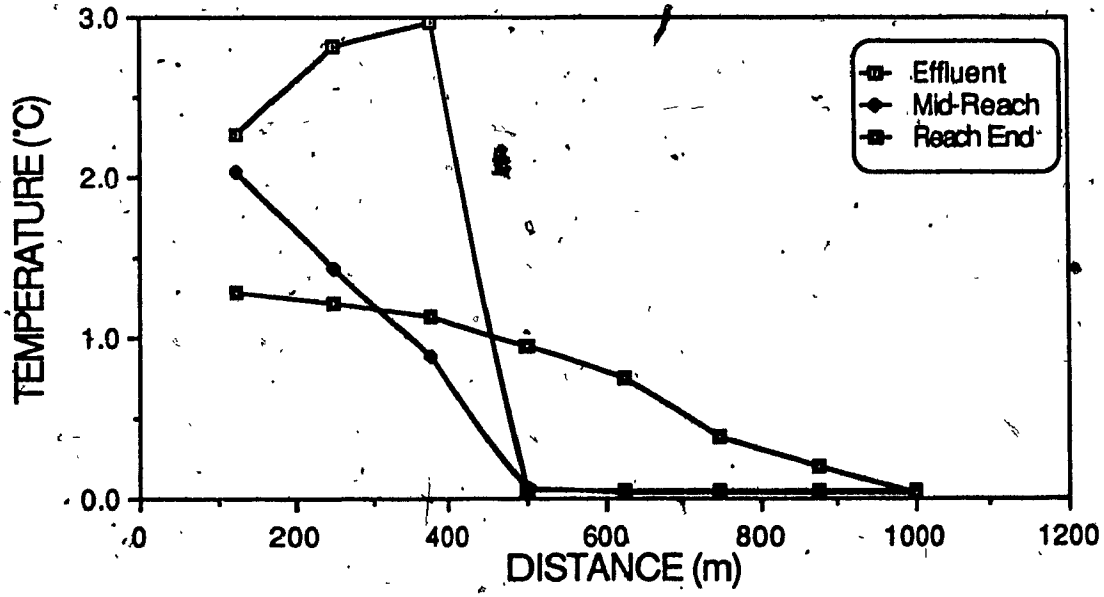

Fig. 4.54 Water Temperature Profiles

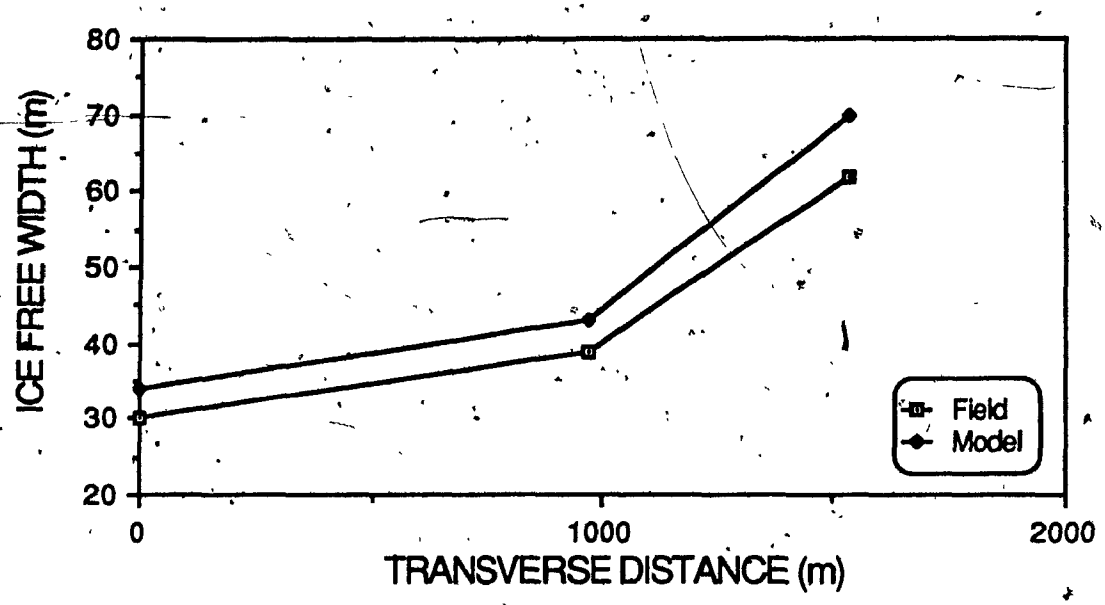

Fig. 4.55 Ice Free Width Comparison

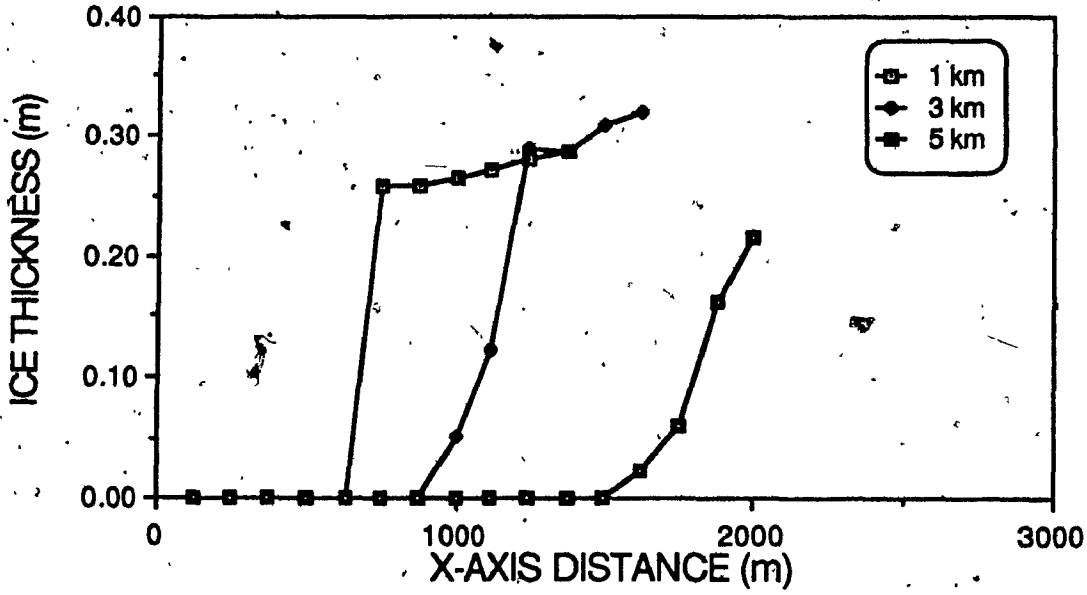

Fig. 4.56 Ice Thickness Profiles

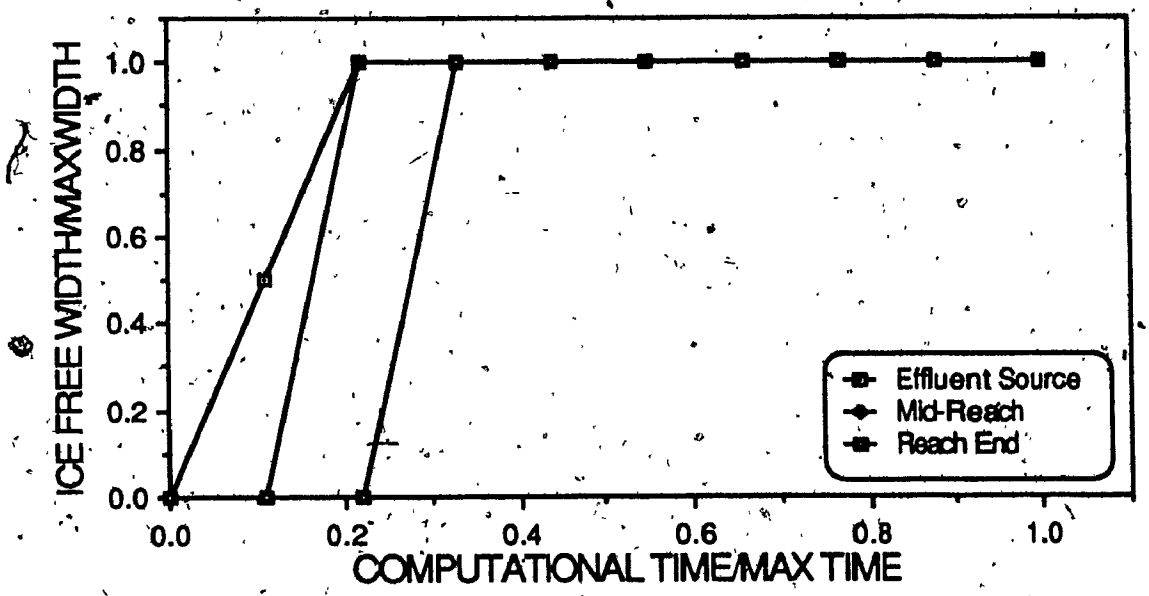

Fig. 4.57 Ice Free Widening

CHAPTER 5

CONCLUSIONS

In the present work the melting of river ice by a side discharge thermal effluent is modelled. The model developed here allows the effect of a thermal effluent discharge to be predicted and the possible development of a beneficial design.

The river hydrodynamics are simulated by use of the shallow water equations. Incorporation of the ice cover effects in these equations permits modelling of the flow in the vicinity of a floating ice cover. An extensive heat budget evaluation allows for the effect of different meteorological conditions to be considered. Air temperature has an important effect on the extent of the open water area, as well as the undisturbed ice thickness. Tests indicated that warmer effluent discharges increased open water reaches in length and width. Ice cover melting is observed to occur predominately downstream of the effluent source, with some thinning of the ice cover upstream of the outfall. Furthermore, suppression of the ice cover was found to be related to flow velocity. Higher stream velocities produced longer ice free reaches. The warm water is more quickly carried downstream with less cooling and increased heat transfer occurs to the ice cover underside. The ice cover thickens quickly in the direction transverse to the flow but thickens slowly in the main flow direction, due to a lower water temperature gradient. Thickness of the ice cover, in the vicinity of the effluent outfall, is strongly dependant on the heat transfer at the underside of the ice cover. This heat transfer is based on water temperature, flow velocity and depth of flow.

The McCormack finite difference scheme produces a good simulation of the flow field. Temperature distribution modelling is performed by use of an upwinding finite difference scheme, due to the inability of central difference schemes to provide useful

results.

Comparison is carried out with an analytical solution of the energy equation indicating overall good performance of the model. Comparison with field data shows the validity of the behaviour of the ice cover simulation. The space distribution of ice cover thickness distribution agrees with the field results.

Further research could be carried out to better understand dispersion in ice covered rivers and mixing at the ice cover edge. Introduction of a turbulence model would allow near field mixing to be modelled. Calibration with additional sets of field data would permit more refinement and a better understanding of the model predictions.

REFERENCES

1. Al-Saleh, W., Sarraf, S. and Kahawita, R. (1987). "River Ice Cover Melting by Side Effluents," 11th Canadian Congress of Applied Mechanics Proceedings, Edmonton, Alberta, pp. C-78-C-79.

2. Anderson, D.A., Tannehill, J.C. and Pletcher, R.H. (1984). Computational Fluid Mechanics and Heat Transfer, Hemisphere Publishing Company, Washington, D.C.

3. Ashton, G.D. (1979). "Suppression of River Ice by Thermal Effluents," CRREL Report 79-30, U.S. Army Cold Regions Research Engineering Laboratory, Hanover, N.H., Dec.

4. Ashton, G.D. (1980). "Unpublished Field Data," Mississippi River Study Personal Notes Received During Visit at U.S. Army Cold Regions Research Engineering Laboratory, Hanover, N.H., November 1986.

5. Ashton, G.D. (1981). "River Ice Suppression by Side Channel Discharge of Warm Water," IAHR International Symposium on Ice Proceedings, Quebec, Quebec, pp. 65-81.

6. Baldwin, B.S., McCormack, R.W. and Diewart, G.S. (1975). "Numerical Techniques for the Solution of the Compressible Navier-Stokes Equations and Implementation of Turbulence Models," AGARD Lecture Series No. 73, NATO, London, Eng., Feb., pp. 2-1 - 2-22.

7. Burrell, B. and Davar, K.S. (1982). "Flow Conveyance With Ice Cover on the Nashwaak River, N.B.," Canadian Journal of Civil Engineering, Vol. 9, pp. 674-677.

8. Chow, V.T. (1957). Open Channel Hydraulics, McGraw Hill, New York, N.Y.

9. Dingman, S.L., Weeks, W.F. and Yen, Y.C. (1967). "The Effects of Thermal Pollution on River Ice Conditions, Part 1, A General Method of Calculation," CRREL Report 206, U.S. Army Cold Regions Research Engineering Laboratory, Hanover, N.H., Dec.

10. Dingman, S.L. and Weeks, W.F. (1970). "Temperature and Ice Distribution in the North Saskatchewan River Below the Edmonton Generating Plant," CRREL Special Report 152, U.S. Army Cold Regions Research Engineering Laboratory, Hanover, N.H., Oct.

11. Elder, J.W. (1959). "The Dispersion of Marked Fluid in Turbulant Shear Flow," Journal of Fluid Mechanics, Vol. 5, pp. 544-560.

12. Engman, E.O. (1977). "Turbulant Diffusion in Channels with a Surface Cover," Journal of Hydraulic Research, Vol. 15, No. 4, pp. 327-335.

13. Garcia, F.R. (1983). "Mathematical Modelling of Two-Dimensional Hydraulic Problems Using a Fully-Dense Finite-Difference Scheme," M.Sc.A. Thesis, Ecole Polytechnique de Montréal, Aug.

14. Hayes, F.D. and Ashton, G.D. (1979). "Turbulent Heat Transfer in Large Aspect Channels," CRREL Report 79-13, U.S. Army Cold Regions Research Engineering Laboratory, Hanover, N.H., May.

15. Hayes, F.D. and Ashton, G.D. (1985). "River Ice Suppresion by Thermal Discharges," CRREL Preliminary Report Work Unit No. 322 89, U.S. Army Cold Regions Research Engineering Laboratory, Hanover, N.H., April.

16. Leonard, B.P. (1979a). "A Survey of Finite Differences of Opinion on Numerical Muddling of the Incompressible Defective Confusion Equation," ASME, Finite Element Methods for Convection Dominated Flows Symposium Proceedings, New York, N.Y., Dec. 2-7, pp. 1-17.

17. Leonard, B.P. (1979b). "A Stable and Accurate Convective Modelling Procedure Based on Quadratic Upstream Interpolation," Computer Methods in Applied Mechanics and Engineering, Vol. 19, pp. 59-98.

18. Paily, P.P., Macagno, E.O. and Kennedy, J.F. (1974). "Winter-Regime Surface Heat Loss from Heated Streams," IIHR Report No. 155, Iowa Institute of Hydraulic Research, Iowa City, Iowa, March.

19. Paily, P.P. and Macagno, E.O. (1974). "Thermal Response of Heated Streams, Solution by the Implicit Method," IIHR Report No. 165, Iowa Institute of Hydraulic Research, Iowa City, Iowa, May.

20. Paily, P.P. (1974). "Winter-Regime Thermal Response of Heated Streams," Ph.D. Thesis, University of Iowa, May.

21. Patankar, S.V. (1980). Numerical Heat Transfer and Fluid Flow, Hemisphere Publishing Company, Washington, D.C.

22. Raithby, G.D. (1976). "A Critical Evaluation of Upstream Differencing Applied to Problems Involving Fluid Flow," Computer Methods in Applied Mechanics and Engineering, Vol. 9, pp. 75-103.

23. Roache, P.J. (1976). Computational Fluid Dynamics, Hermosa Publishers, Alburquerque, N.M.

24. Shen, T.S. and Chiang, L. (1984). "Simulation of Growth and Decay of River Ice Cover," Journal of Hydraulic Engineering, ASCE, Vol. 110, No. 7, July, pp. 958-971.

25. Wake, A. and Rumer, R.R. (1979). "Modelling Ice Regime of Lake Erie," Journal of the Hydraulics Division, ASCE, Vol. 105, No. HY7, July, pp. 827-844.

26. Wankiewicz, A. (1984). "Analysis of Winter Heat Flow in an Arctic Stream," Canadian Journal of Civil Engineering, Vol. 11, pp. 430-443.